Array Combiner for GMRT

A Thesis
Submitted for the Degree of
Master of Science (Engg.)
in the Faculty of Engineering

By
T. PRABU

Department of Electrical Communication Engineering
INDIAN INSTITUTE OF SCIENCE
BANGALORE-560 012 (INDIA)

JUNE 1997

ABSTRACT

Background :

The hardware designed and developed provides the single beam modes for the GMRT Array

Today Radio Astronomy has developed to be a highly complex, inter-disciplinary subject. Many radio astronomical problems need technologies from different engineering fields and knowledge from many scientific fields, at times well beyond the state-of-the-art. Large number of unsolved problems in the area of the meter-wave radio astronomy, led to the conception of the world's biggest meter-wave telescope array facility in India, known as the Giant Meterwave Radio Telescope (GMRT). It consists of 30 dish antennas operating in six different center frequencies of astronomical interest. Some of the important studies that are planned with GMRT are the inter-planetary scintillation study, pulsar searches, studies of known pulsars, radio recombination line observations, and lunar occultation observation etc. All these observations can be efficiently carried out only if a suitably combined output is available from the GMRT array .The instrumentation design and development details presented in this thesis, facilitates the above described observations with GMRT by providing such single beam outputs in two modes.

The Design and Development :

The design requirements were carefully studied. The GMRT array simultaneously requires the Incoherent and the Phased Array mode Single Beam outputs for efficiently conducting certain important astronomical observations. After the array outputs are digitised, delay corrected and Fourier transformed, the signals can be tapped for producing the single beam mode outputs. These are complex spectra, represented by digital numbers.

Large Number of Inputs: There are about 120 complex numbers each being 12 bits wide, contributing 1,440 input signal bits to the system. Handling so many inputs is a major task.

Large Processing Power: There will be about 16 million such 120 complex numbers to be processed every second. This calls for a high speed digital processing hardware with capabilities to do 17,280 Million Multiplications, and 8,488 Million Additions every second. The computational power required in producing the two single beam modes cannot be met by any readily available commercial hardware.

The major engineering challenges arise from the magnitude of the number of inputs to the system and from the required speed of operation. It is required to design a suitable instrument to meet these requirements.

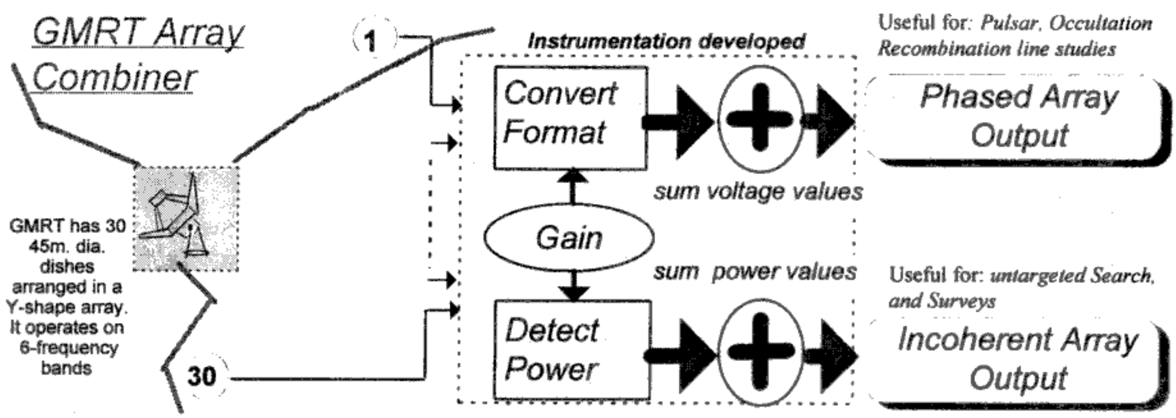

The design was carefully analysed and the two main sections were identified. Techniques were found out to simplify the design complexities. To validate the design, a reduced version of the instrument, working at 16 MHz, was built and tested at the telescope site with astronomical signals. The tests showed that the basic design was working satisfactorily. Currently it is being used for the astronomical observations. In this design, the major computations were simplified using the look-up tables, and erasable programmable logic devices were used for performing the addition. In the final design, two more important considerations were included, viz., 1) simplification of the hardware complexity by running the system at twice the speed, 2) optimisation of the quantisation levels (in the look-up tables) in accordance with each independent input-signal level.

Then the final instrument design work was taken up. It has been designed with a scalable architecture. The system speed of operation is about 32 MHz. Running the system at the higher speed introduced new constraints. The hardware technology required was completely different from what was used in the proto-type design. The realization of the final system hinged on the availability of faster components in the market and the knowledge from literature for building such high speed systems. For this purpose, the high speed circuit design aspects were carefully studied. The techniques for performing processing of signals at the required speed were identified and circuit layouts were carefully made to suit for the high speed design. The full system design was completed. The design taking into account all the additional factors is implemented in the final version of the hardware. The PCBs required for a main section of the instrument, supporting an eight dish system (two polarisation) were made, assembled and tested.

The details about the design and development of this Instrumentation outlined above, is presented in the Thesis.

Results and conclusions:

The *Array Combiner* operations were analysed by simulating the system operation using *computer programs*. These simulation studies yielded useful information about the choice of parameter to optimise the performance of the Array Combiner. After the instrument was brought to the final form, it was tested with the simulated signals in the laboratory as well as at the telescope site. Tests carried-out include observation of the noise sources. The test results show that the design goals are adequately met in the hardware. Using the proto-type, even *pulsar* signals were observed by connecting the outputs to the Pulsar search pre-processor back-end. The following are the two typical results (observed *pulsar* profiles).

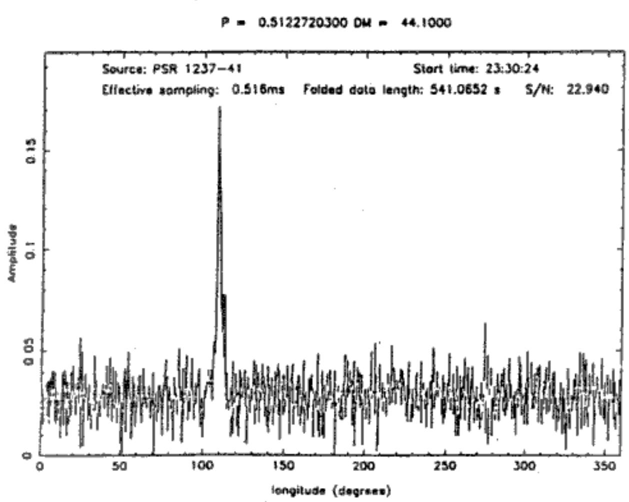

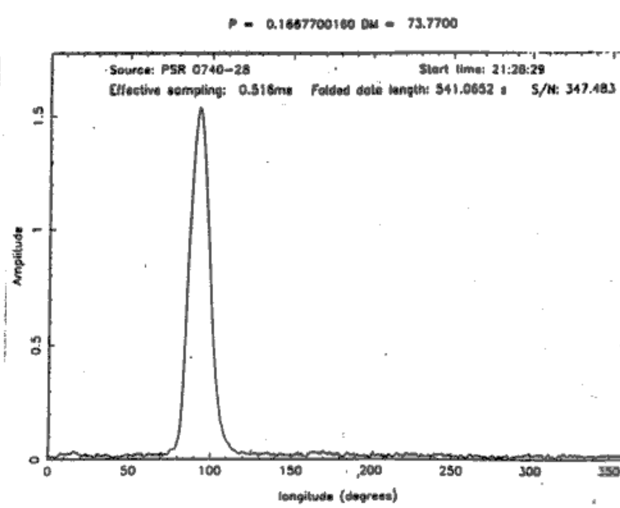

I acknowledge . . .

As I, discover myself at the tail end of this program, I recollect many indispensable events, that enabled the proper and smooth completion of this work. I am undoubtedly thankful to everyone of the people, who were in the background for such events to materialise, and I wish to recollect, and acknowledge everyone of them.

I thank both my guides, Prof T. S. Vedavathy, and Dr. A. A. Deshpande. Your guidance and the suggestions were timely, and very much valuable. Your patient teaching elevated my thoughts. I will honour them always!.

The complexity of the work, clearly indicates the presence of the hard working team members. I wish to acknowledge this and thank, (vijay), gopalakrishna, kamini, moorthy, jacob, (ravi), and (suresh). Your hard efforts and the full hearted support is helping in the physical realisation of such a big system possible. I respect your skills and capabilities!.

I also thank the other friends in the lab for their encouragements and suggestions. Special thanks to ramkumar and desh, for their timely help during my entry into the Institute of Science. I also thank desh, for all his suggestions during the initial and final stages of the system development. I also wish to thank the pulsar group, for their constant feed back and suggestions while testing and using the Instrument at the observatories. Thanks to all the Team members of the Pulsar Search Pre-processor, for we have used your machine (ramkumar, sridhar & mark). I thank Dr Ravindra, for providing the various resources and supports for the project. And special thanks to GK and Uday for, they have extended the supports to the field stations. I thank, all the colleagues in the library for, their helps, and especially Mr Chowdappa for all the neat reprographic works. I also wish to thank, Mr. Gangathar and other friends (suresh, muthu, mohan, gokul, gopal and others) for their support in making the cages. Coming out from the hardware, I wish to thank mamatha for organising various works required for the project.and the observatory staff at Ooty and Pune, for their kind support during many testing hours in the day and night. Also I wish to thank the staff at the food facilities in all these places.for their support during our requirements.

Last but not the least, I understand, and value all the co-operation, help and the sacrifices you had to undergo, jeba and the little one. I wish to tell you something, you know it is only now, I had a chance to stay in-station for such a long stretch of time!. Grand pa, mas, and pa, ma, I respect all the encouragements and teachings from you, that brought me here, to be in this project. I wish to be a useful part too, in the endeavours to come.and pray for that!.

T Prabu

Contents

Page No.

Chapter 5 Results and Discussion

Chapter 6 Conclusions

Appendix - A Full System Details

Appendix - B Simulation

Appendix - C Eight-Dish System

Chapter 1 *Introduction*

Chapter 1

Introduction

1. 1 Topic of Interest

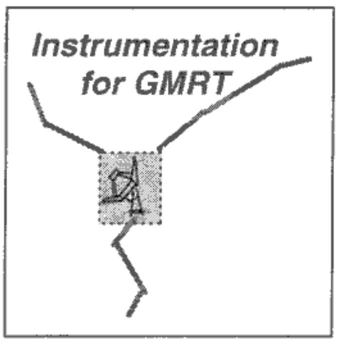

Since the *World War-II*, astronomers have been probing the sky, also in wave-length windows other than that of the visible light. Most of the radiation whose wave-lengths are shorter than that of the visible light, like ultraviolet and X-rays, is all blocked by the Earth's atmosphere. Ultra-violet and X-ray observations can be made by sending detectors to high altitudes using balloons and rockets. For X-ray observations, Geiger and Scintillation counters are used. Now there are unmanned UV observatories orbiting around the Earth. Gamma rays are hundreds of thousands of times more energetic than X-rays. Practically the whole universe is transparent to them. Hence, they seem to be the only strong signals to reach Earth from the farthest places in the universe. Having survived many light years of journey, they are stopped by the Earth's atmosphere. These cosmic gamma rays can be indirectly studied by looking at the sub-atomic particle shower, they produce while interacting with atoms and molecules of the atmosphere at the high altitudes. Orbiting gamma-ray observatories are also used for direct observations.

In the case of infra-red observations, the temperatures of the celestial bodies are studied. Most of these wavelengths penetrate the Earth's atmosphere. Infra-red observations are little complicated due to the fact that nearly every object, including the instruments used, emit infra-red (heat) radiations. Telescopes and photographic emulsions made to operate at the visible light wavelength could well suit for infra-red radiations that are close to visible light wavelengths. In olden days direct sensation or thermo-meters were used to measure the infra-red radiations. Later on thermocouples and gas expansion schemes were used for measurements. Recent equipments are vacuum shielded to prevent radiation from outside and cooled to absolute zero to prevent the equipment from producing infra-red radiation. And these techniques increase the sensitivity to a great extent [1].

The radio waves can pass through the Earth's atmosphere and even through the clouds. Radio Telescopes are used for receiving these radio frequency signals. These telescopes revealed celestial objects which were never seen before even by the biggest optical telescopes. Systematic surveys of the sky led to the discovery of thousands of objects emitting radio waves. Some of them don't have any significant emission at the optical wavelengths.

Generally, the quality of radio observations is limited by three major considerations; they are, the low resolution of the telescopes, the low intensity of the signals being received, and the terrestrial radio Interference [2]. Interferometry and aperture synthesis techniques were developed to improve the observational capabilities. These techniques are very powerful and complex too. Today, there are many powerful radio telescopes that are operated based on these techniques.

In the early days of radio astronomy, many interesting experiments were carried out, which helped in improving our understanding of the solar system. Large antennas with high sensitivity and angular resolutions, improved data-processing methods, the use of interferometers and specialised instruments have enabled studies of farther objects beyond our solar system with greater details. These improved techniques showed the evidence for the existence of new kinds of extraordinary objects like, the *Quasi-stellar Radio Stars (Quasars) at high red-shifts (receding), the highly magnetised rotating Neutron Stars (Pulsars), continuously varying Active-galaxies and objects with escape velocity greater than that of the velocity of light (Black-holes)* [3]. Detection of many of these objects helps in the understanding of the state of the *Early-Universe* apart from unveiling many other new scientific fundamental facts. The centre of our galaxy, heavily obscured at optical wavelengths by thick curtains of interstellar dust is still another interesting area for exploration at radio wavelengths. *Hydrogen* is the basic building block of the universe, whose *line emission* at 21.1 cm is studied and has resulted in important insights; for example the shifts in the line frequencies due to the *Doppler* effect has helped understanding the *Galactic* rotation. Detection of the Carbon monoxide (CO) *line emission* at 2.6 mm (115.3 GHz.), gives the indirect evidence for the presence of the second most abundant component in the Galaxy, the molecular hydrogen (H_2). The simplicity of the CO emission gives useful information about the interstellar clouds, which are also the potential regions of star formation [3]. Another interesting research area is related to the question whether other stars have planetary system. It is too difficult to use any direct methods for this purpose. Detection of the wobbling of a star could be associated with presence of a rotating massive planet around that star. For this purpose, as one of the methods one looks for *Doppler-induced wavelength shifts* in a star's spectral lines using highly specialised spectrographs.

Today, the nearly 60 year old Radio Astronomy has developed to be a highly complex, inter-disciplinary subject. Many *practical* problems in radio astronomy can only be solved by applying suitable techniques from various engineering, and scientific fields, at times well beyond the state-of-the-art.

Large number of unsolved problems in the area of the meter-wave radio astronomy, many other new scientific objectives and the absence of a powerful metrewave telescope anywhere in the world, led to the conception of the meter-wave radio telescope array facility known as the Giant Meter-wave Radio Telescope (GMRT) in India. When it is completed, it will be the World's biggest meter-wavelength synthesis radio telescope. GMRT will be a very powerful tool in the investigations of phenomena ranging from stellar systems to universe as a whole. The Y-shaped GMRT array consists of 30 dish antennas of 45 metre diameter, operating in six different frequency bands [4].

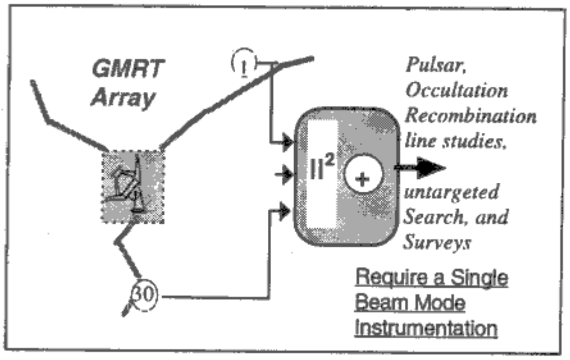

Although the GMRT is basically an Aperture-synthesis instrument, a single beam mode is desirable for studies such as inter-planetary scintillation, pulsar searches, studying known pulsars, radio recombination line observations, and lunar occultation observations etc.. Such a single-beam mode essentially involves combining the different dish outputs suitably and is best suited for studying temporal and spectral variations of sources smaller than the effective beam width of the single-beam. In such cases, a single-beam mode helps in simplifying observations in terms of reduced hardware and data rates etc.

The hardware designed and developed provides the single beam modes for the GMRT Array

The special instrumentation designed, developed and presented in this *thesis*, is aimed to provide two simultaneous single-beam modes for the GMRT Array.

In some applications, for example in untargeted survey/search, it is desirable to have more sky coverage at the expense of reduced sensitivity. If the outputs from all the '*N*' dishes are combined incoherently (after detection), then the effective collecting area would be about $\sqrt{N}$ times the area of a single dish, which is approximately 5,500 square metres for 30 dishes, with a field of view of approximately 0.3 square degree (at 610 MHz). In some applications, it is required to have the highest available sensitivity, although field-of-view may be very small (for example, while studying known pulsars). This would involve combining the dish outputs coherently (before detection) where the effective collecting area would be approximately N times that of a single dish (30,000 square metres for 30 dishes). However the field of view would be very small (at best 1/N th of the former case) [5, 6].

1. 2 Single Beaming: Possible solutions

- **Based on Analog Devices**

In the case of a relatively small telescope arrays, the single-beam can be achieved by suitably arranging variable delay elements in signal paths and then adding the detected signals (Incoherent Addition) using suitable power combiners. For the coherent combination, however, the delay parameters need to vary in very fine steps. Hence to provide very fine steps in the beam positions and in many directions it would require large amount of duplication of the networks and lot of switching elements in the system which is a cumber-some task. It is not practical to attempt such beam forming techniques for the 30 dishes of the GMRT array, where the long and continuously changing baselines will pose serious difficulties in achieving such networks and will result in serious limitations in the performance of the single beam system.

- **Based on Off-line Processing**

Single beam can also be simulated by first recording the dish outputs, and then processing it off-line through suitable computer software. To do such operation in real time it needs mammoth data acquisition, a terra sample storage (30 x 2 x 32 million data word to be recorded/processed every second, for the entire observation duration!), and processing capabilities.

There is no off-the-shelf ready made solution available to meet these requirements.

- **Based on Digital Technology**

Presently the digital technology is increasingly progressing every day. For most of the design problems, now it is possible to find a spectrum of elegant digital solutions. Many analog problems can be dealt with easily in the digital mode. Such designs will also benefit from programmability, easy change of parameters, good repeatability and at times remarkable compactness.

The GMRT design has already incorporated a digital front-end hardware to process the base-band signals. From each of the GMRT dishes, two bands of 16-MHz, for each of the two circular polarisation will be available. These 4-bands of 16 MHz each are sampled in parallel, and after signal propagation delay between antennas are corrected, the sample sets are Fourier transformed separately to produce 4 complex spectra each with up to 512 spectral channels at Nyquist intervals. These output complex spectra are available sequentially at a rate of 32 MHz per side band. Thus in all there are 60 such data streams that are available in parallel.

It is most convenient to tap the digital signals from the array at this stage, and digitally combine them to produce the two simultaneous single-beam modes. Such a system, apart from meeting the observing requirements, would be relatively compact, flexible, quickly configurable, and can incorporate many additional desirable features like channel wise, dish wise gain control etc.

1. 3 What is attempted in the present project?

The aim in this project was to design and fabricate a suitable digital hardware to realise the two single-beam modes discussed above. It should be noted that such a hardware would be required to work at 32 MHz rate, where digital design is generally very complex. Facilities are provided for combining or not combining any specific combination of dishes. Test facilities are built-in for testing this as well as any other hardware that would use the single-beam output. A PC based control enables programmability and hence flexibility.

In the present study, the design for a model is worked out. A detailed quantitative analysis of the performance evaluation is carried-out using computer simulations. A pilot model which can cater 4 dish inputs was considered, built, tested, installed at the telescope site and has been validated by using it for the astronomical observations. The model was developed for the complete final system with all the required facilities. An up-gradable final system for 8 dishes was fabricated, tested and installed at the site. The system was evaluated by several tests. The test results are presented here. The test results show that the design goals are adequately met in the final system.

1. 4 Layout of the Thesis

The thesis presents brief introductions to radio astronomy as a subject, various techniques adopted in the radio telescopes, about the GMRT instrumentation, and its scientific goals. Then a detailed description about the single-beam hardware design development and test results are presented.

Chapter-2 presents a brief *introduction* to radio astronomy and *radio telescopes.* It describes the receiver electronics aspects and gives an outline of the various type of receivers used in the radio telescopes. It also gives an overview of the different techniques adopted in *radio telescopes* to enhance observational capabilities and a brief introduction to some of the big *radio telescopes* in the world.

Chapter-3 describes briefly the *Giant Metre-wave Radio Telescope (GMRT),* its Scientific goals, followed by an outline about the receiver instrumentation, and digital back-ends available in the *GMRT.*

Chapter-4 contains a detailed discussion of the *design and development* of the instrumentation for incorporating *single beam modes* in the GMRT.

Chapter-5 gives detailed account of the various *tests*, their importance, *results* and a discussion of the results.

Appendix - A
Contains the thirty dish Array Combiner system Plan details.

Appendix - B
Contains the Simulation Programs [Provided in a floppy disk].

Appendix - C
Contains the complete details about the eight dish hardware installed at the GMRT Site. Related programs are provided in the floppy disk.

Appendix - D
Contains the testing/diagnostics lookup programs used during the development of the system [Provided in a floppy disk].

Appendix - E
Contains the details about the proto-type system. Related programs are provided in the floppy disk.

Chapter 2 ***Introduction to Radio Telescopes***

Chapter 2

Introduction to Radio Telescopes

2. 1 An Introduction

Today Radio Astronomy has developed to be a highly interdisciplinary field with connections to various fields of science and engineering. Observing the night sky on a clear day using an optical telescope has been the traditional tool for *Astronomy*. Although these telescopes have revealed the vast size of the universe, the universe turned out to be bigger than one had ever imagined. Often, we have serious limitations while using optical wave-lengths to learn about how the universe looks. Some regions like the centre of the our Galaxy are heavily obscured by thick curtains of interstellar

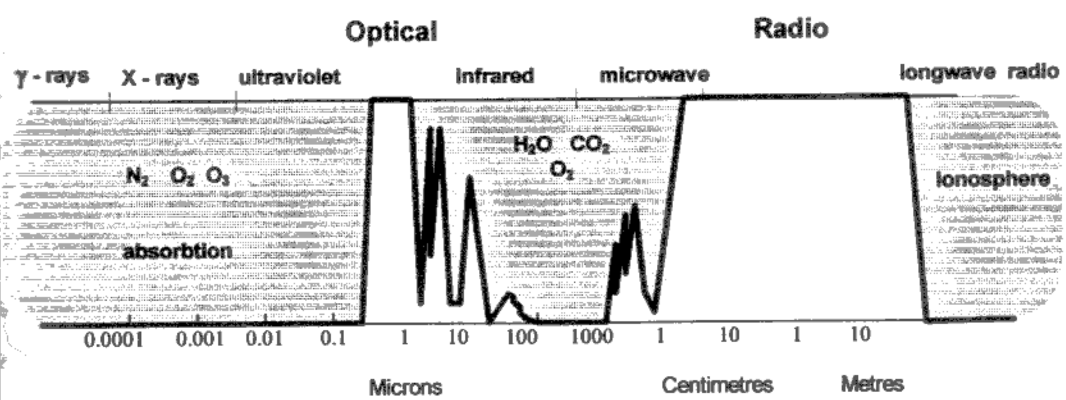

The electromagnetic spectrum, showing the wavelength range of the 'windows'. The radio range is limited by the ionosphere at wavelengths greater than a few metres, and by atmospheric absorbtion at wavelengths shorter than about 2 cm. (ref. Burke & Smith, 1997)

FIG. 2 - 1

dust, other objects like most of the Neutron Stars don't radiate enough at optical wavelengths.

One of the ends of the electro-magnetic spectrum, that is beyond the infra-red, is occupied by radio waves. This spectrum can broadly be classified as microwaves, millimetre-waves, and metric-waves. These radio waves can pass through the Earth's atmosphere and even through the clouds. *Antennas* are used to pickup these radio signals. This 100 year old technique originated from *Maxwell* and *Heinrich Hertz*, has now evolved to be a very sophisticated technology.

Just before *World War-II* Bell Laboratory radio engineer *Karl G Jansky* investigating radio disturbances interacting with trans-oceanic telephone service, found that the static he was receiving was originated from our galaxy, the *Milky-way*. Followed by this, an amateur astronomer *Grote Reber* built his own radio antenna and systematically mapped the sky and found many intense sources of radio emission. During the war British radar technicians found that Sun is the intense radio emitter. Then the astronomers from many countries began to make radio observations.

Astronomers have learnt to design and use special antennas for receiving radio frequency signals from celestial objects and they have named these antennas as radio telescopes. These radio telescopes revealed enormous number of celestial objects which were never seen before even by the biggest optical telescopes. Systematic scanning over the sky led to the discovery of thousands of celestial objects emitting radio waves. Some of them don't emit any light and are not obviously visible to the optical telescopes.

Using this new tool for astronomy many interesting experiments were carried out. Radio signals were sent to the Moon and reflections were obtained. These RADAR experiments revealed day time meteor streams, which were never visible to the optical telescopes. Reflections of radio signals from Venus revealed an accurate measure of its distance. Radio signals are also used to get a closer look at the Venus clouds. Radio experiments gave the conclusive evidence for the correction to the apparent rotation period of Mercury. Radio and radar studies of the Moon revealed the sand like nature of its surface before the landing experiments were attempted. Information about planets, their temperatures, surfaces, and magnetic fields were obtained using radio observations. Observations on Sun revealed much finer details. As the receiver is tuned to receive higher frequencies, the radiation received comes from increasing depths within the Sun's outer layers, and it became possible to study these layers separately. Solar flares and Sun-spots are found to be strong radio sources.

Getting radio signals through interplanetary ranges posed great technological difficulties. As the strength of the echoes decreased with the fourth power of the distance, it became very difficult to detect them. Such problems were solved by smarter techniques. Large antennas, improved receivers, data processing techniques, and the use of interferometer enabled astronomers to study farther and weaker sources and to obtain great details.

Usually radio observations suffer from low resolution, low intensity, and interference. The resolving power of the telescope is directly related to the diameter of the dish. For a given wavelength of operation the bigger the diameter of the dish, the better the resolving power of the telescope. At very long radio waves, images become fuzzy because of the large diffraction fringes. This problem is not solved easily because it is not very easy to build bigger telescopes. A dish of about 30 meters diameter operating at 21 cm wavelength can have a resolving power of only 0.5 degree. This number here means this telescope cannot distinguish details smaller than the size of the Moon in the sky. Constructing still bigger telescopes is much difficult an effort.

A solution to this problem has been found by using interferometry techniques. Using two or more radio antennas simultaneously, it is possible to simulate the effect of one very large antenna. The farther apart the antennas are the better the resolving power that can be achieved. Optical telescopes typically have a resolution of 1 to 2 arc seconds. Radio telescopes used in the combination have managed to achieve resolutions better than these figures. This technique is very powerful and complex too. It requires the precise knowledge of when a particular radio wave arrives at the given antenna. Such interferometry can also be tried between an orbiting radio telescope with a ground based one.

The second handicap is the low intensity of the radio signals. The energy of the photon depends on the wavelength. Photons of radio energy have such long wavelengths that their individual energies are quite low. To get strong signals focused on the antenna, the collecting area of the dish must be large.

The interference is the third handicap for radio observations. Man-made interferences are thousands of times stronger than the astronomical signals. These interferences drown the radio signals that they can never be detected at all. The only way out is to construct the radio telescopes at the remote radio quiet places.

2. 2 Radio Telescopes - *A History Remembered*

It is now more than 60 years since the discovery of cosmic radio waves by *Karl G. Jansky*. The radio antenna that he used was about 100 *ft* long by 12 *ft* high. It had a vertically polarised , unidirectional fan shaped beam with its half-power width of about 30 degrees. The antenna was a *Bruce-Curtain* type. The antenna was mounted on a horizontally rotatable base structure. A synchronous motor was used to turn the structure once every 20 minutes. The antenna output was connected to a sensitive receiver and the receiver output was observed using a pen-on-paper (chart) recorder. The receiver had a long response time. This first ever successful radio telescope operated at a wave-length of 14.6 metres (at 20.5 *MHz*).

Jansky's experiment gave him a very good estimate of the background sky radiation and how it sets a limit on the smallest detectable signal strength. He quickly realised that it is not the receiver but the antenna sensitivity that has to be improved. He felt that it would require larger antennas with sharper beams, with capabilities to point easily in different directions to make progress in this field (*radio astronomy*). This led him to propose construction of a hundred-feet diameter parabolic-dish antenna for use at metre-wave-lengths. Although *Jansky* did not get the support, many others got influenced by his ideas and started building more sophisticated radio telescopes.

2.3 Modern Radio Telescopes

Today the modern radio telescopes built using the state-of-the-art technology, has capabilities to operate from decametre-wavelengths down to sub-millimetre wavelengths. Some of these telescopes facilitate angular resolutions as fine as 1-milli-arcsecond.

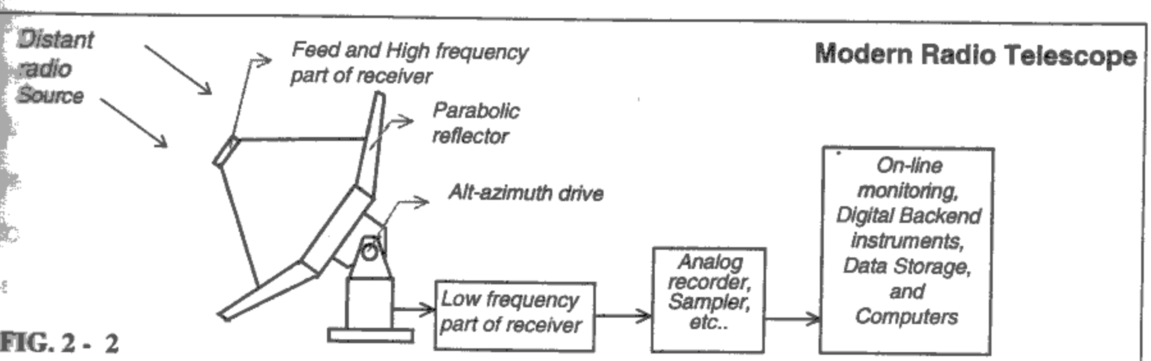

FIG. 2 - 2

The telescopes and the receivers vary quite widely. The picture shown here explains the principle parts of a radio telescope with a common example. A distant celestial source emits signals. The parabolic reflector is made to point towards the source. This is usually done by a computer based control system. The radiation incident on the reflector gets focused and is picked up by a feed located at the prime focus of the reflector. The high-frequency low-noise amplifiers are located right close to the feed. The pre-amplified signals are brought down to a suitable place, where they are further amplified, detected, integrated, and the outputs are recorded for further processing. Some times the data rate may be too high for direct recording. In such cases, real-time data processing using dedicated hardware is performed, and the output information at reduced rate is recorded for further processing.

2.4 Receiver Systems

The receiver system of a radio telescope is as much important as the telescope antenna itself. The Receiver must be sensitive enough to record the very small voltages that the aerial feeds into it without much distortion. Amplifiers are used to convert the small input voltages to a convenient level for further processing or recording. Moreover such an amplifier or any lossy element introduces additional 'noise' of its own into the receiver. This additional unwanted noise introduced has characteristics similar to that of the signals received from the astronomical sources. Most often the signals coming from the radio astronomical sources are several times weaker than the locally generated receiver noise. Distinguishing the celestial 'noise' from this unwanted noise is a fundamental task in a radio telescope receiver. Hence sensitive observations are possible only if all the operations in the receiver are optimised.

Generally radio astronomy observations fall into two main types. They are, the spectral line observations, and the continuum observations. There are receivers built specifically to facilitate these observations. In the case of spectral line observation the precise frequency of reception is critical. Generally spectral resolutions of tens of kilo-Hertz to few mega-Hertz will be required for such observations. In the case of continuum observations, the total amount of power emitted over a wide frequency band is of interest. In this case, the details in narrow frequency bands is not very critical.

The front end of a radio telescope receivers is basically similar in construction to that of a communication receiver. The most common type of receivers used in the radio telescopes are of the superhetrodyne type. Here the signals from the source are coupled to the receiver by an antenna. The source signal's frequency characteristics are shifted to an intermediate frequency band, which is then amplified and fed into a back-end system. There are different kinds of back-ends used for observations. For the spectral line observations, a spectrometer back-end is used. In the case of continuum observations the total power detection systems are used. The exact configurations and capabilities of these back-ends differ in detail based on the frequency resolution required, nature of the signals, required bandwidths and sensitivities.

2. 4. 1 Traditional Receivers in Radio Astronomy

Traditionally there are many different types of receivers being used for the general radio astronomy observations [24]. Some are listed below:

Total Power Receiver:

This receiver simply measures the total noise powers from the antenna and the receiver. Square-law detector is used to get the signal envelope. An integrator averages the fluctuating signal power for a specified length of time (τ). As the inverse of the pre-detection Bandwidth (B) determines the interval between the independent estimates of the average power, the product $B\tau$ gives the number of independent estimates averaged. Usually the averaging time used are in the order of few seconds. This value is a compromise between too short a period, for which the output noise is excessive and too long a period causing excessive smoothing and loss of information over short time scales. In this type of receiver, gain variations in the pre-amplifier stage; due to changes in operating temperature or power supply fluctuations can affect the sensitivity of the receiver.

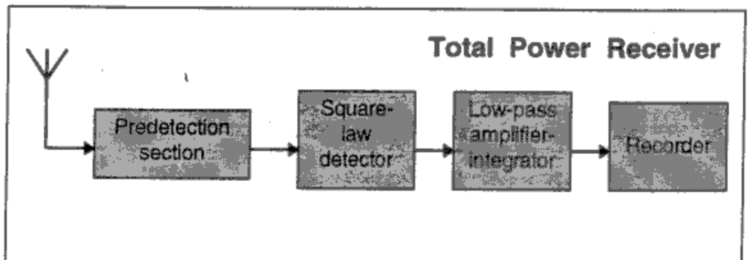

FIG. 2 - 3

Dicke Receiver:

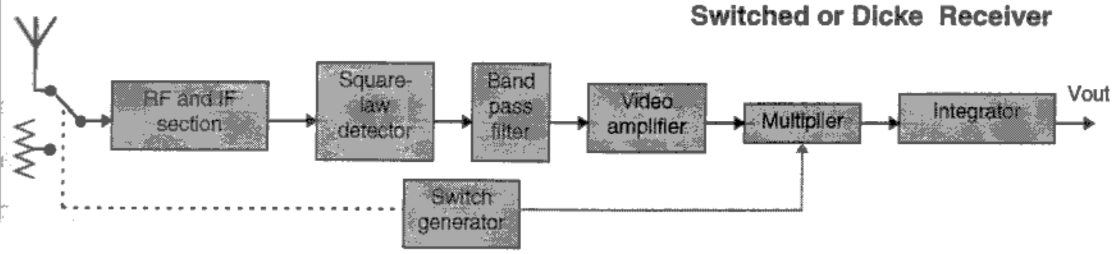

FIG. 2 - 4

In this type, the relatively slow gain variations do not affect the sensitivity of the receivers. Here the receiver's input is continuously switched between the antenna and a comparison noise source at a rate higher than the rate of possible significant gain changes. This allows continuous calibration of the gain of the receiver assuming that the comparison noise power at the input is constant.

Graham's Receiver:

In the case of a Dicke receiver the signal power is observed only half of the time. Such observation results in observing time inefficiencies and consequent reduction in the attainable sensitivity. The situation is improved in the Graham's receiver. Here there are two Dicke type receivers, while one receiver is connected to the source, the other one is connected to the noise reference source. The telescope input is switched between the two receivers. The outputs from both the receivers are averaged and recorded.

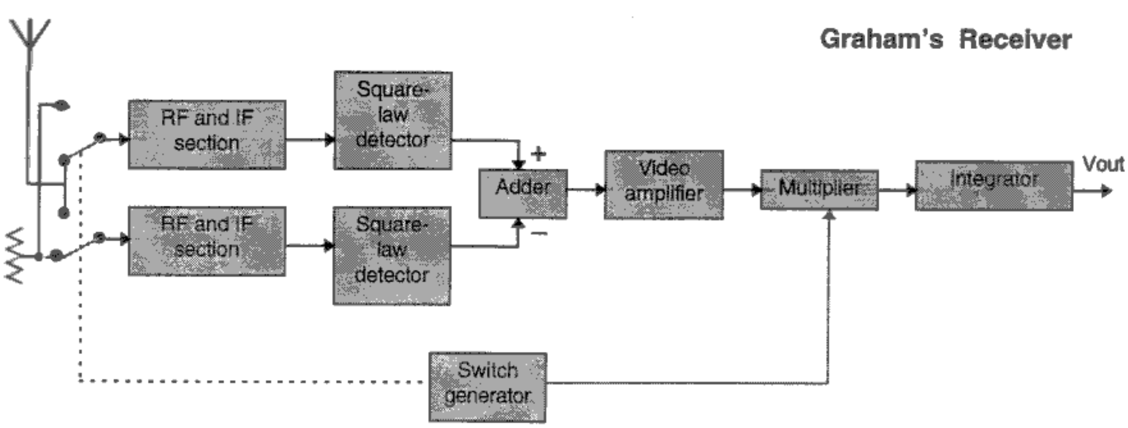

FIG. 2 - 5

Adding type Interferometer:

In this case the signals from a pair of (interferometry) antennas are added, detected, and averaged. In this case the maximum sensitivity is twice the sensitivity attainable with a single antenna. This type of receiver also suffers from gain variations and is less preferred.

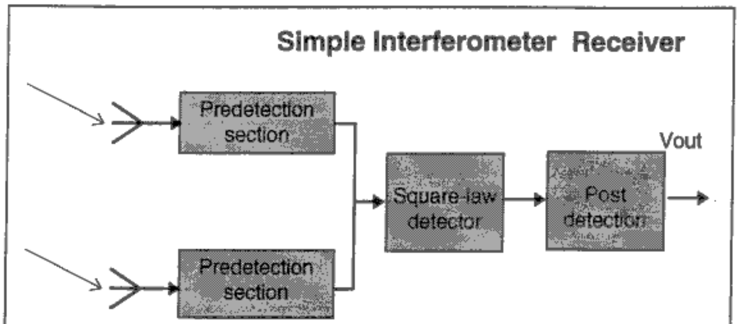

FIG. 2 - 6

Multiplying type Interferometer:

Here the IF voltages from a pair of interferometry antennas are multiplied (instead of being added), then detected, and averaged. In this case, the receiver gain variations affect the sensitivity to a lesser extent as the generally large DC due to the uncorrelated noises in the two front-ends is absent. However, any random phase variations in the receiver amplifiers can affect the sensitivity directly. Therefore, phase scintillations in the ionosphere can reduce the system sensitivity. In this type of receivers there is no switching involved between the antenna & the receiver and hence the losses are reduced. This results in reducing the receiver's noise temperature and hence has an advantage over the switching type of receivers. However such correlation type receiver has $\sqrt{2}$ times less sensitivity by nature compared to an adding type.

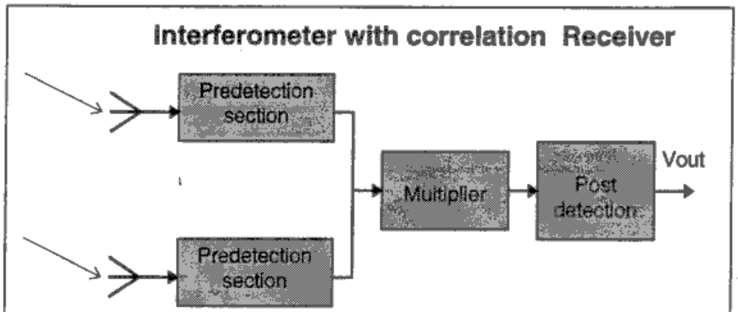

FIG. 2 - 7

There are many other improved versions of the receivers that are used in the modern radio astronomical observations.

2. 5 Single-Dish Radio Telescopes

Often inadequate in resolution at the long wavelengths.

Even the Moon, would look as a fuzzy blur object in the sky
in the 1000 ft Single dish telescope at the metre wave-lengths. " -SKY & TELESCOPE

Single-dish radio telescopes suffer from poor angular resolutions. The angular resolution or resolving power is the ability of the telescope to discriminate between closely spaced point sources and to map the finer features of the sky. The angular resolution is inversely proportional to the aperture size expressed in units of the wavelength of operation. Generally radio telescopes have much less resolving capabilities than the optical telescopes. In the case of radio telescopes their operating wave-lengths are hundreds of thousand times longer than the optical wave-length ranges. This difference dictates that a radio telescope operating in such long wave-lengths has to be that many times bigger to get the similar resolution. An optical telescope of moderate size can easily yield resolutions better than that of the 0.7 cm wide human eye. But for a radio telescope operating, for example at the 21 cm wave-lengths, it is a very big task. The telescope will have to be kilometres wide to get the same resolution. Constructing such big telescopes is also not so easy. The biggest single-dish radio-telescope is about 300 metres in diameter (*Arecibo*).

2. 6 Interferometer Telescopes

Early this century, radio scientists have made use of the interferometry principle for selective beaming or receiving of radio communication signals. This background knowledge was right in time for the radio astronomers to sophisticate their observations. Radio interferometers nearly surpassed the capabilities of even the biggest optical telescopes in terms of their sensitivity and resolving powers.

A radio interferometer in its simplest form consists of two antennas spaced many wave-lengths apart. The signals from the two antennas are, after equalising the delays in the signal path, combined using a sensitive radio receiver. The interferometer has sensitivity that depends on the collecting areas of the elements while the angular response consists of finely spaced fringes, where the fringe lobe separation depends on the distance between the two antennas. This telescope's direction of maximum

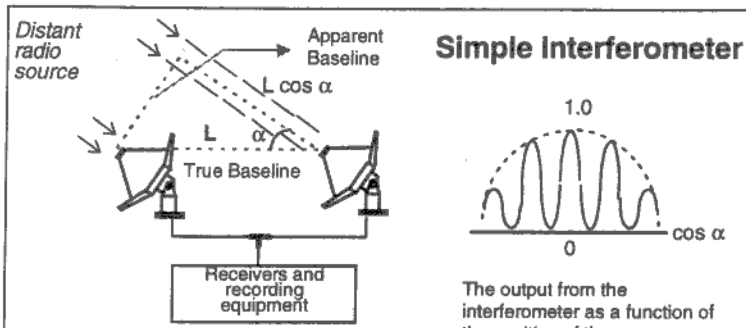

Two antennas separated by L wavelengths, connected as a radio interferometer and receiving plane waves from direction α

The baseline is effectively the diameter of an equivalent single-dish antenna that would have to be built to obtain the same resolving power

The output from the interferometer as a function of the position of the source.

FIG. 2 - 8

sensitivity can easily be steered by introducing time delay in the signal path of one of the antenna with respect to the other. The incoming electromagnetic signal from sources at sufficient distance is a plane wave. If the two antennas are separated by a distance L, the signals reach the antennas in general at different times. The two antennas receive the signal voltages with the corresponding delay. At a given observing frequency the outputs from the two antennas, when combined will interfere either constructively or destructively depending upon the phase shift corresponding to the relative delay. If the paths differ by an even number of wave-lengths, the waves arrive in step or in phase and combine constructively to yield a peak output. In the case when the phases differ by an odd number of half wave-length, the waves are out of phase, and they combine destructively, yielding no contribution in the output. As the celestial source crosses the antenna beam(s) of an interferometer this relative path gets altered and the signals arrive in and out of phase repeatedly with smooth transitions in-between. If this interferometry array is receiving dominant signals from one discrete radio source, a simple oscillating output will result. This is also known as the fringe pattern.

Using the normalised amplitude of such a fringe pattern one can estimate the angular size of the radio source, and the phase of the fringe consists information about the source direction in the sky. The accuracy in the estimation of the source position depends, apart from the signal to noise ratio of the fringe, on the distance between the interferometer array antennas, and to a lesser extend on dimensions of the individual antennas. In the case when two or more sources of similar intensities are present simultaneously in the beam, then the resulting interferometer fringe output will not appear very different from the response for a single point source unless observed over large hour-angle range or/and the source separations are large.

2.7 Aperture Synthesis Telescopes

The design of radio telescope arrays to map the radio sky exemplifies general physical and mathematical principles. One of the most spectacular findings by *Fourier* is the foundation for many advanced signal processing techniques today. *Fourier* had demonstrated that any complex, transient wave-form can be expressed as the sum of an infinite series of simple sinusoidal wave-forms characterised by frequency, amplitude, and phase. The distribution of radio brightness across the sky can be treated mathematically in a similar manner, as a sum of an infinite series of simple wave-forms of varying spatial-frequencies. The broader feature of the radio sky can be analysed in terms of components of relatively low spatial-frequencies and the very fine narrow features (especially of discrete sources of very small diameter or complex structures) can be reconstructed by incorporating also the information on the high spatial-frequency components. A single dish or a filled aperture telescope samples the lower spatial frequency with increasing redundancy. Such redundancy, although ensures high surface-brightness sensitivity, is not necessary for the sampling of the possible spatial frequency range. It is, therefore, enough to measure the complex contribution over the desired spatial frequency span using minimum redundancy possibly with a suitable unfilled aperture.

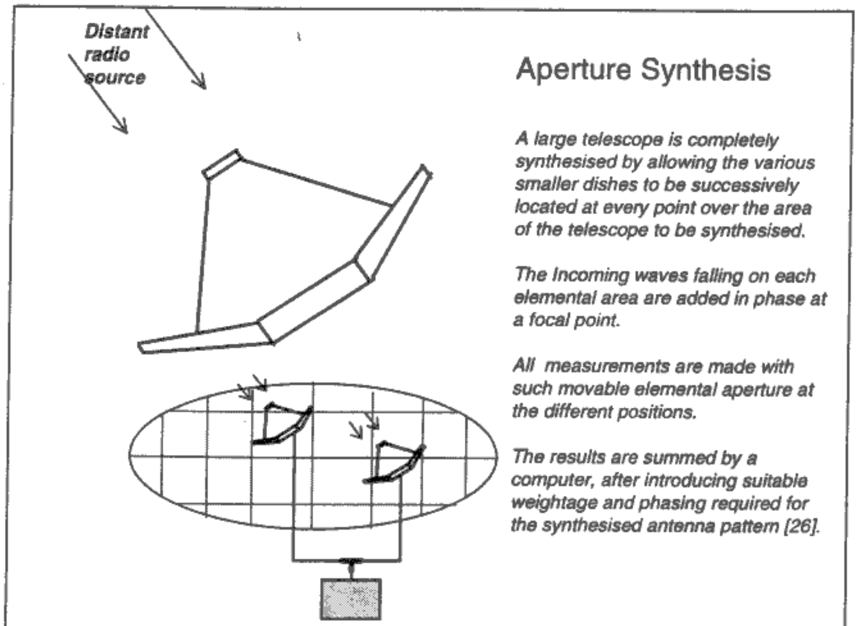

FIG. 2 - 9

In the case of sources that do not change significantly over long time scales, another technique is possible. An aperture equivalent to that of a large antenna can be synthesised by sampling a desired spatial frequency span with a variable spacing interferometer and measuring the source (complex) visibility at each of the chosen spacings using a suitable correlation receiver. Usually antennas are mounted in trolleys or on rail trucks to facilitate such movements. Many such interferometer pairs can be employed simultaneously to enable a quicker coverage. If 'N' array elements are used, it is easy to show that (N-1).N/2 independent interferometer pairs can be realised with suitable arrangements of the elements. In this case, if 'N' is large, adequate sampling in the spatial frequency domain may be obtainable even in a snap-shot mode to make meaningful images. Additional major increase in the spatial frequency coverage is gained if the observation extends over a large hour angle range as each of the interferometer pairs samples systematically changing spacing and orientation as seen by the source with changing hour-angle. Such aperture synthesis is known as the Earth rotation synthesis.

Aperture Synthtesis

Use of the rotation of the Earth

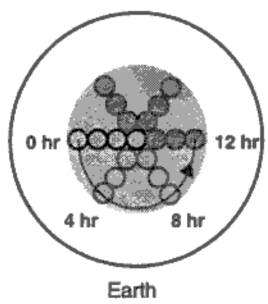

Suppose we observe a north polar region using a line of telescopes located at the north pole, continuously for one twelve-hour period, the rotation of the Earth causes this line to sweep out a half a circle. The data collected over the twelve-hours can be processed using a computer to mimic the angular resolution of a single dish with the aperture equal to the full circle (shaded area)[25].

FIG. 2 - 10

2.8 Some Big Radio Telescopes in the World

***ARECIBO* Telescope**

The world's largest single dish radio telescope is about 300 metres diameter built into a valley in *Arecibo, puerto Rico.* This is a fixed spherical reflector telescope. The spherical surface allows the beam to be steered over a large range of angles by moving a specially designed feed in the focal plane. This telescope is capable of detecting very weak signals with good resolution. This factor makes this telescope one of the most important and powerful radio telescope in the world:

Ooty Radio Telescope

The world's largest single steerable radio telescope is located in *Ootacamund, India.* It has a reflector, which is a single parabolic cylinder. This telescope is 530m by 30m in size. This telescope is built along a hill slope parallel to the Earth's rotation axis and thus has an equatorial mount. While the hour angle tracking involves simple mechanical rotation of the reflector in the East-West direction, the steering of the beam in the North-South direction is realised using electronic phasing of the feed array along the length of the array.

Today the world's most powerful radio telescopes are the interferometer types. Some of them are listed below.

5 Km CAMBRIDGE Radio Telescope

The 5 *km* telescope at *Cambridge* consists of 13 metre diameter dishes. Four of which can be moved to different positions along a 1.2 *Km* long rail track.

Very Large Array

Another interferometer facility is in the deserts of New Mexico, where 27 radio telescopes of 25 metres diameter are connected together to simulate a bigger telescope of about 40 Km in diameter achieving a resolution of about 0.1 arc seconds. The radio telescopes are arranged in a Y-shaped array. This telescope can map regions of the sky with angular resolutions of sub arc seconds. New techniques are employed to obtain superior images from this telescope [7, 8].

MERLIN

MERLIN the *Multi-Element Radio Linked Interferometer Network* in *Great Britain* has baselines up to 127 *Km.* This telescope has relatively smaller no. of antennas than the *VLA* telescope, but has better angular resolution compared to VLA in some frequency bands.

Most of the extra-galactic radio sources are of fraction of an arc second in diameter. To observe and study such sources, radio astronomers have coordinated observations using radio telescopes in Europe, the United States, Canada, and Australia into a planet-wide radio interferometer network, when the information from various baselines is combined the angular resolution is equivalent to that of a radio telescope of nearly 8000 miles (Earth's diameter) in diameter. This technique is called the ***VLBI*** (Very *Long Baseline Interferometry*).

Currently there are two principal VLBI arrays in the world. The Very Long Base Line (VLBA) Array of *USA* consists of ten identical radio telescopes, from Peurto Rico to Hawaii. This will span nearly quarter of the Earth's circumference. *This interferometer will have the resolving power capable of reading a news paper 960 kilo-metres away, That is nearly 1000 times better than any ground-based optical telescope.* The *European VLB Network* (**EVN**) consists of a co-operative arrangement of radio telescopes in the *UK, Netherlands, Germany, Italy, Poland, Russia, Ukraine, China and Japan*. The *EVN* and the *VLBA* cooperate to form a world-wide net. The *Australia Telescope* (*AT*) also cooperates with the other *VLBI* arrays of the world [9].

With such wide distribution of the *VLBI* array elements, the separate telescopes cannot be easily connected directly, and hence the data are simultaneously recorded along with the timing information at each independent stations and are subsequently collected together and correlated.

The *radep* interferometer telescope proposed by a group of Soviet Scientists could measure the distance of objects out to the full radius of the universe (*15 billion light-years*). Three units would be deployed in space, two near the orbit of Saturn and one near the Earth [9].

Australia Telescope (AT)

Another set-up in *Australia* is a continent spanning radio array similar to the *VLBA* of *USA*. This consists of a 6 *Km* long compact array containing rail mounted 22 metre diameter 6 antennas, and a long baseline array including many other telescopes in the continent [10].

Giant Metre-wave Radio Telescope (GMRT)

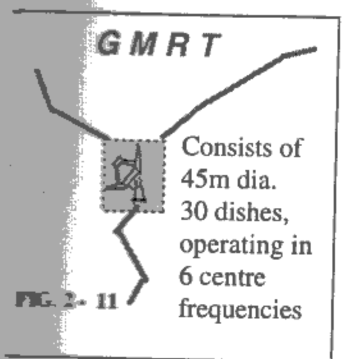

FIG. 2- 11

When completed, the *GMRT*, being constructed near Pune, India, would become the World's largest meter-wavelength Earth's rotation synthesis radio interferometry telescope. This radio telescope consists of 30 radio telescopes, each being 45 meter diameter, arranged in a Y-shape array [4,7, 11]. Some important details about this radio telescope are presented in the next chapter.

Chapter 3 *The Giant Metre-wave Radio Telescope*

Chapter 3

The Giant Metrewave Radio Telescope

GMRT, the *Giant Metrewave Radio Telescope* coming up in India is a front-line research facility for astronomy and astrophysics. *GMRT* will be a very powerful tool in investigations of phenomena ranging from stellar systems to universe as a whole.

3.1 Where it is located

Locating a suitable place for such a big telescope is an important task. The radio signals coming from the astronomical sources are thousands and millions times weaker (typically in the order of 10^{-26} *Watts per sq. meter* per unit bandwidth) than from the terrestrial radio and *TV* transmissions. Radio Telescopes employ extremely sensitive equipment designed to detect the weak celestial signals with remarkable accuracy. Man made radio interference is every where. This problem is rapidly becoming very critical because of the fact that transmitters are becoming numerous and more powerful while the radio telescopes are becoming more sensitive. Although the International frequency allocation measures give some protection for the radio observatories, any radio interference from a poorly designed or faulty equipment such as transmitters, Earth satellites, automobile ignition

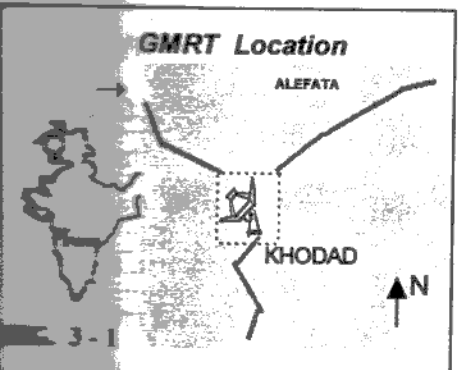

Fig. 3-1

systems and so on can easily drown the weak astronomical signals. Hence it has now become almost necessary to locate the radio telescopes as far from the industrialised area as possible in order to *listen* to the signals from the sky. Additional important considerations relate to the accessible area of sky from a given location in the Earth and the properties of ionosphere that depend on the geomagnetic latitude of the place.

After a careful study of the Indian terrain with all these considerations, *GMRT* is located in a suitable site, near the village *Khodad*, about 80 Km north of *Pune* and 150 *Km* east of *Mumbai*. Low-lying hills and the western ghats protect the telescope site from the industrialised cities. This place is about 1000 metres above the mean sea level and 10 degree away from the Earth's magnetic equator. The wide southern sky coverage that is possible from this location makes *GMRT* very useful for the astronomical observations.

3.2 A brief introduction to GMRT

World's Biggest Metre Wavelength Synthesis Radio Telescope

GMRT consists of 30 fully steerable 45-metre-diameter parabolic dishes that use a novel design. Twelve of these dishes are placed in a compact central array within 1 sq. Km. area. The remaining 18 dishes are placed along the three arms of a Y-shape configuration with each arm extending to about 14 *Kms* from the array centre.

The *GMRT* is designed to operate in six separate frequency bands between 50 and 1420 *MHz*, centred at

50, 150, 233, 327, 611, and 1420 *MHz*.

All these are internationally allocated special radio astronomy bands.

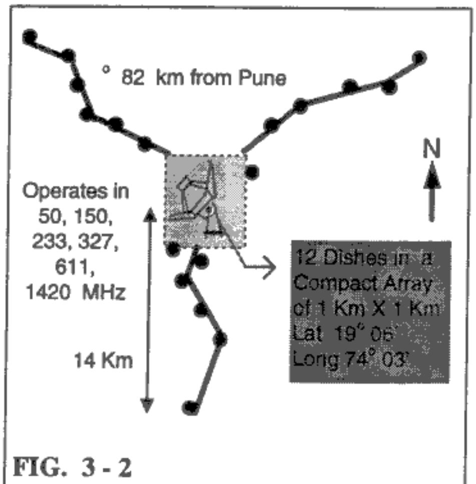

FIG. 3 - 2

The reflecting surface of the *GMRT* dish consists of a wire mesh made of a 0.55 mm stainless steel wire. The mesh is required to be finer than about twentieth of the shortest wavelength of operation to prevent transmission through the mesh. The wind loading is also reduced in such non-solid structures. The cost of fabrication also comes down. A novel SMART concept (*Stretched Mesh Attached to Rope Trusses*) is employed to achieve the curved surfaces of the dish. Many innovative techniques are employed in the design of the *GMRT* dishes. Each of these dishes weighs about 90 tonnes, and the counter weight is additional 40 tonnes. Seventeen-bit encoders are used to obtain a positioning accuracy of about 1 arc minute. The *GMRT* dishes are designed to operate up to a wind speed of about 40 *Kmph* and are capable of withstanding the wind velocities of 133 *Kmph*.

Multi-frequency and dual-polarisation operation are possible with the *GMRT* dishes. The feeds and the low noise *RF* amplifiers are placed on a rotatable turret at the prime focus of the antenna. A dual-band capability is provided by placing 233 *MHz* and 611 *MHz* feeds in the same face of the turret. Similar provision is available for the 50 and 1420 *MHz* bands. The desired feed will be rotated to lie at the focus by computer control. Optical fibre links are used to distribute the coherent local oscillator signals to the receivers at each of the antennas and then to bring the *IF* signals to the central laboratory.

GMRT with all the 30 antennas will give a collecting area of about 30,000 sq. metres. This is comparable to the effective area of the *Arecibo* 1000 *ft* radio telescope and three times that of the *Very Large Array* (*VLA*) in *USA*. *GMRT* primarily operates as the *Earth-rotation Synthesis Radio Telescope*.

GMRT

Frequency (MHz)	Primary beam (Degree)	Synthesised beam (Arcsec)
50	9.0	60
150	3.0	20
233	2.0	13
327	1.4	9
611	0.7	5
1420	0.3	2

FIG. 3 - 3 Ref. [11]

When completed, *GMRT* would become the World's largest meter-wavelength Earth's rotation synthesis radio interferometry telescope. The thirty 45m diameter dishes are arranged in an array forming Y-shape. Each arm of this array is about 14 *Km* long with baselines extending up to 25 Kms. The 30 antennas form 435 (30 x 29/2) interferometer pairs. *GMRT* antennas are carefully positioned in the array to get the desired sampling of spatial frequencies. The spacing between the nearest antenna is about 100 metres and the farthest is about 25 *Km* long. But a celestial object being observed sees these 435 combinations of these physical distances as a continuously varying projected baselines with changing orientations, while the source moves from the East to the West. This effect provides finer coverage in the spatial frequency domain even with physically fixed pairs. The *electronics* and the *computation* involved in processing this interferometry pair outputs become highly sophisticated and numerously complex. For most applications the outputs from each pair of the antennas are integrated and recorded every 10 seconds. Each interferometer measures one *Fourier* component of the brightness distribution of the radio sky. In the GMRT set-up, there would be about 2 million *Fourier* components to be measured and processed in about 12 observing hours. Highly sophisticated Instrumentation with very powerful computing back-ends is used for this purpose.

3. 3 GMRT - Scientific Goals

GMRT is being constructed in *India* with many outstanding scientific objectives in mind. Many radio telescopes in the world could not attempt certain important problems in the meter wavelength radio astronomy. It is becoming increasingly difficult to work at meter wavelengths in most parts of the world, because of increased radio interference at these wavelengths. Currently a meter wavelength telescope site in India is a best option. We have much less radio interference as compared to most other countries. Another difficulty is related to the relatively higher cost involved in the construction of the large antennas that are required at these wavelengths. In addition, the adverse effects due to the ionosphere disturbances increase at these wavelengths. However all these problems are tackled in the *GMRT* design by adopting or developing suitable techniques.

The high sensitivity and good angular resolutions of the *GMRT* telescope will aid in investigating a range of interesting astrophysical phenomena. The geographical location of the telescope will help in looking at also the relatively unexplored regions of the sky.

Solar system can be well explored with *GMRT*. Exciting new results are expected in the studies of ionosphere and magnetospheres of our Earth. These studies can be carried out by looking at the refraction and scintillation of radio waves coming from distant radio sources. High resolution maps of the solar active regions of the sun may yield many interesting results and reveal completely new features.

The neutral Hydrogen line emission and shift in their observed frequency due to their motion can be well mapped with *GMRT*. It will be possible to understand the complex plasma processes that make some radio stars to emit intense radiation hundreds of time stronger than those from the sun.

Pulsar study is another important area of research planned with the *GMRT*. Many intriguing problems in this field are yet to see a convincing answer. Pulsars, the most stable clocks known, found in a binary system with an eccentric orbit will be the best laboratory for testing the gravitational theories. It is possible to do the accurate timing studies of these pulsars with *GMRT*. Also it is possible to detect many new pulsars with *GMRT* due to its good sensitivity and sky coverage. Pulsar studies with *GMRT* in the phased array mode can help in carrying out high sensitivity studies of the known pulsars and probe many important properties of the interstellar medium as a whole.

These are only few examples of the wide ranging scientific programs planned for the Giant Metrewavelength Radio Telescope. For this work a powerful back-end instrumentation will have to support the telescope hand-in-hand. There is a brief presentation about the *instrumentation* used for the *Giant Metrewavelength Radio Telescope* in the next section [4, 11].

3.4 GMRT Receiver System#

Feed

GMRT telescopes have independent feeds at each of the six frequency bands, where each feed caters to the two (linear) orthogonal polarisation states. Thus at a given frequency band two outputs corresponding to two polarisations is available. This 2 outputs are fed to the Quadrature Hybrids.

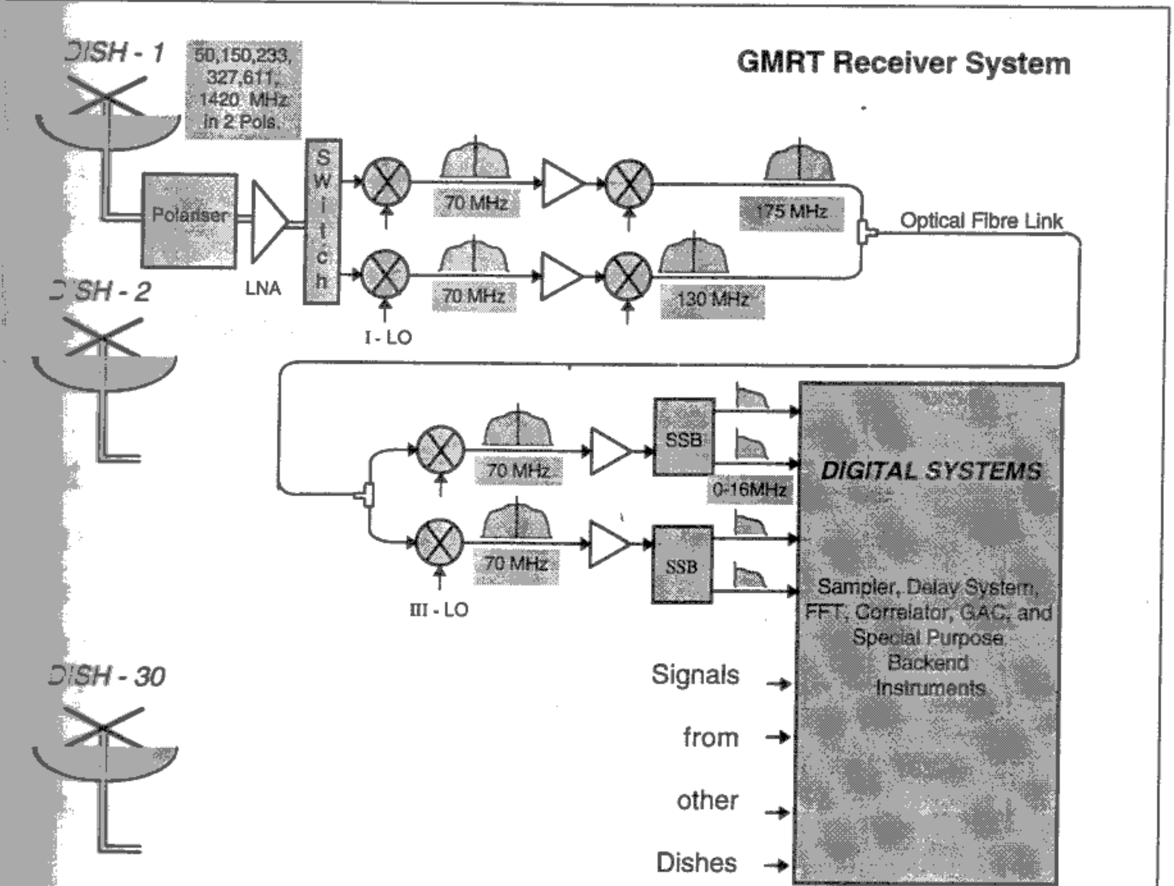

FIG. 3 - 4

Quadrature Hybrid (Polariser):

In this stage, the two linearly polarised inputs are converted into Right circularly polarised and Left circularly polarised signals. The outputs from this stage is given to the low noise amplifiers.

[12, 13, 14, 15, 16, 17]

Low Noise Amplifiers:

The output signals from the Polariser are first amplified using the low noise amplifiers (LNA). Usually noise performance of this stage determines to a large extent the Receiver's Noise Temperature. Outputs from the LNAs pass through a Switching stage.

Up to this stage the electronics are separate for each of the six separate operating bands.

Switch:

The switch selects one of the six operating bands and passes the signal down to the next stages. The next stage is the First Mixing stage.

After this stage the electronics are common to all the operating bands.

First Mixer stage:

First Local Oscillator is a synthesiser that generates frequencies from 100 MHz to 1700 MHz with a step size of 5 MHz. This synthesiser is phase-locked with a 'global' 200 MHz reference signal. This reference is generated at the central electronics laboratory and send to all the 30 antennas through the Optical Fibre cables. A Mixer down converts the selected operating band to an Intermediate Frequency band centred at 70 MHz with an appropriate of choice of LO frequency.

The IF outputs from this stage are fed to a Second Mixer stage after buffering.

Second Mixer stage:

The IF bands corresponding to the two circular polarisations enter this stage. These bands are centred at 70 MHz frequency and it is required to transmit both the bands to the Central electronics lab in the same optical cable. Hence they are translated to 175 MHz and 130 MHz bands. The Local Oscillator frequencies used are 105 MHz and 200 MHz respectively. This Local oscillator is also phase-locked to the central reference signal. The signals now enter the Optical Fibre system.

Optical Fibre System:

Optical fibre cables are used to carry all the signals between the antenna base and the central electronics room. They carry the local-oscillator-reference signal, control, and monitor signals from the central electronics lab to the antennas and bring the IF signals, control and status monitor signals from the antennas to the central electronics lab. Each of the 30 antennas get an independent fiber cable connection from the central ac. Fibre cables aid in reducing the signal degradation. Laser diode is used as optical transmitter and avalanche photo diode is used as optical receiver in the optical fibre link. Once the fibre cables coming from the antennas reach the central lab, the signals enter the Third Mixer stage.

Third Mixer stage:

This stage converts the signal bands centred at 175 MHz and 130 MHz, back to signal bands both centred at 70 MHz. IF processing is also done before these bands are converted to the Base Band signals. Signals now enter the Single Side-band (SSB). Receiver

SSB Receiver stage:

The Local Oscillator is from a frequency synthesiser that generates frequencies from 50 to 90 MHz with a step size of 100 Hz. It translates the two side-bands around 70 MHz (70 MHz $\pm$16 MHz) into two channels, each having 0 to 16 MHz band. The signals are passed through Automatic Level Controller (ALC) circuit and are then sent to the digital back-end systems.

Digital Back-end systems:

The base-band analog signals with 16 MHz band width are digitised. The sampling is done at 32 MHz rate. The digitised data is 4 bits wide. Then the data are send to the Delay correction system.

Delay Correction System:

Delay correction system stores the digitised numbers in a memory. A computer controlled readout system is used to appropriately delay the data before it is send to the next stage. The delay stage is required to correct the signal propagation delays between signals received from the antennas. The delays depend on the source direction, and the location of the antennas with respect to the central lab. The delay correction steps possible here are in integral multiples of the sampling interval. Fractional part of the delay can be corrected for in the next (Fast-Fourier-Transform) stage [18, 19].

Fast-Fourier-Transform System:

This stage is equivalent of a 256 Channel Filter Bank. It uses sets of successive 512 time samples and for each set performs a Fast-Fourier-Transform to produce a time multiplexed sequence of 256 spectral voltages. Fractional sampling period delay corrections are performed at this stage, by applying a suitable phase gradient correction to the complex spectra.

The signals from this stage go to the digital Correlator. Spectral outputs are also tapped at this stage (FFT outputs) by the GMRT Array Combiner to produce the single beam outputs [20].

Correlator System:

Here, the signals from all the 30 antennas and up to 256 channels over a 32 MHz bandwidth are cross correlated and integrated giving 2,38,080 product terms. Then the products are averaged and recorded in the computers. This correlator data will be used for obtaining high resolution images of the radio sky [20, 21, 4].

The GMRT Array Combiner System:

Signals from all the 30 antennas and up to 256 spectral channel signals from two bands of 16 MHz each are combined at the full speed to produce two simultaneous single beam outputs. One is the Incoherent Array output and the other is the Phased Array output. The pass-band ripples and other gain variations are corrected in this stage before the signals are combined [5, 6, 22].

The development details about this instrumentation are presented in the thesis (Next chapter).

Instruments that will use outputs from the *GMRT Array Combiner:*

The outputs from the *GMRT Array Combiner* will be send to the following systems for further processing and recording.

1 The Pulsar Search pre-processor:

This system can take in either the incoherent array outputs or the phased array outputs. This on-line hardware is a part of the scheme mainly aimed at detecting new Pulsars using the GMRT Telescopes [22].

2. The Pulsar Polarimeter system:

This system takes the phased array output from the GMRT Array Combiner and processes it in a variety of ways. The Pulsar Polarimeter will enable high time resolution and high sensitivity studies of known pulsars with full polarisation information.

3. The Coherent Dedispersion System:

This system also takes in the phased array output, and processes it. The Coherent Dedispersion System is mainly meant for doing very high time-resolution studies of the Pulsar radiation using the GMRT telescopes [23].

4. Very Large Base Line Interferometry (VLBI):

For this purpose the single beam outputs from the *GMRT Array Combiner* is directly recorded using the very high speed Data Acquisition Systems (DAS). The collected data will be correlated with data collected simultaneously from the other VLBI telescopes in the world.

Apart from this, any future instrument that requires a single beam output from the GMRT telescopes can be connected to this system. Details about the *GMRT Array Combiner system* development and the design details are described in the next Chapter.

Chapter 4 *The Array Combiner*

Instrumentation Development for Incorporating Single-Beam Modes in GMRT

Chapter 4

The Array Combiner

Instrumentation Development for Incorporating Single-Beam Modes in GMRT

4.1 Introduction

This instrumentation work is aimed at developing a hardware to facilitate the single beam mode observations for the Giant Metrewave Radio Telescope (GMRT). Some of the astronomical observations planned with GMRT can be efficiently carried out only if the single beam modes are available. Two of the possible single beam modes are considered here. One of which is the Incoherent Array (IA) mode output and the other one is the Phased Array (PA) mode output.

The PA output is formed by coherently combining the voltage signals from the array

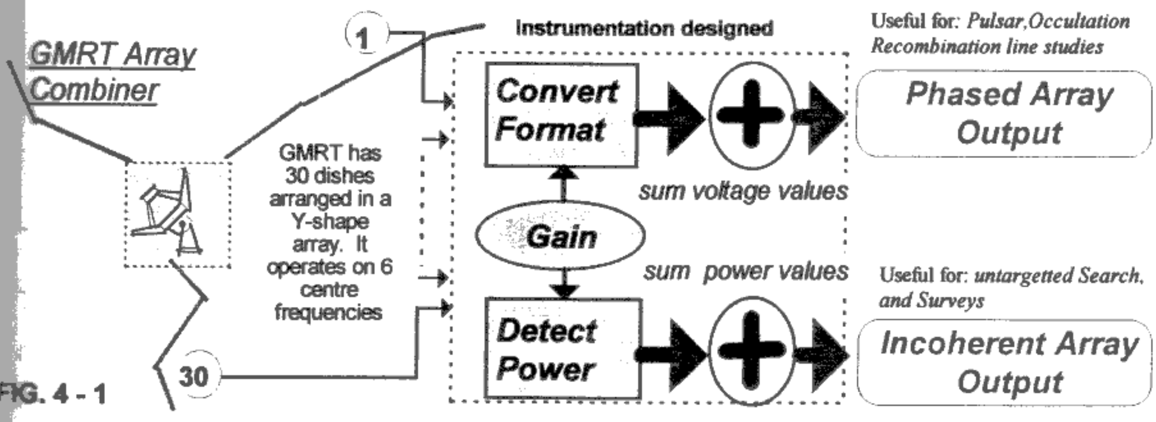

FIG. 4 - 1

elements. This is useful for observations of small sky area that require a very high sensitivity. The *incoherent array output* is formed by combining the detected power outputs from the array elements. This combined output yields a broader sky coverage at the expense of reduced sensitivity. However it is very useful for the survey kind of observations. Both are required simultaneously to facilitate more than one kind of observations at the same time.

The observations that will use the PA and IA single beam mode outputs are:

Pulsar search and general study observations
Pulsar polarimetry study observations
Pulsar profile microstructure study observations
Recombination line observations
Occultation study observations
VLBI observations, etc.

Few of these observations use only the PA outputs and the others use both outputs.

Each GMRT dish provides outputs corresponding to the two orthogonal polarisations. After the front-end RF processing at the antenna base, the signal is brought to the remotely located receiver room. Optical fibre cables are used for the IF signal transmission. They connect the signals at antenna base to the receiver room typically a few kilometres away. In the receiver room a single side band (SSB) receiver splits the incoming 32 MHz IF band into two side bands of 16 MHz each. There will be 120 such 16 MHz bands available from the GMRT array corresponding to 30 antennas, 2 polarisations and 2 side bands.

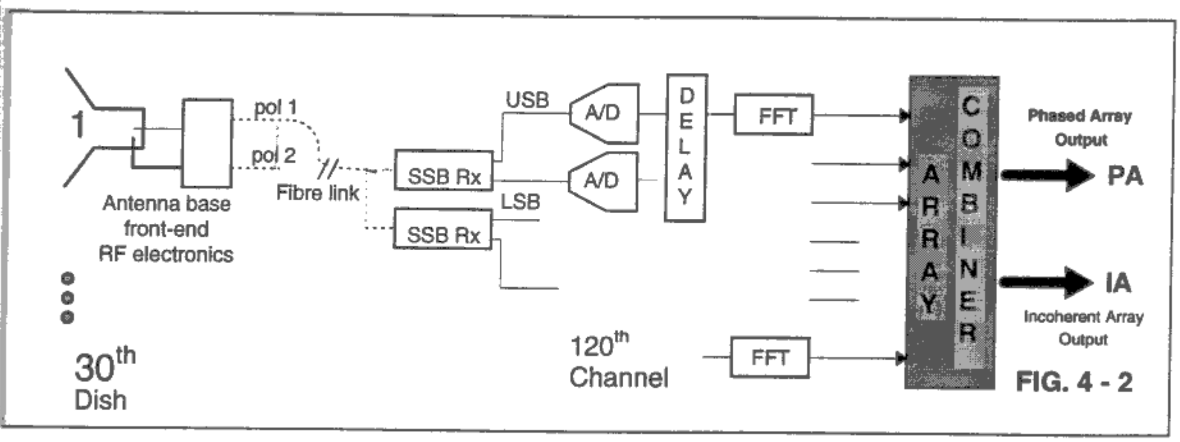

FIG. 4 - 2

The 16 MHz bands are digitised and the signal propagation delays between antennas are electronically corrected (The nearest antenna is few hundred meters away, and the farthest is about 14 kilometres away). A series of Fast Fourier Transform (*FFT*) modules produce complex spectra of 256 frequency channels for each of the 120 signals. The FFT output spectral channels are time multiplexed and are available sequentially. Each spectral channel outputs corresponding to one of the polarisation is time multiplexed with that from the other polarisation. Therefore the apparent output rate is doubled to 32 MHz. The multiplexing operation reduces the cabling complexity by a factor of two.

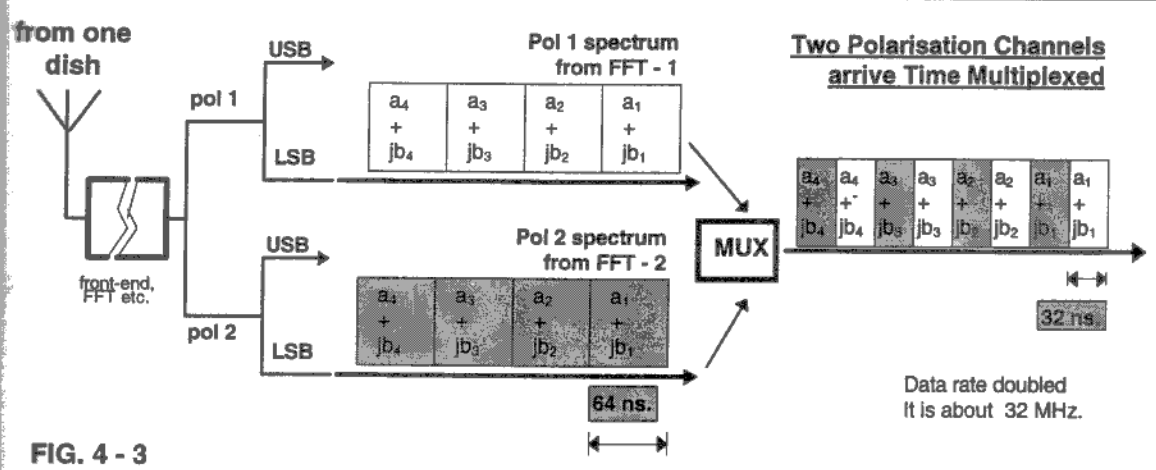

FIG. 4 - 3

Now the output data change at the 32 MHz rate on 60 channels carrying 120 complex spectra. Each of these spectra consists of 256 spectral channel voltages represented using the complex numbers of the following format.

$$a.2^{-c} + j.b.2^{-c}$$

Here, 'a' and 'b' are 4-bit wide numbers in a sign-magnitude format. The common exponent, to the base 2, is given in 'c'. This is a 4-bit implied negative number. In total 'a', 'b', and 'c' together are a 12-bit wide data represented in a 4,4,4 format.

This 12-bit data can be tapped at this stage and suitably combined to produce the two single beam modes.

The *IA outputs* can be formed by adding all the modulus squares (power terms) of the complex numbers as shown here.

$$IA = \sum_{i=1}^{30} (a_i^2 + b_i^2)\, 2^{-2c_i}$$

FIG. 4 - 4

The *PA outputs* can be formed by adding all the complex numbers (voltage terms) as shown here.

$$PA = \sum_{i=1}^{30} a_i .\, 2^{-c_i} + j\sum_{i=1}^{30} b_i .\, 2^{-c_i}$$

FIG. 4 - 5

4. 2 Design Considerations

The design considerations mainly arise from the observational requirements and the nature of signals.

1. Whenever a source is being observed in the PA mode, it will be possible to do either a survey or an un-targeted search around the same area using the IA mode outputs. Hence if the two beam modes are available simultaneously, the telescope time can be used in an efficient way during such concurrent-observations.

2. It is possible that not all the dishes will be used for observation at a given time. Some times one or more dish may not be operational due to maintenance or repair related works. It is also possible that not all the dishes may be required for a given type of observation. The outer array may not be included for some observations, when there is increased ionospheric scintillation. In such cases, for example the Phased Array mode observations may use only the central array dishes. Given such possibilities it is required to have a provision to control the inclusion of the of the dish signals while producing the single beam outputs.

3. It is also required to equalise the amplitude gains of different dishes, before combining their signals, to ensure optimum output.

4. Variations in the input power across the band can cause the combiner to operate either in saturated (too-small steps) scale or in coarse (too big) steps for the channels with widely different input powers. Such quantisation errors invariably lead to signal to noise degradation. Hence it is required to equalise the gain difference across the pass band.

5. The signals from the upper side band and the lower side band arrive separately and are available in parallel. Hence, they can be processed independently.

6. The two polarisation channels arrive time multiplexed. The combined signal output corresponding to these polarisation channels are to be produced separately.

7. It should be possible to facilitate dual frequency observations, by producing the sub array group outputs.

8. It should be possible to control the final output data format and width.

9. A diagnostic aids should be incorporated, to enable testing of the combiner or any other hardware that would use the single-beam outputs.

10. A computer-based flexible control and configuration facility is to be incorporated.

The facilities that are required can be summarised as

- *Simultaneous IA and PA outputs*
- *Masking and weightage facility for every dish inputs*
- *Masking and weightage facility for all the frequency channels*
- *Separate outputs for the side-boards*
- *Separate outputs for the polarisation channels*
- *Sub-group combiner facility*
- *Output format control*
- *Diagnostic facility*
- *Computer based control*

The above considerations would imply a complex system with a relatively simple modular design. But the major engineering challenge arise from the data rate and the number of inputs to the system. This design challenge can be visualised from the fact that there are 1.92 X 10^9 complex data to be handled every second. These signals arrive through 1440 input connections (12x2x60). To produce the two single beam mode outputs there will be about 17.28 X 10^9 multiplications and 8.488 X 10^9 additions to be performed every second.

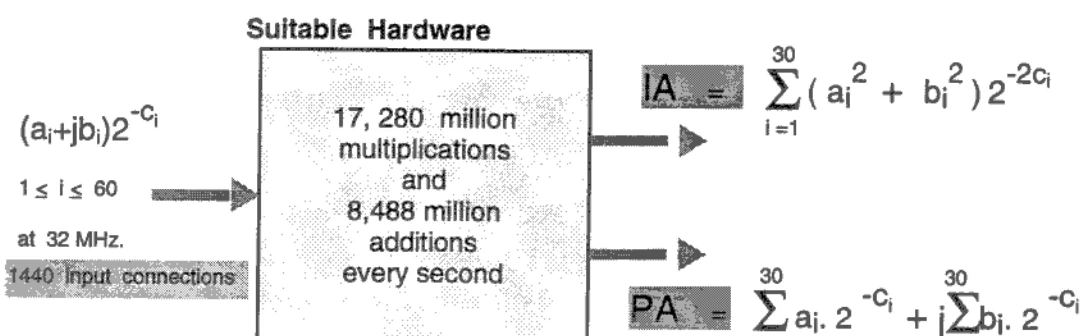

FIG. 4 - 6

These capabilities are not provided by any commercial hardware available readily.

4.3 Design Development

The potential options to realise the above in electronic circuitry can be broadly classified as based on

- *Processor based hardware*
- *Discrete ICs*
- *Erasable Programmable Logic Devices (EPLDs)*
- *Memory based lookup tables*

There is a remarkable growth in the capabilities of all these technologies in the past few years. An analysis of these options and the conclusions we arrived at are presented below.

Usually a Processor based design offers very good flexibility and can solve many complex design requirements. If the design requirements are carefully implemented then, most of the future requirements also can be accommodated by suitable software changes. Although more powerful and fast processors are available today, further analysis revealed that, to meet the desired processing capabilities, many processors will have to be used in a processing network. The design complexities and the connectivity that may be required, in such a case, will be too complex and very expensive.

Discrete ICs are the conventional choice for most of the designs. High speed discrete ICs are easily available at relatively less cost. For implementing big designs, large number of ICs will be required, resulting in a complex design with large amount of connectivity and big-size circuit boards. Some times the cost that may be saved in the ICs will have to be used up in making the circuit layout and in manufacturing such big circuit boards. However, the availability of the miniature surface mount devices (SMDs) makes the compact designs possible. The short lead lengths of the SMDs are the useful features for the high speed design. For some specific sections in the design, use of such components will be inevitable. One inherent limitation with the discrete IC based design is that, it may not easily accommodate the future requirements.

The EPLDs are the state-of-the-art technology devices. They essentially work as programmable circuit chips. Computer-aided circuit development tools facilitate easy circuit design and verifications. The circuit operations can be simulated in the development system, and hence its operations can be verified before the chip is actually used in the circuit board. Future design changes can be easily incorporated, by erasing the old circuit (like erasing an EPROM or EEPROM), and by programming a new circuit. The other big advantage is that, it can easily incorporate many TTL equivalent circuits (typically 20 to 30 times for the EPM 5128 chip). Much higher capacity devices are also available in the market now. But the speed at which these devices can work purely depends on the circuit complexity and some times the resource utilisation factor. As the circuit complexity increases the maximum operating speed generally comes down. However, this limitation may be overcome if much higher speed versions of the EPLDs are available. A careful analysis is therefore required to find the suitability of EPLDs for this particular design. Other important factors to be considered are the power consumption and bus driving capabilities. EPLDs decipate a lot of power in a relatively smaller area, hence sufficient cooling is required. The EPLDs have relatively less signal driving capabilities and I/O pins (e.g. 5000 series) suffer from the *latch-up* problems, hence all the I/O signals have to be buffered for proper functioning of the EPLD. In 1993, the cost of these devices was still higher than that for the equivalent discrete chips. However, the EPLD prices were expected to come down in the future. When compared with the reduction in the board size, flexibilities in design efforts, future advantages, and the reprogrammability, the higher cost of the chip may not be such a big disadvantage.

A Memory device (like RAM, PROM, EPROM, etc.) based solutions suit to many specific type of problems. Usually complex combinatorial circuits can be easily implemented using the memory devices. This scheme is referred here as the lookup table technique. Any kind of direct computations can also be performed using such tables. One of the important advantages with this technique is, its predictable speed of operation. As any location in the memory can be accessed with the unit access time, input data size or the amount of computation involved can not affect the 'processing' time (input to output). Although, lookup tables can be used to solve variety of design problems, the availability of a high speed and suitable size component limits such utilisation. But in the recent times, a number of combinations of speed and density memory devices are becoming available in the market. Although the cost of the high speed memories is generally higher, it is expected to come down soon. As the memory devices are programmable, any future design changes are easily accommodated. It will be very useful to consider the lookup tables for all the suitable sections in the design. In a given design, if the parameters are going to be changed quite often, only then a RAM based option is preferable, otherwise it is more appropriate to use a PROM or EPROM based implementation. It should be remembered that the RAM based tables however need additional circuits to load the contents.

4. 4. Possible Schemes for the Different Stages

The single beam mode operation can be divided into two stages. The first stage is the *input conversion stage*, and the second is the *summing stage.*

For the IA mode

Input Conversion stage: The modulus squares (power terms) of the incoming complex numbers (voltage terms) are obtained.

Summing Stage: The power terms obtained in the previous stage are added together.

For the PA mode

Input Conversion stage: The mantissa - exponent format complex numbers (voltages) are converted to a fixed length real format.

Summing stage: The real format complex voltages obtained in the previous stage are added together.

The various possible designs for these computations are carefully analysed to find the suitable implementation scheme.

• Input Conversion Stage:

Calculation of the Modulus Squares

The logical blocks involved in the computation of this are shown here. In this scheme we would need 4 multipliers, 1 power computation unit and 1 adding unit. It is clear that, even if one is able to meet the high speed requirements, this scheme would require too many hardware components for the implementation.

Computing the
Incoherent Array output

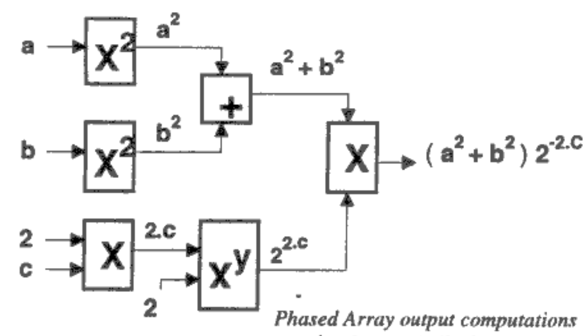

Phased Array output computations can be shown similarly

FIG. 4 - 7

As an attractive alternative, the *Input Conversion stage* can be easily implemented using suitable lookup tables. The steps involved for this are as shown below:

In the present design, Erasable and Programmable Read Only Memories (*PROMs*) are used as the lookup tables. The picture shown next illustrates this implementation. The sizes of the PROMs specified in the diagram are the minimum sizes required.

This diagram shows the first stage implementation for both IA and PA modes. In the IA

To compute $(a^2 + b^2)\,2^{-2.C}$ using the PROMs (lookup table method)

- *Pre-compute the values of $(a^2+b^2)\,2^{-2C}$ for all possible values of a, b, c.*
- *Arrange these values in the appropriate locations of an array (here it is a 3-dimensional array) in such a way that $(a^2+b^2)\,2^{-2C}$ is obtained when a,b,c values used as index.*
- *Whenever a new value of a,b,c occur, get the contents of the array at location (a,b,c).*

Memory chips (PROMs) can be used as an *Electronic Array.*
Memory chips address lines can be used as the array Index.
When a,b,c are given as address, pre-stored values of $(a^2+b^2)\,2^{-2C}$ appear at the output

Similarly *Phased Array output* computations can be done using the PROMs

FIG. 4 - 8

mode, for computing the power values the sign bits of the real and imaginary parts are ignored. Hence, a 1024 location PROM addressed by a, b, c (3, 3, 4-bits) is sufficient. For converting the real part, a 256 location PROM addressed by a, c (4, 4-bits) is sufficient. Similarly, another 256 location PROM addressed by b, c (4, 4-bits) caters for the imaginary part. The width of these PROMs decides quantisation noise contribution of this stage. The PROMs can be replaced by any other memory element (EPROMs, RAMs, etc.,) as long as the organisation and the speeds are matched. It can also be a single memory element addressed by a, b, c (4, 4, 4-bits) and wide enough to give power, real, imaginary part outputs in the data-out lines.

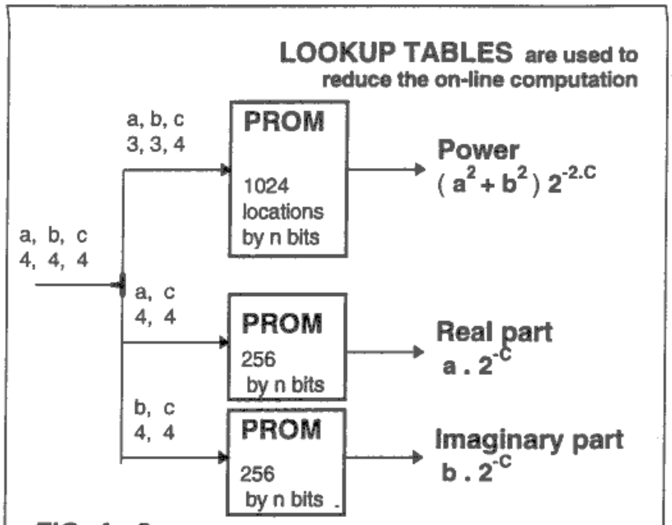

FIG. 4 - 9

This technique of using such look-up tables simplifies the hardware implementation particularly for complex arithmetic operations and hence is most suited for both IA and PA mode input conversion stages.

• Summing stage:

The output real, imaginary numbers and the power values thus produced corresponding to all the 30 dishes are added here. This stage can be realised by many different techniques, but the speed of operation limits the options. A processor based scheme is not practical. Multi-input adders are not available to realise the simple addition of the 30 inputs. Hence, it is required to design a suitable adding network which can handle the required data rate and the given number of inputs. Various choices are explored. A comparison between the 2 most suited schemes are given here.

Lookup Tables	Hardware Addition
• Predictable speed of operation. As any location can be accessed with unit access time, input data size need not effect the 'processing' time.	• Speed of operation varies for different bit size adders.
• Usage depends upon the availability of the high speed and high density Memory chips.	• If implemented inside EPLD design, component count reduces.
• Costs are relatively high.	• High speed components are available
• Memory chips used are programmable, hence the entire design can be re-configured by programming the memory devices again.	• Cost of the component is less
	• Needs large boards, if implemented in discrete chips.
	• Hardware will be frozen for only one kind of operation, if discrete chips are used

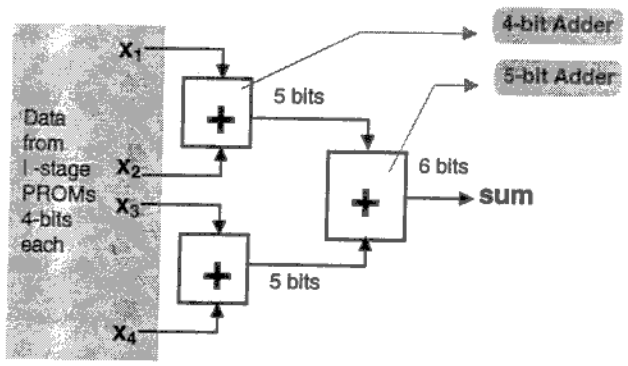

Binary Tree Adder
An illustration for 4-input, 4-bit wide data addition

FIG. 4 - 10

At this juncture, it is important to evolve a scheme which can easily meet the 32 MHz data rate with reduced hardware complexity. As 2 input adders are readily available, it is possible to cascade them to produce a multi-input adding network. The binary tree addition can be adopted for this purpose. The advantage of such a binary network is that the addition of 'n' inputs (where $n=2^m$; 'm' is an integer) can be completed in $\log_2(n)$ levels of addition and a total of (n-1) adder modules. Thus the 30 inputs can be added in five levels.

There are two constraints with such a scheme. Although it can cater to many number of inputs, each level of addition introduces delay in processing and hence after the 'm' levels of addition, there will be at least 'm' times the single adder delay introduced. Such a delay in an asynchronous scheme will cause limitations in the speed at which the binary network can operate. As a general consideration, one should note that when the inputs are added at each stage the data size grows. Hence it will be required to use progressively bigger sized adders in the network. But the standard adders are available only for catering to 4-bit wide data. The schemes described in the following section addresses these aspects.

Pipe-line Adder

It is possible to achieve very high processing rates using the pipe-line or stream-line techniques. In cases where the processing can be split into partial processing stages and if the computed results are not required to be fed back during the following clocks, it is possible to adopt pipe-line processing to increase the rate of processing. In this scheme, if part of addition is completed at the required data rate the rest are performed by using the additional processing stages. The first stage adder is released after a clock for accepting a new set of data. The illustration shown here explains how a 4-bit 4-input pipeline adder works. At each stage, part of the addition is completed, the partial sum is stored and forwarded to the next stage for further processing. At the same time, a new set of data enters the inputs for fresh processing.

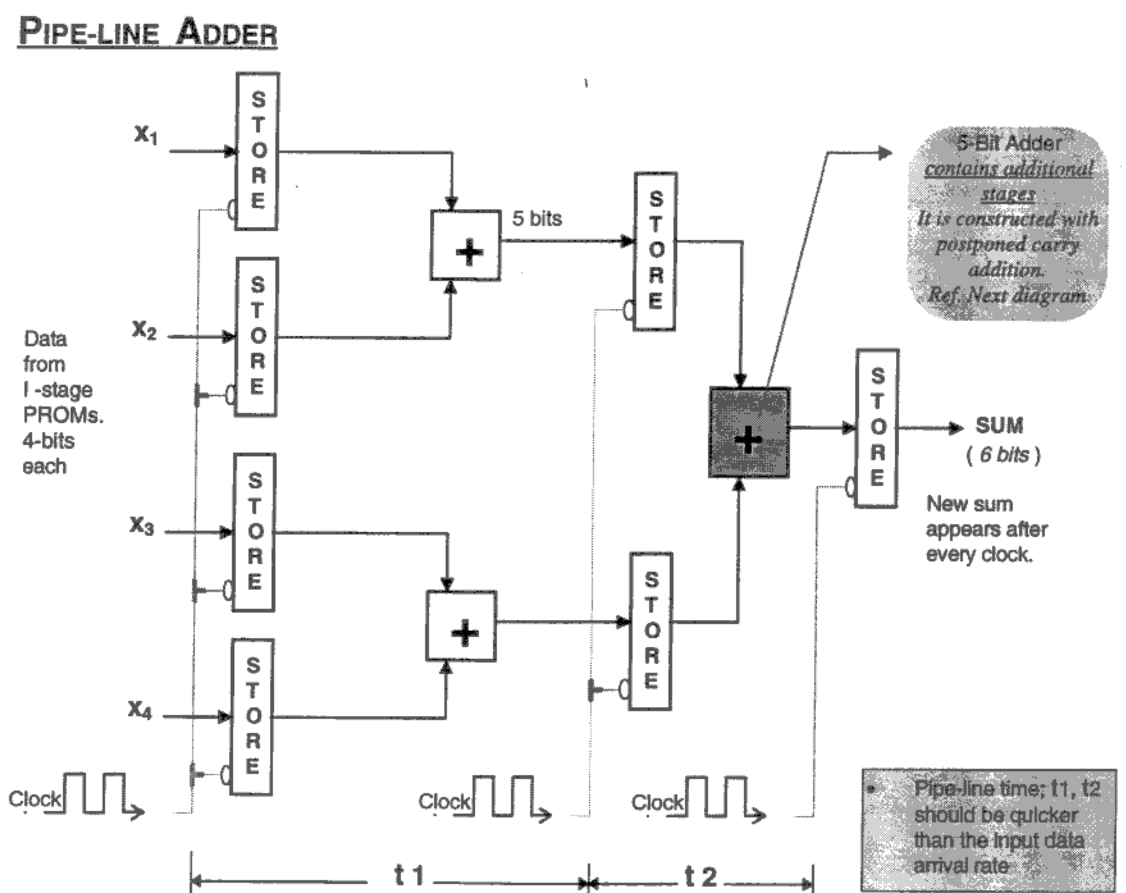

FIG. 4 - 11

In this illustration (fig.4-11) x1, x2, x3, x4, each 4-bit wide input data, are added together using the pipe-line binary summing network. Here, the input data rate is always equal to the pipe-line processing rate. In the first stage of pipe-line, x1+x2, x3+x4 additions are performed and the results are stored. After the first clock the second stage takes in these values and produces the final sum. While the second stage is performing this addition, new set of data arrives at the first stage. The final stage output (x1+x2+x3+x4) appears after the second clock. In case, if the 5-bit adder used in this network is not available as a standard unit, it can be constructed with two adders working in an extended pipeline as described in the next figure.

Five Bit Adder Stage

The 5-bit adder implementation is shown here. In this network, the portion of the addition which is not completed in the first part of pipe-line is carried out in the second part of the pipe-line. This kind of postponed-carry addition is essential to meet the processing speed. Otherwise the carry propagation of the first pipeline adder will cause additional delay and will result in slow processing. This delay is avoided by introducing the second step in the pipe-line. Using this method much bigger adders to cater for the 30 input addition can be easily constructed.

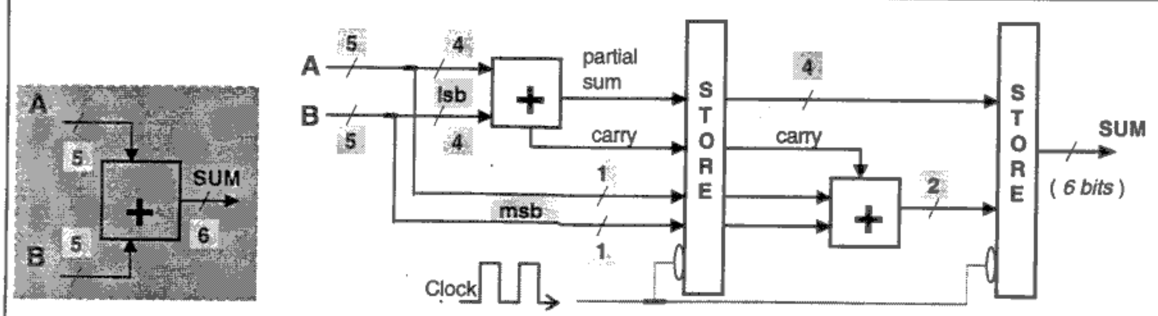

5-BIT ADDER STAGE

FIG. 4 - 12

• Verification of the pipe-line adder design

A discrete integrated circuit based pipe-line adder was constructed and tested to assess practical implementation. The test results yielded useful information about the practical limitations in the pipe-line operations. The clock and the data relations are understood more clearly. The diagram shown here, depicts this experiment.

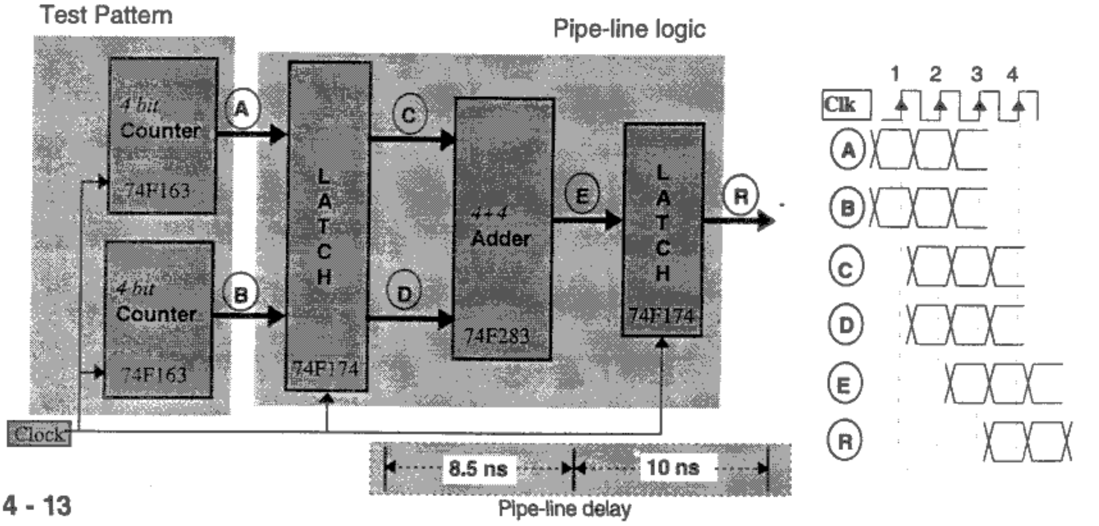

FIG. 4 - 13

This circuit has a built-in pattern generator and an adding element. The test pattern at the required speed is generated using a suitable clock. The sum outputs produced by the circuit are verified using a logic analyser system. The timing relations at the different stages are carefully analysed.

The suitability of the EPLD based design is also analysed. The circuit required for 4 input, 4-bit wide data addition pipe-line network is implemented inside an EPLD chip. The diagram below shows the details:

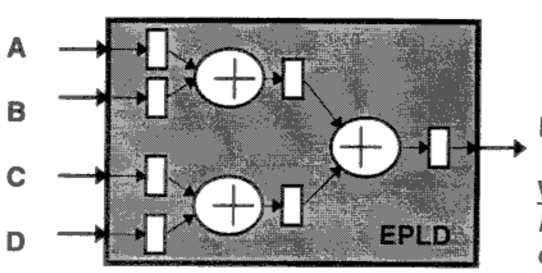

Worked up to 17.6 MHz Speed
Result 'R' verified for various combinations of A, B, C, and D inputs

FIG. 4 - 14

Although there is huge reduction in the board-space, the circuit operating speed is directly related to the complexity of the stages inside. It is found out by using EPM5128-1 chip, the maximum speed of operation achieved is about 17.6 MHz for this circuit. It is a trade-off between the speed of operation and the design complexity inside the chip.

The conclusion arrived from this experiment was that, in the prototype design an EPLD based summing network would be used, as the operating speed of 16 MHz was adequate for the prototype planned. The choice for the final design will be made based on its performance and considering the new fast component availability in the market.

Following these preliminary tests, verification of some of the crucial design idea using a pilot model was undertaken. The details are described in the next section.

4. 5 Prototype-four-dish Array Combiner

The reduced version of the final system is referred here as 4-dish array combiner. The specifications of the system are given below:

Combines 4 dish inputs.
(2-polarisations and 2-side-bands per input)
Facility to mask or include any given dish.
Four-bit quantisation in power, real, & imaginary.
Facility to accommodate 4 input-signal ranges.
Built-in diagnostic aids.

The inputs to the combiner are the polarisation multiplexed ECL differential level data from the FFT hardware coming at the rate of 32 MHz. Prior to the demultiplexer/ diagnostic stage the data enters the ECL-TTL converters, where the ECL differential signals are converted to the TTL levels. Then the signal enters a latch-cum-counter stage. During the normal operation, the signals are latched and forwarded to the next stage. During the diagnostic operation, FFT signals are ignored and the counters are activated. The counters produce a ramp pattern. There are separate 4-bit counters for a, b, c inputs. The counters can be operated either in Up or Down count mode. The selection of the latch or the counter mode of operation is governed by the control computer. The signal corresponding to a selected mode enters the demultiplexer

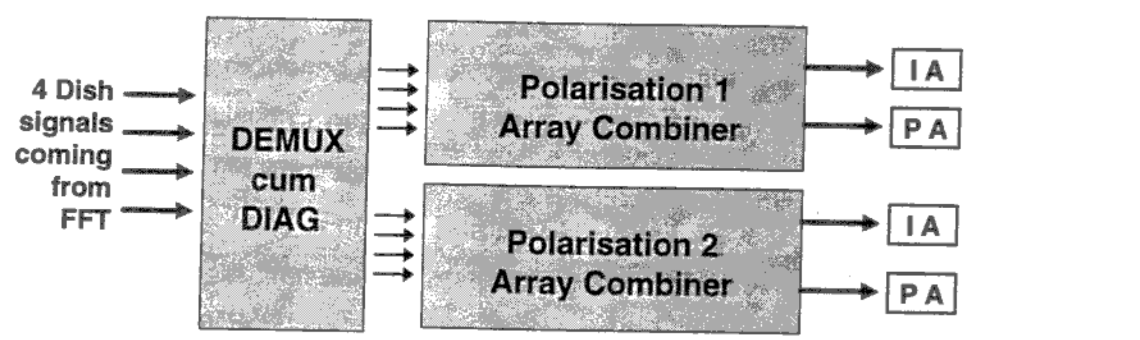

Four-dish Array Combiner (proto type) FIG. 4 - 15

stage. At this stage the 2 polarisation channels are separated and synchronised. In the case of diagnostic mode the even and odd (up count mode) patterns (ramp steps 0, 2, 4,... and 1, 3, 5,... respectively) will get separated. The demultiplexing operation reduces the data rate from 32 MHz to 16 MHz. There by the processing speed requirements are reduced and the prototype development is simplified. The demultiplexed data is sent to two identical array combiner boards. They process the polarisation-1, polarisation-2 data separately.

Each board of the combiner hardware accepts 4 inputs from the demultiplexer and produces the IA and PA mode outputs. The first stage of the array combiner is the input converter. These are PROMs, that converts the 12-bit complex number into power, real, and imaginary terms (4, 4, 4-bit wide numbers). There are four set of such PROMs, one corresponding to each dish.

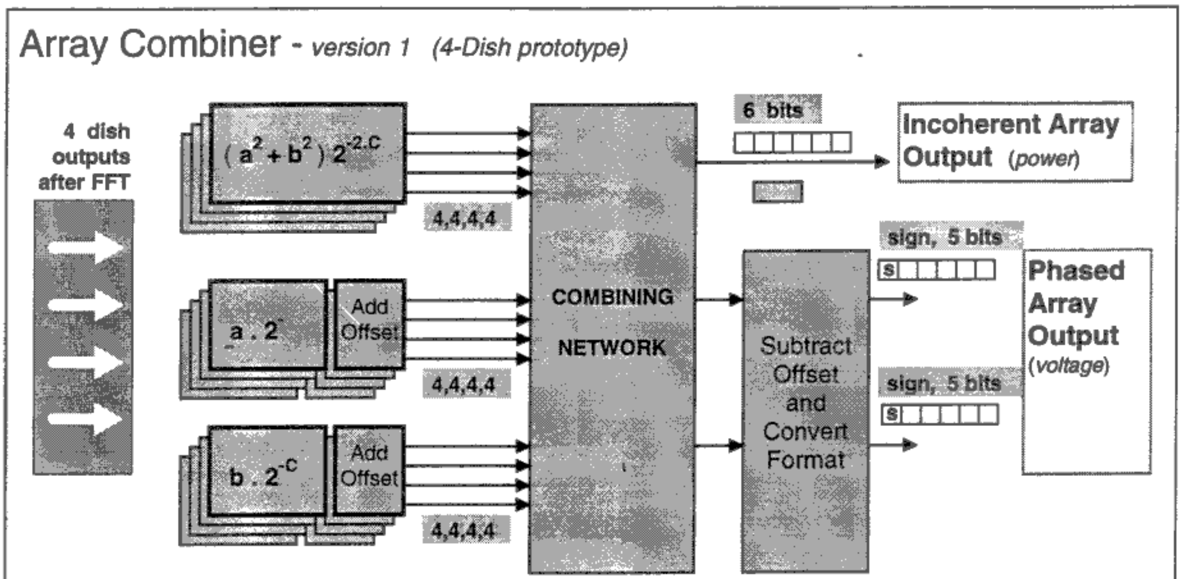

FIG. 4 - 16

The power value produced are positive numbers, whereas the real, imaginary numbers can be either positive or negative. If they are only positive numbers even for real and imaginary parts the summing network's complexity can be reduced and the three of them can be identical. For this purpose an offset scaling is introduced. The offset scaling in the Real, Imaginary input conversion stage of the PA shifts the output to change in a positive range. After the offset scaling, they change from 0 to (2 x positive maximum). Now the output magnitude '0', (positive maximum +1), (2 x positive maximum) corresponds to input negative maximum, '0', positive maximum respectively.

Thus in the summing network, there are three identical networks performing power, real, & imaginary summation. Each of the network is implemented inside one EPLD chip (EPM 5128JC-1). All these three EPLD circuits are made identical to simplify the design and testing complexities. These networks combine all the four dish data for one polarisation. The offsets introduced in the input conversion stage will be removed at the last stage of the real, imaginary summing networks. With the knowledge of number of inputs that were present, a corresponding offset value will be supplied to the offset subtractor. The offset subtractor result can be now either positive or negative depending upon the input values. The power summing network also has an offset subtractor to maintain similar pipeline. However it is loaded with a dummy offset value (e.g. value corresponding to '0') and it doesnot modify the data.

The format conversion stage converts the results to a sign-magnitude format. This is needed to match the requirements of the instruments that follow the array combiner. The format conversion stage, present in the IA network is programmed to do no operation on the data. This section is retained here for uniformity even though it is not required.

The summing network EPLD contains a programmable register to configure the circuit to suit to power or real-imaginary mode operation. The dish selection facility is provided by the Antenna Mask register. Another register holds the input range (lookup table) selection number. These registers can be pre-loaded from the control computer.

This design consists of many pipe line stages, hence it is required to tell when the first data appears, to the back-end systems, to enable them to start collecting the data. For this purpose a pipe-line delay register is incorporated in the EPLD circuit. This can be programmed from the control computer to generate a clock valid (start) signal after a predetermined number of clocks. When the Array Combiner output has the very first valid data output the clock valid signal appear. The back-end instruments can use this flag to start acquiring data.

The other polarisation Array Combiner board also works the same way. The data rate handled by each of them is 16 MHz.

The clock for the Array Combiner is synchronised and derived from the clock control circuit. This circuit is implemented inside an Erasable Programmable Logic Device (EPLD). The control computer can command to start or stop the operation of the combiner by controlling the clock circuit. It synchronises the Array Combiner operations with the FFT system, and generates the 2 phase clocks required for demultiplexing the data, and the diagnostic clocks.

This version of the design was realised in hardware. Printed Circuit boards are made. Circuit boards are assembled and tested. The complete hardware is checked and installed at the observatory site. Now it is presently being used for the astronomical observations. Details about the results are described in the next section

4. 6 SECOND PHASE - Final System Development

After the successful completion of the proto-type, the work on the final system was taken up. The final system will have to work at double the clock rate that of the proto-type (the clock rate will be 32 MHz, instead of the 16 MHz). This 32 MHz operation reduces the design complexity, system size, and hence the cost, provided that suitable components are available.

• High-Speed Design Aspects

Designing big digital circuit boards for the 32 MHz operation, however, have new constraints. Actually it is a migration into a new technology. Usually for circuit boards operating around this speed, a special attention is required in the design and circuit layout. At these speeds the signals start to behave more differently as the high frequency effects start to dominate. PCB design without adequate care will result in the deterioration of clock shapes and consequent malfunctioning of the circuits. Most low frequency components would practically stop working.

Here, the new technology products catering to very high frequency operation come into use. Invariably these new products operate with different signal and electrical characteristics. Their power ratings are different as power consumption increases as a function of the operating frequency. Proper planning of the power distribution on the circuit board, therefore becomes one of the major considerations.

These high speed devices make very sharp signal level transitions. The signal rise and fall times are, typically in the order of 1-3 nanoseconds. These sharp edges enable them to work at the high clock rates. Therefore, unless the circuit boards also allow this kind of signal transitions, square-wave-clocks and signal edges would start jittering, which can jeopardise the circuit operation. Such problems are very difficult to diagnose and correct. The practical solutions are to choose the right component and to take sufficient care on the circuit lay-out design.

For proper operation at the high speeds, the circuit board layout should be made so as to smoothly handle every clock in the circuit. Usually it is enough, if the circuit layout can handle, the 5th harmonic of the fastest square wave clock. This rule is not sufficient in many other cases. The high speed components used in the circuit produce very sharp signal edges. Often these edges have their contributions, beyond the 5th harmonic of highest operating frequency. So it turns out that the kind of components used decide finally the restrictions on the board layout. The practical solution is to use only the appropriate speed components given the clock speed. Also when high frequency components are used on the relatively slower clock speed applications, it unnecessarily adds complexity in the circuit and layout designs.

The high speed operation also pose, variety of other demands in terms of test equipment. It was required to use high bandwidth equipments to reveal true nature of the signal particularly when the signal is non-ideal. For proper trouble shooting and testing circuits involving in the BiCMOS technology components it is required to have 300 - 500 MHz bandwidth scopes, even when the maximum clock frequency is only 32 MHz.

It was important, therefore, to understand these various aspects of the high-speed technology before final circuits can be realised. The necessary requirements were identified. Suitable components were located. The high density surface mount versions of the buffers and latches from the FCT series were found to be the best choice. These chips are made with additional pins for power supply and ground. These additional pins handle the high speed switching current requirements comfortably. Also, there are separate power supply pins close to the output pins. These supply pins can be separately de-coupled with suitable capacitors, so that the load variations will not affect the ICs internal operating characteristics. This offers a definite advantage in the circuit design. There are also special bus driving ICs, where balanced and higher output currents are available. This feature reduces the bus driving problems. Then, there are also ICs with a built-in series termination (FCT 2 and T series). These ICs are suitable for driving signals over a short distance (point to point use). The series resistor reduces unwanted current swing, and there by eliminating problems such as the ground bounce, and those related to signal reflections. Typically, these double density chips replace two numbers of the TTL dual-in- line IC equivalent chip but occupying only 1/4 th the space. PCB routing is also relatively easy when the density of the chips is compared. These chips are available with different speed grades. The new thing that was to be learned about those chips, however, is related to their soldering on the circuit boards. For this purpose, some special tools and techniques had to be acquired.

Appropriate de-coupling techniques were identified. Considering the speed of operation and the technology of the IC chips in use, it was found that the circuit required two kinds of de-coupling. One on them is meant for de-coupling the low frequency range of switching noise. Other one is for de-coupling the high frequency range, produced chiefly by the fast signal edges. For most circuits, it was required to use a ceramic 0.01 μF (for 10 - 30 MHz range) and a NPO type 470 pF (for the 160 MHz range). It was also required to place the de-coupling capacitors at the right places in the layout. These placement details were studied carefully and implemented in the board design.

The importance of proper termination of the high speed signals cannot be under-estimated. Different termination techniques were carefully studied and some related experiments were tried-out. The ‘parallel termination’ was found to be the most suitable method. Different critical signals were identified and their signal routing strategies were worked-out with extra care.

4. 7 Design Philosophy

The core of the design consists of the Input Conversion stage followed by a five level binary tree summing network. The design is divided in two stages. The first stage is implemented in 8 identical boards. These boards are called as the '4-input cards'. They combine 4-dish inputs in one card to produce power, real, and imaginary outputs. The second stage is implemented in 3 identical boards. These are called the '8-input cards'. The 8-input cards combine 8-data inputs of one kind (e.g., power, real, or imaginary terms) available from the eight '4-input cards'.

Design complexities are simplified by using the lookup tables in the place of computational hardwares. The over all processing speed of 32 MHz is achieved by using pipe-line techniques. In this design, long operations that could not meet the required speed are divided in to suitable sub stages and implemented in multiple pipe-lines. The IA, PA computations are implemented in 12-pipe-line stages (input conversion -1, summing network - 8, additional features - 3).

A high-density, 25 nanosecond CMOS EPROMs are used for the input conversion stage. Four-bit wide R/W RAMs are used to select the input signal range. A five-level binary tree adder network is used to implement the summing hardware. High speed CMOS EPROMs (20, 25 nanoseconds) are used to implement the adding elements in the network. High speed FCT series SMD devices are used to meet the high speed latching and buffering requirements. FCT series low-skew (0.5 ns) 1:10 clock-buffers are used to distribute the clock signals in the circuit boards.

Worst case estimates of the power consumption (for the 32 MHz operation) were taken into account while deciding on the power supply distribution. Power supply decoupling is achieved by using 0.01 μF and 470 pF capacitors. These two capacitors filter the 20-40 MHz and ~160 MHz components respectively

It is important to appreciate that different portions of the circuit work at different speeds. They can be classified as follows.

1. High Speed Section: Clock and control signal had the fastest edge to edge transition of about 32 nanoseconds. Very short trace lengths and stringent component placement control are required for proper operation.

2. Medium Speed Section: It is identified that for the pipe-line processing if the clocks are transiting at 32 MHz rate, then the 'signal-lines' can transit only at 16 MHz. This fact helped to group the data lines in the medium speed section. In this section, while it is desirable to avoid long PCB traces, the components need not be placed in a compact way.

3. Low Speed Section: These are the low speed control and set-up lines. Some of them usually stay static except during the configuration operation controlled by the computer. In this section long traces and liberal component placement are allowed.

This identified grouping has helped to suitably plan the PCB layout. The layout looks as shown in figure below.

The 'clock' and 'init' signal buffers and delay circuitry fall in the High Speed section. It is located in a strategic place in the board. The circuits are implemented in a compact area and it is very close to the input and output connectors. From this place the clock radially reaches to the other sections of the board with almost equal delays. The high speed signals are daisy-chained and routed with additional isolation, ground guards and terminated at the last point to achieve a stable high-speed operation.

High Speed Board Layout

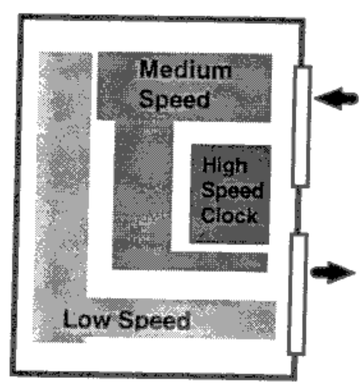

FIG. 4 - 17

The pipeline data processing (Input Conversion, Gain RAMs, and Summing) stages fall in the Medium Speed section. The input data enters via one of the connectors, and the processed data comes out through the other. In the pipeline architecture of the design, there is minimal cross connectivity in the circuit. The processed data moves between different stages like a plane wave front. This kind of connectivity avoids the use of long traces and naturally supports the easy implementation of a high speed layout.

The Low Speed sections in the layout consists of the programmable registers, display drivers, low speed buffers, control and setup-decode-logic circuits. They operate at relatively very slow speeds. Here, the components placement restrictions are minimal. Length of the tracks may not be of much significance for the proper operation. The component and the track density in this section is also relatively small.

4. 8 The functional block diagram

The functional block diagram of the system is shown here.

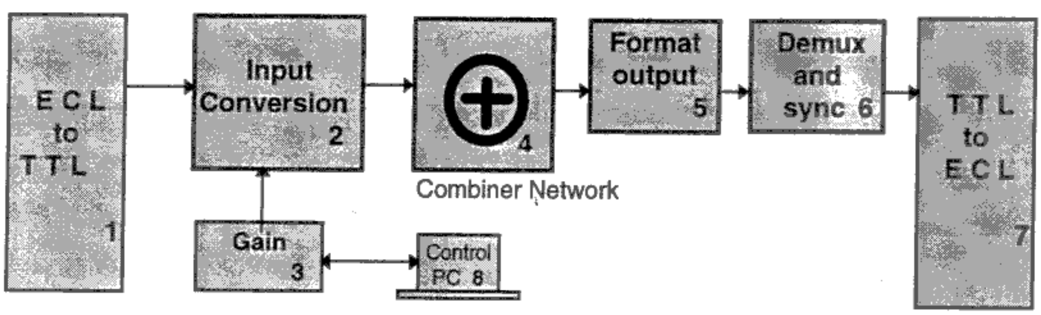

Array Combiner Functional Block Diagram

FIG. 4 - 18

1. The ECL to TTL Section.

The complex spectral data are coming from the FFT as ECL differential signals. There are inputs corresponding to data from 30 FFT modules. These signals are converted to TTL levels, latched and forwarded to the Input Conversion stage.

2. Input Conversion section:

The mantissa exponent format complex numbers entering this block are converted to the corresponding power, a linear format real, imaginary terms. The conversion is carried out by using EPROM based look-up tables. The power terms produced are 6-bits wide and the real, imaginary are 5, 5-bits wide. The EPROMs contain 2 banks of 16 tables suitable for measuring different input signal ranges. Presently one of the bank is used for storing the diagnostic signals. The bank selection is activated by programming a control register. The range control bits coming from the gain RAMs selects one out of the 16 tables in the given bank. The gain control bits are commonly available to both IA and PA tables (power, real, imaginary sections).

3. Gain Control Section:

A 4-bit wide R/W RAM (one RAM per dish) addressed by a channel counter (10-bits wide) supplies the range control bits to the input conversion section. Contents of the RAMs are loaded from the control computer. This gain control feature is available to all the 30 dish inputs, the two polarisations and for the individual spectral channels.

4. Combiner Network Section:

The Combiner network combines the 30-inputs (power, real, imaginary) using a 5 level binary adder network. There are 3 identical networks meant for summing the power, real, imaginary terms. The adder network for the power terms is configured to add positive numbers and the real, imaginary networks are configured to perform the 2's complement addition. The entire network is implemented using suitable high speed EPROMs in multiple pipe-lines stages.

The first two levels of the binary network (6, 7- bit adders) are implemented in 2 pipe-line stages (one pipe-line per level). The last 3 levels (8, 9, 10- bit adders) are implemented in 6 pipe-line stages (2 pipe-lines per level). The hardware up to the second level addition are implemented in the 8 identical boards. The antenna masking provision is provided at the inputs of the first level adder itself. Selective inclusion or masking of any combinations of antenna inputs are possible at this level. There are separate masking provisions available for IA and PA networks.

Another additional stage of masking is provided at the inputs of the third level adder. From this level hardware is implemented in another set of 3 identical cards. At this stage onwards, the summation of the power, real, and the imaginary terms are carried out in separate card. The masking provision helps in avoiding any set of inputs for further addition if the corresponding previous stage cards are not present.

5. Format Control Section:

The final sum output data format can be suitably altered to match to the requirements of the back-end instruments. The format conversion section is implemented using an EPROM. This section accommodates up to 8 formats with a maximum data size of 11-bits. Suitable data scaling is also possible at this stage.

Sub-Group Facility:

A provision is available to bring summed outputs corresponding to two independent groups to the back-end instruments to facilitate sub-array observations. In this, each group can have a maximum of 16 dishes. These are the partial sums from the network tapped out before performing the last level addition. This provision is available for both the IA and the PA mode outputs.

6. Demultiplexer Section:

The Array Combiner processes the time multiplexed 2-polarisation channels. They are separated (demultiplexed) into individual channels only at this last stage. The IA, PA mode outputs, including the sub-group outputs are demultiplexed to produce a corresponding polarisation 1 and 2 channels with a reduced data rate of 16 MHz.

7. TTL to ECL Section:

These are buffer driver stages, facilitating proper distribution of the array combiner outputs to the different back-end instruments. The TTL outputs from the array combiner are converted to ECL differential signals and distributed using twisted pair cables.

8. Control Computer:

The Array Combiner operating parameters (mask registers, gain values, etc.) are loaded from a control computer, which also monitors the system status during the operation. A control software gives the user interface to the Array Combiner system.

4. 9 Implementation Details

The hardware required to produce the two single beam modes are divided in to two main sections and implemented in two types of circuit boards. They are:

1. Four Input Cards (eight cards)
2. Eight Input Cards (three cards)

[details are for one side band]

• Four Input Cards

The Four Input Card (FIC) combines four dish inputs. There are eight such cards to handle the 30 dish signals. The basic functions of these cards are:

1. Accepts the complex spectral voltages from four FFT modules (coming from 4 dishes x 2 Polarisations).
2. Converts the complex voltages into Power (6-bits), Real, Imaginary terms (5,5-bits) after adjusting for the expected input signal range.
3. Combines the 4-dish Power, Real-Imaginary terms.

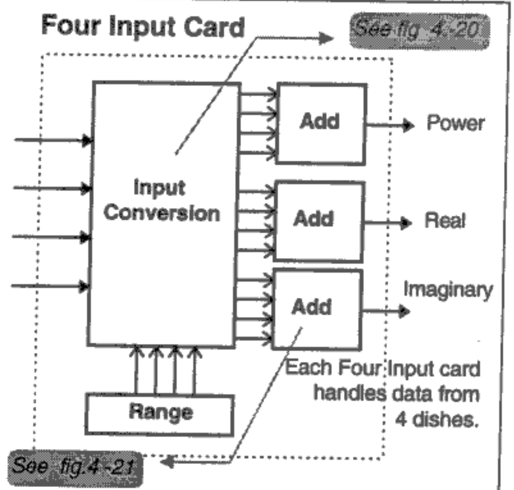

FIG. 4 - 19

Hardware details

The spectral voltage outputs from the FFT system enters ECL to TTL converters and are converted to the TTL levels. These signals are latched using the tri-statable input registers[1]. The register outputs are tri-stated for the diagnostic operations. The mode control register (M_0 bit) has to be programmed for this purpose. During the diagnostic mode it is possible to tri-state the input register and feed a common 12-bit number from a programmable register to the IPC inputs. It consists of two numbers of 128K X 8 EPROMs[2] per dish input. There are 4 such sets of EPROMs in the Four Input Cards.

[1] 74FCT16374 SMD
[2] CY27H010

The IPC stage produces the Power (6-bits) , Real (5-bits), & Imaginary (5-bits). The first EPROM (for example U16) outputs the power (6-bits) and the 2 LSBs of the real part. The second EPROM (U17) outputs the remaining 3-bits of real part and the 5-bits of the imaginary part.

Input Conversion and GAIN Control Section

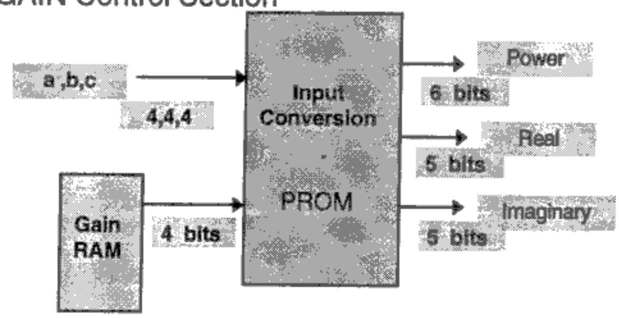

- Independent gain correction possible for each channel of the pol, side-band and for any dish.
- Pol channels arrive multiplexed, their gain values are located in successive locations of Gain RAM

FIG. 4 - 20

The EPROM (IPC stage) gets the expected input signal range information from the Gain RAMs. For this purpose the upper 4 address bits (A12 to A15) of the EPROMs are used to select one out of the 16 possible 4K size tables. These tables contain the optimum look-up outputs corresponding to the different input ranges. During the operation of the system, gain corrections are accomplished by suitably changing to an expected table for every channel of the spectral inputs. The details about the gain tables to be used (4-bits wide data) are coming from Read/Write RAMs[3]. There are 4 such RAMs in each cards corresponding to the 4 dish inputs. The gain values corresponding to 256 spectral channels and for the 2 polarisations for the 4 dishes are stored in these RAMs. Using these RAMs it is possible to store up to 512 range values[4] per polarisation. The RAM locations are pre-loaded during the set-up operation. The RAMs are addressed by a 10-bit channel counter. The channel counter is implemented inside an EPLD[5]. This channel counter operates in synchronisation with the FFT system. When a specific channel data from FFT arrives at the IPC stage inputs, the corresponding RAM locations are accessed and the stored range values are supplied to the IPC lookups. The odd and the even numbered sets of locations in the RAM contains range table numbers corresponding to the two polarisation channels. The synchronisation signal (XINIT) is derived from the clock sequencer EPROM[6] located in the Clock-Controller card. The control computer

[3] CY7C150
[4] Synchronisation has to be adjusted
[5] EPM5032
[6] CY7C245A

loads two Gain RAMs at a time using the 8-bit data path. Gain RAMs corresponding to Dish-1, Dish-2 RAMs are loaded together. Similarly, data corresponding to Dish-3 and Dish-4 Gain RAMs are loaded together. After loading, the computer can read back and verify the operations. The integrity of the data stored in the RAMs is checked using the pre-computed parity bits stored in a parity RAM. The parity RAM is also addressed by the channel counter, hence the parity errors are checked automatically when each time a new location is accessed. The contents of the parity RAM can also be read by the control computer for verification, if required.

The output data from the IPC stage enters the binary summing network. At first the power, real and imaginary terms are latched in the clearable registers[7]. The 'clear signals' are taken from the antenna mask register (U60). The mask register can be programmed to exclude any combination of the dishes in the summing. As already mentioned, separate masking provisions are available for power, and real-imaginary (IA mask, PA mask) summing networks.

First Level Addition (Dual 6-bits plus 6-bits adders):

After the clearable register, the data enters the Level-1 summing stage of the binary network. At this stage successive two inputs are added together. The adders are implemented using EPROMs[8]. These EPROMs take in two 6-bit inputs, adds them and produces a 7-bit sum output. In the case of real, imaginary terms the inputs are only 5-bits wide, hence the most significant bits (MSB) are tied to ground at the clearable register inputs while the same 6-bit adders are used for summing. The real, imaginary term network adders ignore these MSBs. Then the sums produced are stored and forwarded to the next pipeline stage using a latch[9].

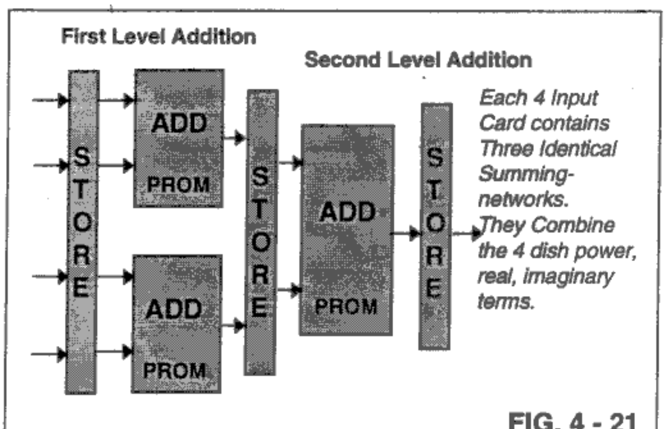

FIG. 4 - 21

[7] 74FCT162823 SMD
[8] CY7C264
[9] 74FCT162374 SMD

Second Level Addition (7-bits plus 7-bits adder):

The second level of summing produces the output corresponding to the four input sum. The power term will be 8-bits wide, the real and imaginary are 7-bits each. These 7-bit adders are implemented again using EPROMs[10]. All the three sums (power, real-imaginary terms) are further latched and forwarded to the 'Eight-Input Cards' through the back-plane.

In the 4-input cards, a provision is available to adjust the phase delays for the clock and Init pulse so as to meet the proper timing synchronisations. The parity error status is displayed using LEDs and also available to the control computer as a status flag. The IA and PA mask values are displayed on the front panel. An EPLD based decoder circuitry is used for selectively writing and reading the programmable registers and the Gain RAMs present in the card. The input conversion stage has a provision to switch to a second bank for any diagnostic purpose. This is accomplished by programming the Bank selection bits in the mode control register. The gain RAMs are loaded from the control computer by tri-stating a 10-bit latch that is feeding the channel counter outputs to the RAMs address lines. The RAM address values are supplied from the control computer while loading and reading the contents. The tri-state control is achieved by setting a (M1) bit in the mode control register. There are general purpose lines provided in the board between the EPLDs and the back-plane euro connector to accommodate any future requirements. A 1:10 low-skew FCT clock driver[11] is used to distribute the clock to the different sections of the four input card. There are 4 pipeline stages in this card.

All the 8 first stage cards simultaneously receive the synchronisation signal through the back-plane.

---

[10] CY7C276

[11] 74FCT807 SMD

• Eight Input Cards

Eight sets of the four dish sums, thus obtained are available to the *Eight Input Cards (EIC)* for further addition. There are 3 identical Eight Input Cards handling the Power, Real & Imaginary terms separately. The basic functions of this card are given below:

1. Accepts the 4 dish sum terms from the Eight four input cards.
2. Sum all the 8 terms
3. Demultiplex the Polarisation Channels.

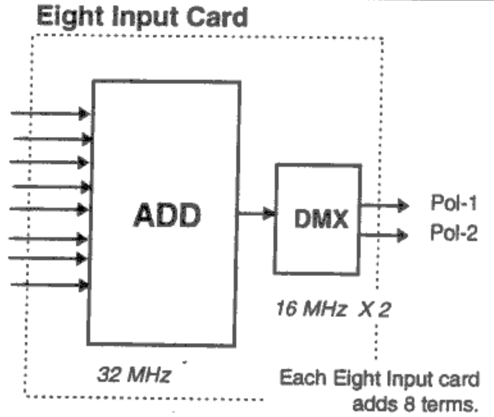

FIG. 4 - 22

Hardware Details

There are eight power, real-imaginary terms each 8,7,7-bits wide, at the 8-input cards (EIC) for summing. All these 3 cards have identical hardware circuit, but are programmed to perform simple addition in the case of power, and 2's complement addition for the real and imaginary terms. One of the card is described here. The details are given here.

The input data enters the first stage clearable registers[12]. All of the 8-inputs may not be present during the operation, hence a masking provision is available to exclude any given set of inputs in the summing. The register clear signals are coming from the Card Enable register (U43). The control computer configures the Card Enable register. The data outputs from these registers are fed to the next stage of the binary network (first adder stage in this card) for further addition.

The addition of 8 inputs can be carried out in 3 levels using the binary tree network. For this purpose it is required to have 8, 9, 10-bit wide adders corresponding to the three levels. Due to hardware implementation considerations, each of these adders are

[12] 74FCT162823 SMD

split into 2 pipeline stages (postponed carry addition refer Fig. 4-12) and implemented in the EIC.

Third Level Addition (8-bit adders):

The inputs are 8-bits each, and there are 8 of them.

Pipeline-1 adds the successive two least significant 6-bits and produces 7-bit outputs. There are four such adders implemented in four EPROMs[13] to cater to the 8-inputs. The results are latched and forwarded to pipeline-2.

Pipeline-2 adds the two most significant 2-bits along with the corresponding carry produced in the previous pipeline. These are implemented as four numbers of 2, 2, 1- bit adders. Two such adders are implemented in one EPROM[14]. There are two such EPROMs.

The final sums here, are four 9-bit wide numbers. These outputs are available for the second level addition.

Fourth Level Addition (9-bit adders):

The inputs for this stage are four 9-bit numbers from the previous stage.

Pipeline-1 adds the successive two least significant 6-bits and produces the 7-bit outputs. There are two such adders at this stage, they are implemented in two EPROMs[15]. The results are latched and forwarded to pipeline-2.

Pipeline-2 adds the remaining successive two most significant 3-bits along with the corresponding carry produced in the previous pipeline. These are implemented as two numbers of 3, 3, 1- bit adders. Each adder is implemented in one EPROM[16].

Here, there are two outputs, each 10-bits wide.

---

[13] CY7C264

[14] CY7C291

[15] CY7C264

[16] CY7C291

Fifth Level Addition (10-bit adder):

The inputs for this stage are two 10-bit numbers from the previous stage

Pipeline-1 adds the two least significant 6-bits and produces the 7-bit output. The adder is implemented using an EPROM[17]. The result is latched and forwarded to the next pipeline

Pipeline-2 adds the two most significant 4-bits along with the carry produced in the previous pipeline. This is implemented as a 4, 4, 1-bit adder. It is implemented in one EPROM[18].

Here, the 2-inputs are added together to produce a 11-bit output.

Sub-Group: One of the inputs to this stage (sum of data from dish 1 to 16) is brought out as a sub-group output. The main summing stage is also optionally bypassed to produce the second input of the adder (sum of data from channels/dish 16 to 32)[1] as another sub-group. The data output from both these groups are format converted, demultiplexed and are available to the back-end instruments. The hardware implementation of this will be discussed in detail.

Output Format Control:

The sum output after the last stage addition is fed as the lower 11 address bits (lower 10-bits in the case of sub-group outputs; where the 11th address bit is grounded) of the Format-control EPROM. The upper 3 address bits of the EPROM are supplied from a Format Select register (U47). These 3-bits can select up to 8 different formats. This Format Select register is configured by the control computer. The output data corresponding to the selected format will

Output Format Section

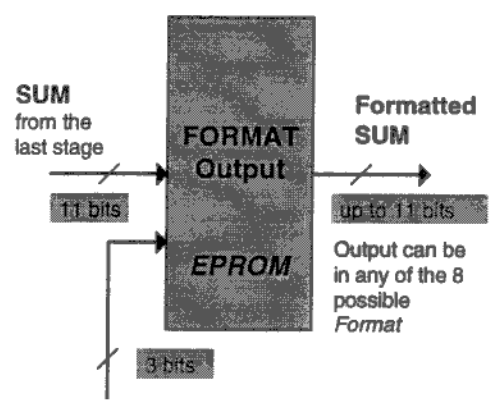

FIG. 4 - 23

---

[17] CY7C264

[18] CY7C291

[1] There are 32 inputs to the summing hardware

appear with a maximum data size of 11-bits (10-bits in the case of sub-group outputs).

Since the real, imaginary terms are combined in independent cards, they have separate *Format-Output* sections. However care must be taken in the control software to handle them identically.

Sub-Group:

The sub-group outputs, representing the sum of 4-input-card-0 to card-3 sum outputs, are available. The outputs are 10-bits wide. The main group output can be programmed to give either the full sum of all the 4 input card outputs (dish 1 to 30) or bypass the addition and give only the sum belonging to the second group, i.e. card 5 to 7. This bypass mode is activated by setting the M_0 bit in the SubGroup/PolEnable register (U45). This M_o bit forms an additional (address) input to the 10-bit adder stage (last level) EPROMS (U25, U33) and configures them to work in Adder or By-pass mode.

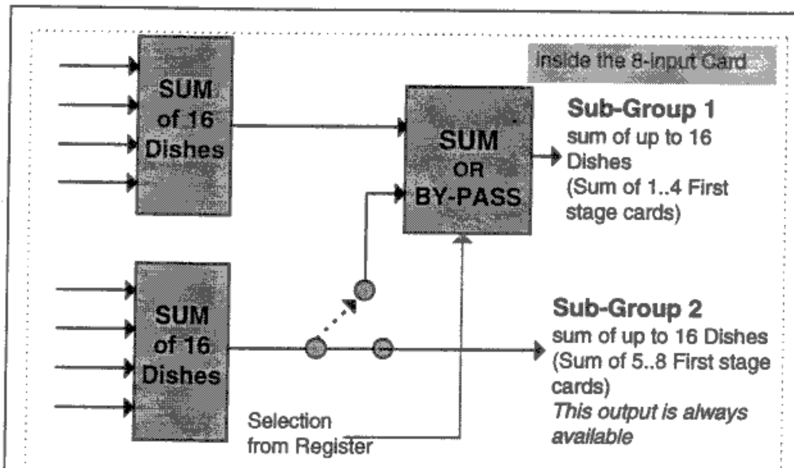

Sub-group Facility FIG. 4 - 24

De-multiplexer:

Now the formatted data enters the de-multiplexer stage. The two phase clocks (CK1 and CK2) coming from the Clock Control section demultiplexes the data. The data which appears for the even clocks are latched by the CK1. and the odd ones by CK2. After de-multiplexing the Polarisation-1 data appears first and Polarisation-2 data one clock later. This

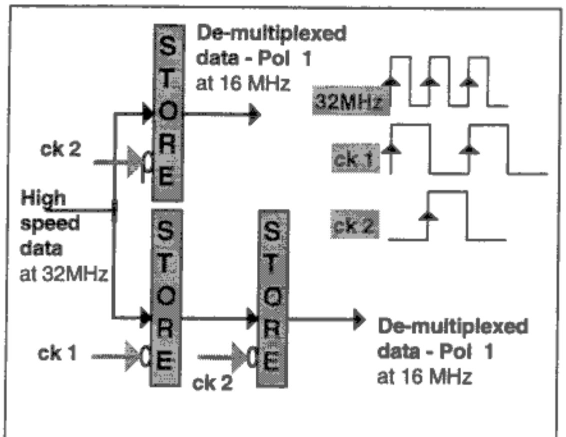

FIG. 4 - 25

delay differences are compensated by, again latching the polarisation-1 data using CK2 clock. The two polarisation channels will have a data rate of 16 MHz per channel.

Control Interface and Control Software:

The controller interface provides access to the programmable registers. The interface consists of two data buses each 8-bits wide, one for reading and another for writing data. A 4-bit address bus is used for selecting a particular register inside the card. The card select line is used to select a specific card. The read and write signals are used to specify the read/write operations. One reserved line is provided for future use. Error status indication is available to the controller interface from all the cards. The computer communicates to the array combiner through a 144-line I/O card.

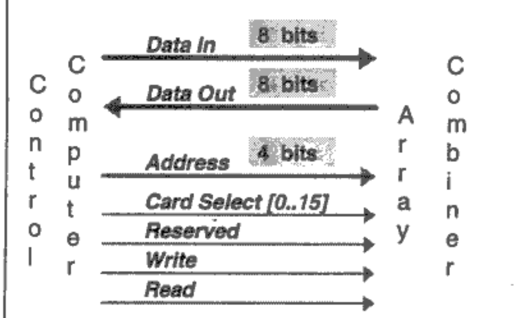

FIG. 4 - 26

The Control Software is divided into, Four main Modules. They are

1. *Lower Level : I/O routines and Interface specific routines.*
2. *Card Specific: It is specific to a type of card in the system. e.g. FIC control, EIC control routines etc.*
3. *Diagnostics: These routines serve mainly as an aid for testing and debugging.*
4. *User Routines : These are Application Specific routines. They call the other routines and provide the user interface.*

Usually the lower level routines need not be changed for writing any application programs. On the other hand, if the hardware control interface is changed then only the Lower most routines would need to be changed.

Timing Sequencer:

A timing Sequencer is used to generate proper timing signals for the system. This block receives the synchronisation signal from the GMRT clock distribution system. This module translates the input signal timing information to suit the Array Combiner requirements. The counters used in the Array Combiner obtain their synchronised-reset signal from this stage. The Sequencer is implemented inside a clocked-EPROM. The following Timing signals are available from this Sequence.

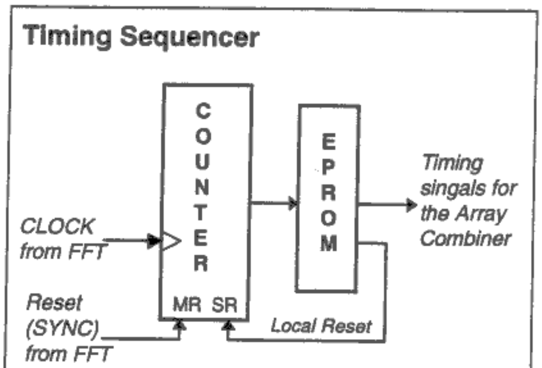

FIG. 4 - 27

1. *Local synchronisation (reset) signal*
2. *Init signal for the GAC Channel Counters*
3. *Init signals for the Back-end instruments*
4. *Gated 16 MHz Clock for the Pulsar Machines*
5. *Clock Valid signal for the back-end systems*

Programmable Control Registers:

These features are activated from the control computer.

The Antenna Mask: This is a programmable register present in the Four Input Card. The content of the register decides the dishes to be included while combining the signals. There are separate *Antenna Mask* registers present for the *Incoherent Array* and for the *Phased Array* section.

Polarisation Channel Masking: The Antenna Masking masks both the polarisation channels for the specified set of antennas. There are times when only one of the polarisation of a given dish may need to be excluded. This provision helps to mask one of the polarisation of any given dish. As the Polarisation channels arrive in a time-multiplexed manner, they will have to be masked during the alternate clock cycles. This operation is achieved by appropriately loading the Gain tables to point to an "all zero" (a special table which is kept as the 0th table) locations in the Input Conversion stage. For this purpose the alternate location of the Gain RAM is loaded with a table number (here, it is 0) containing "all zeroes"

Card Enable: This feature is available in the second stage combiner cards. At this stage the different 4-dish-groups are combined. There are possibilities that, one or more of the 4-dish combiner card may not be present in the system. During such occasions the inputs corresponding to those 'missing' cards should be made zero during the subsequent summing. The Card Enable register is configured to mask the 4-dish outputs that are absent.

Master Polarisation Masking: This feature is available at the De-multiplexing section of the Eight Input Card. This is a static feature, unlike the high speed polarisation masking already discussed. This *Master Polarisation Masking* feature can mask (zero) or allow a given polarisation channel for the entire Combiner network. If a particular polarisation channel happens to be masked, for all the dishes being combined using the polarisation masking in all the 4-dish combiners, and that particular polarisation channel will be masked out at this stage too. Both the sub-groups have an independent *Master Polarisation Masking* facility.

The details about the Tests conducted with the system and the Results are described in the next chapter

Chapter 5 ***Results and Discussion***

Chapter 5

Results and Discussion

5. 1 Introduction

Various experiments and tests were conducted during the development of the GMRT Array Combiner. These tests can be classified into three main types.

- Simulation studies.
- Field tests.
- Astronomical observations.

5. 2 Simulation Studies - *Error Analysis*

The system functions were modelled using computer programs. Then the *Array Combiner* input-to-output relations were studied using this *software model*. Simulated test data were fed as input signal to the *model*. The processed outputs were collected and analysed. The differences between the observed output value and the *true input value* were examined and the various results from analysis of these comparisons are presented here.

The *Array Combiner* input-to-output relations are chiefly affected by the quantisation errors from the first stage (*Input Conversion stage*). Since in the second stage (Combiner network) further quantizations is avoided throughout the network, it does not introduce additional errors. Hence analysis of the operations of the first stage reveals necessary details about the *Array Combiner's performance*. At first, the functions of the input conversion stage corresponding to one channel (dish) of the *Array Combiner* were modelled using computer programs. This model consists of two programs simulating the first stage, one of them produces the IA (*Incoherent Array*) mode outputs and the other one produces the PA (phased Array) mode outputs. These models operate for 15 different Gain-Windows (dynamic ranges), and output bit length, like 4, 5, 6-bits, etc., can be specified. These options enable the complete functional simulation of the system. The Analysis consists of the following steps.

1. Generation of the input data (*complex samples*).
2. Use the PA and IA software models and compute the outputs for the different gain -windows.
3. Analyse the results

Here the term, gain-window relates to the operating gain level or the expected input range. The smaller the Gain-Window, the smaller the input range but with higher gain. Combiner has 15 different Gain-Windows. These windows are arranged in the order of increasing input range. At present, the successive windows are maintained with 1.5 dB power level difference. Thereby spanning a 21 dB dynamic range coverage in power from window-1 to 15.

The aim of this simulation study is to find the optimum operating gain-window (instrument dynamic range) for a given input power. *The optimal region is a compromise region between the maximum power level the system can handle to the smallest variations it can faithfully reproduce.* The input signals are the normally distributed random noise.

5. 2. 1 Test Input Generation

A computer program (in the Matlab environment) is developed to generate the test data sequence. The required test data are the gaussian distributed random sequence of real and imaginary parts of complex numbers. These random complex numbers are nothing but the random points in a complex plane, which can be generated by randomly choosing a value for the ordinates, that is, the real part, and the imaginary part independently. These complex numbers represent the input signal voltages. Each of the values are represented in 4-bit mantissa and a (negative) 4-bit common binary exponent format. The steps involved in the generation of these numbers are given below:

1. Generate normal random numbers; two sets (sequence A, B).
2. Normalise the sequences to their respective root-mean-square values.
3. Divide the sequences by a suitable *scale factor*.

This operation adjusts the mean power of the input data to a desired value. This biasing is necessary to produce the test data distribution similar to that of the actual system inputs.

4. Find the $\log_2$ and convert the sequences into a mantissa exponent-sequences (A', E1, B', E2).
5. Adjust the mantissa to obtain a common exponent such that the mantissa fields are used optimally, and quantize to produce the required limited bit sequence (a, b, c).

Thus the random complex data sequence (represented by a,b.c) are generated and stored in a file. This data sequence are used as test input for the simulation models.

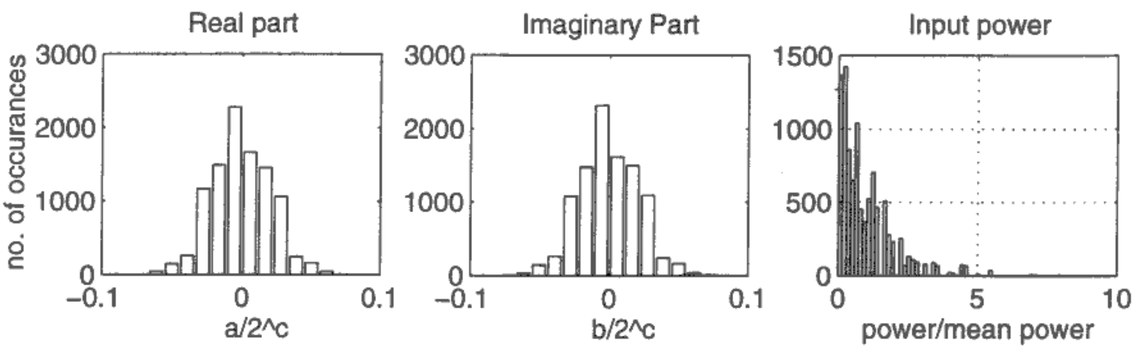

FIG. 5 - 1 *Test data distribution*

Some details about the nature of the input data are presented here. The real imaginary terms $a.2^{-c}$, $b.2^{-c}$ are gaussian distributed random numbers. The exponent 'c' determines the mean input power. From these complex numbers the power value $(a^2+b^2)/2^{2c}$ is computed and stored in the computer. This will be used as the reference input power, to which the outputs from the models will be compared. The probability distributions of the power values are shown here, they have an exponential distribution. In this plot the x-axis units are the output power value normalised to its mean. The x-axis is divided into 64-equal bins. The y-axis indicates the number of occurrences (out of total 10,000 samples) of the power value within a given bin. The discontinuities (gaps) seen are due to the nature of the input data format. It can be seen in this plot that the number of occurrences of small power values are more than the higher values. In this sequence the numbers as big as that of 9 times the mean occurs very rarely and numbers beyond 10 times has not occurred at all indicating that the related probablity is very small. Such is the property of the distribution.

To summarise, a random sequence of complex numbers (voltage terms) were generated. The input power values are computed from these numbers. This complex *data will be fed as input to the IA, and PA models. The power values will be used to compare with the simulation results.*

5. 2. 2 Simulation - *IA Mode (input conversion stage)*

The simulation experiment was carried out for all the 15 gain-windows using the same input data. The experiment was repeated for 3 different cases. They are:

Case 1: output power digitised to 4 bits
Case 2: output power digitised to 5 bits
Case 3: output power digitised to 6 bits

The test data was fed to the IA model. Output power values were computed for all the 15 gain-windows and for all the three cases. Then the results were examined.

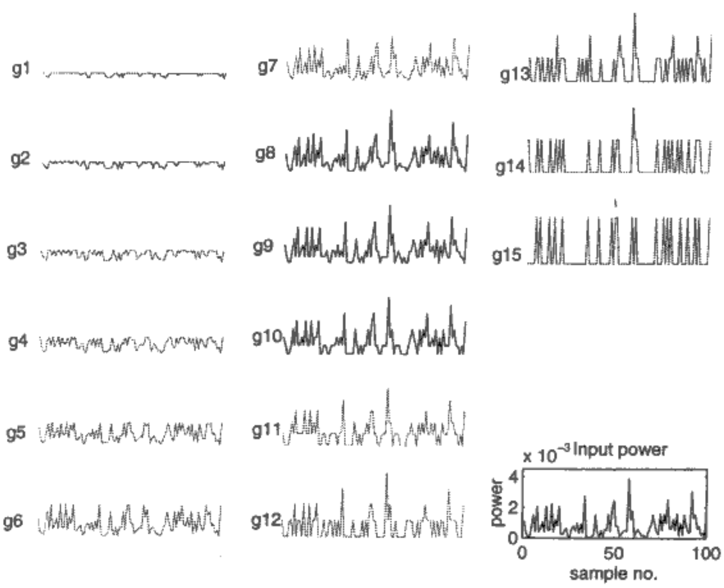

FIG. 5 - 2 *IA outputs from differnt Windows*

A sample sequence of the *outputs* produced are shown here (fig 5-7). These are the power values produced by the 15-different Gain-Windows. The outputs corresponding to only 100 samples are shown here. For the simulation studies a sample size of 10,000 was used. The last plot in fig.5-2 is the actual input power. The plots are arranged here in the order (g1-g15) of increasing input range (decreasing gain). As one can note that the output power value corresponding to many low input range windows (g1, g2 ,..) appear to be saturating and clipping of the signal is seen at the peaks. Outputs corresponding to few other windows (g9, g10) are reproducing the sequence better. In the case of the high input range windows (.., g14, g15) the outputs produced are in coarse steps. Fine details are not visible at all. The last plot shown here is the actual input power.

To summarise, the computed output power for the different dynamic range Gain-Windows appears as shown in fig-5-2. One among them closely reproduces the true statistics of the input signal. The analysis part of the program compares these outputs with the actual input power and estimates the error statistics as a function of the gain-windows used and quantisation step sizes involved.

5. 2. 3 Analysis and Inferences

The steps involved in the error analysis are described here. The output power values belonging to all the 15 gain-windows are taken and for each of them:

1. *The mean power of the input test data is computed (Min).*
2. *The output powers corresponding to each of the gain-windows are taken, and properly scaled to produce the output means (Mop), Then it is compared with the actual input mean (Min). The difference (Min-Mop) is the corresponding error (Ei) introduced in the measurement. These values are recorded.*
3. *The standard deviation of the error sequence (Serr) are computed and recorded.*
4. *The output mean (Mop) and the standard deviations of the error sequence (Serr) are normalised to the input mean (Min). Then the data are plotted for verification.*

This analysis was carried out for the three cases, with differing number of output bits. The input data used in all these cases are the same. The results are presented using the following three plots (fig 5-3, 5-4, and 5-5). Similar trends are noticeable in these plots. The plots shown in fig. 5-3 are the results for the 4-bit power output, fig. 5-4 are for the 5-bit power output, and fig. 5-4 are for the 6-bit output. *The bar plots are shown here to indicate the step size of a given gain-window.*

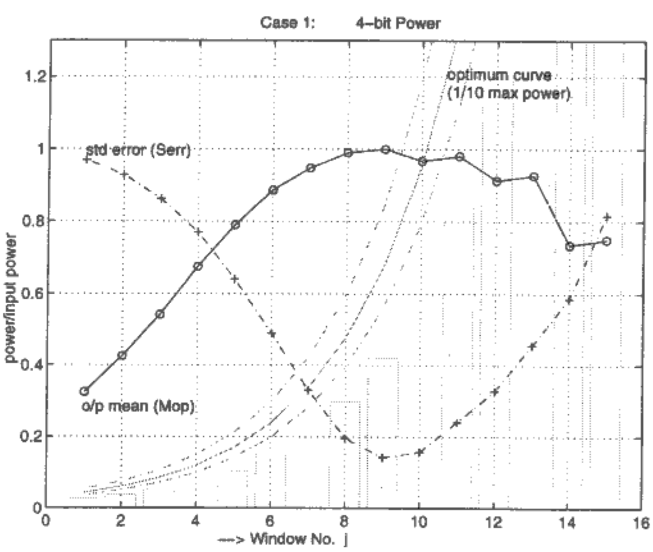

FIG. 5-3 Gain α -(1.5 j)dB *and* input range α (1.5 j)dB

In these plots, the mean of the output power and the standard deviation of the error in the estimation are plotted against different gain-window numbers.

Some of the features that are common for all the three plots (fig 5-3, 5-4, and 5-5) are discussed here first.

Along the x-axis are the gain-window numbers. Progressively each of the gain-window accommodates 1.5 dB more power than the previous one. The y-axis units are the power values normalised to the input mean power. The bar plots indicate the step size of a given gain-window.

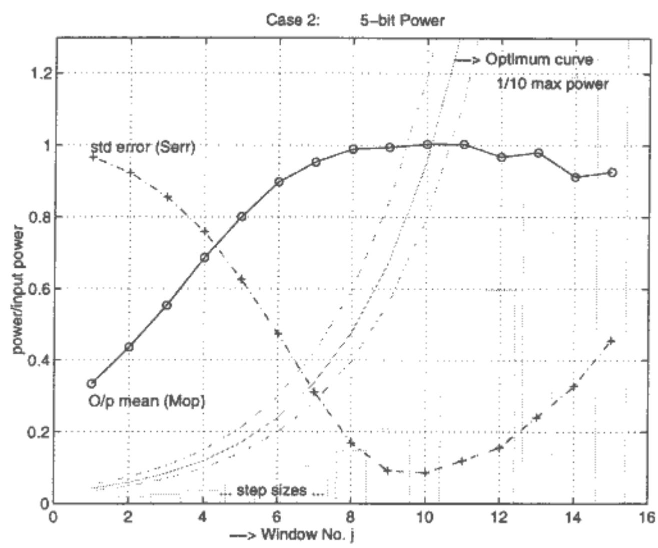

FIG. 5 - 4 Gain α -(1.5 j)dB *and* input range α (1.5 j)dB

Two prominent curves are visible in these plots. One of them is the output mean (Mop), the other one is the standard deviation of the error (Serr) in the output. The output mean is the mean of the output as estimated by the different gain-windows. The input range of the gain-window-1 is not sufficient to reflect the true mean. This window produces clipping of signal due to saturation (see fig 5-2;g1). This causes the estimate of the power to be lower than the input power. The error committed are also very large, it is as much high as that of the input mean itself.

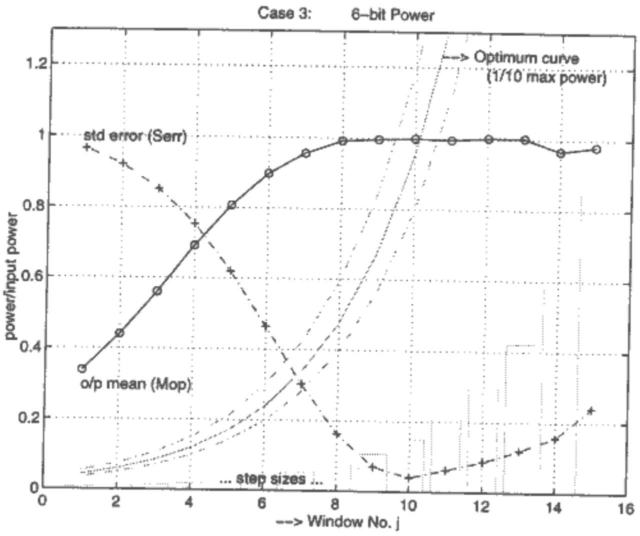

FIG. 5 - 5 Gain α -(1.5 j)dB *and* input range α (1.5 j)dB

As the input range is increased by moving to a higher gain-window number (lower gain), the saturation and the clipping reduces, and the estimated mean (Mop) slowly approaches the true (input) mean. (i.e. y approaches unity). But still the error (Serr) is larger than the estimated mean. The cross-over takes place between the gain-windows 4 and 5. At the cross-over, the estimated mean and the error (Serr) are equal. (the windows differ in ranges by 1.5 dB steps). As the instrument input range is further increased the estimated mean (Mop) output reaches the true mean. At this point the error (Serr) also comes down to a minimum value.

After the point of minimum error, the 3 plots (fig. 5-3, 5-4, 5-5) start to differ significantly. The output mean curve falls-off differently, also the increase in the error (Serr) are significantly different. These differences can be appreciated readily from fig.5-6, where the error curves from fig 5-3, 5-4, and 5-5 are plotted together. It is clear that only when the input range is sufficiently large the errors are dominated by the coarseness of the step, which is smaller, if, more bits are used to represent the output.

To summarise the information indicated from these curves so far,

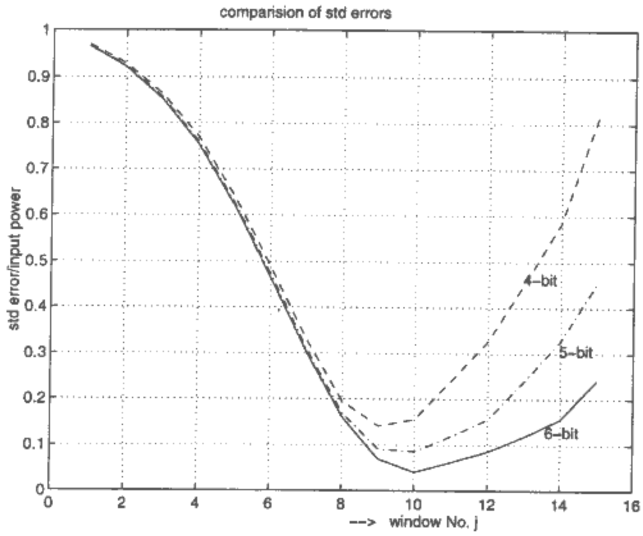

FIG. 5- 6 Gain ∝ -(1.5 j)dB *and* input range ∝ (1.5 j)dB

- In all the three cases, the error shows a well defined minimum at an optimum gain-window.
- The optimum window number shifts towards the left for the 4-bit (smaller bit size) output representation. For the 4-bit output the error minimises at gain-window 9, whereas for the 6-bit output it is at window 10. This aspect is due to the difference in the quantisation steps.
- At the optimum table the error introduced by the 6 bit representation is about 4%, 5-bit representation is about 8%, and 4-bit representation is about 14%
- Six-bit output representation has relatively borad range where the error is small. The output mean follows the input mean linearly in this region. It is useful to have such larger linear region as seen in this case.

The region of the gain-window corresponding to the minimal error is the _optimal operating region_ for the assumed input power. At this region one will get the best reproduction of the signal from this hardware.

The optimal operating window is established by the distribution of the input signal. In this case the inputs are exponentially distributed. From the plots it can be observed that, if the given input signal has a mean power M, then the gain-window (or input range) which just allows up to 10 times the mean, (i.e., input range = 10 x M) gives the best reproduction and the signal-to-noise ratio. This is shown by (see fig 5-3, 5-4, 5-5) the 'optimum curve' corresponding to 1/10th of the maximum (unsaturated) power allowed in a given gain-window. For the test data used, it can be seen that the optimum table for the 6-bit power output, is the 10th gain-window (where the error committed are the minimum).

Hence for 'optimum' performance, given a mean input signal power, a suitable window that gives the best minimum percentage error is to be chosen. As the mean input power is varied along the y-axis, different optimum gain-windows should be selected.

After the optimal region the output mean start to fall below the input mean. This fall-off is very rapid in the case of the 4-bit system. In this region of the plots, the gain windows used become larger and hence the smallest measurable (LSB) value (quantisation step size) becomes comparable to that of the mean input power. For the exponential distribution most signals are below the mean. At this region the mean is comparable to the LSB size, and hence the average output power can't grow too bigger than 1 LSB (one measurable) unit. Also the round-off scheme used in deciding the output value, alters the fine details of the curve by introducing more quanitzation error. These effects are clearly visible in the curves. In the 4-bit output the fall-off is quicker because the LSB size becomes larger than the other 2-cases.

This trend will continue until a gain-window (bigger input range) is reached, where most of the samples will correspond to output smaller than 1/2 LSB. At this point the output mean will fall very close to zero.

5. 2. 4 Simulation - *PA Mode (input conversion stage)*

The simulation experiment was carried out for all the 15 gain-windows using the same input data. The experiment was repeated for 3 different cases. They are:

Case 1: output real, imaginary parts digitised to 4, 4 bits

Case 2: output real, imaginary parts digitised to 5, 5 bits

Case 3: output real, imaginary parts digitised to 6, 6 bits

The test data was fed to the PA model (first stage). Outputs were computed for all the 15 gain-windows. The experiment was conducted for all the three cases and results were examined.

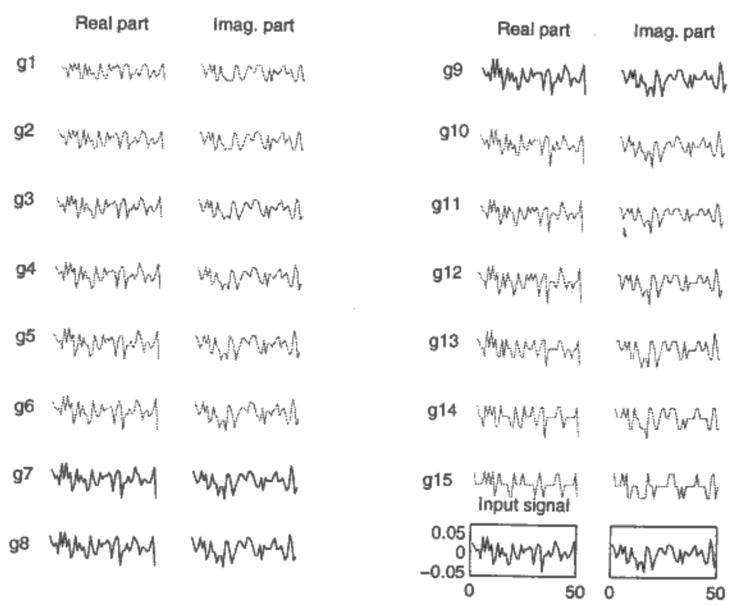

FIG. 5 - 7 *PA outpus from different Windows*

A sample sequence of the outputs produced are shown here in fig. 5-7 These are real, imaginary values produced by the 15 different gain-windows. Outputs corresponding to only 100 samples are shown here. For the simulation study a sample size of 10,000 was used.

The plots are arranged here in the order of increasing input range (decreasing gain). It can be seen that the output voltage (real, imaginary) corresponding to many low input range windows (g1, g2,..) appear to be saturating, and clipping of the signal is seen at both +ve and -ve peaks. Fine features of the signal are over amplified. The outputs corresponding to few other windows (g8, g9) are reproducing the sequence better. In the case of the higher input range windows (g13, g14, g15) the outputs produced are in coarse steps. Fine details in the signal are not visible.

The last plot shown here is the actual input voltage, (the real, imaginary terms). One of the quantised output plot from g1-g15 is a very close reproduction of this last plot

For the analysis purpose, the power terms (modulus squares) are computed from these complex numbers from cases g1 to g15. These power values can be compared with the true input power. The computed power values appear as shown in fig 5-8

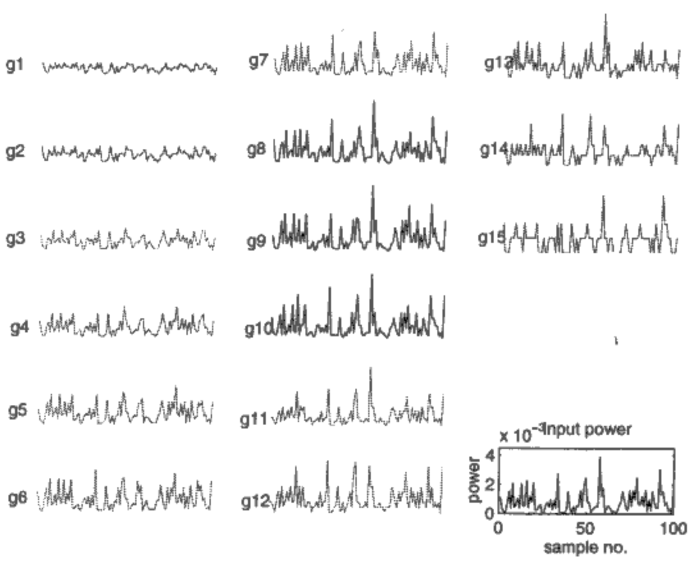

FIG. 5 - 8 *Computed Power values (PA)*

These plots also show similar characteristics as that of the IA mode plots of fig 5-2. The computed power terms belonging to small input range windows (g1, g2,..) are saturating, while that of the high dynamic range windows (g13, g14, g 15) have only the coarse details. And some of the outputs from the middle region (g8, g9, g10) are relatively better representations.

To summarise, real, imaginary terms corresponding to the different gain-windows are produced using the PA model and the corresponding power terms are computed for comparison with the input power.

5. 2. 5 Analysis and Inferences

At this stage the PA mode output voltages are already converted to power values, and hence the analysis becomes similar to that of the IA mode. The details are mentioned here again for completeness

The following are the steps involved in the error analysis of the PA mode outputs:

Computed power data corresponding to all the 15 different gain windows are taken, and for each of them;

1. The mean power of the input test data is computed (*Min*).
2. The output powers corresponding to each of the gain-windows are taken, and properly scaled to produce the output means (*Mop*), Then it is compared with the actual input mean (*Min*). The difference (Min-Mop) is the corresponding error (*Ei*) introduced in the estimation. They are recorded
3. The standard deviations (*Serr)* of the error sequence(*Ei*) are computed and recorded.
4. The output mean (*Mop*) and the standard deviations of the error sequence (Serr) are normalised to the input mean (*Min*). Then the data are plotted for verification.

The analysis was carried out for all the three cases, using the same input data. The results produced from the above experiments are discussed here. The plots show similar trends.

Some of the features that are common to all the three cases (4, 5, 6-bit results from fig 5-9, 5-10, 5-11) are discussed here first.

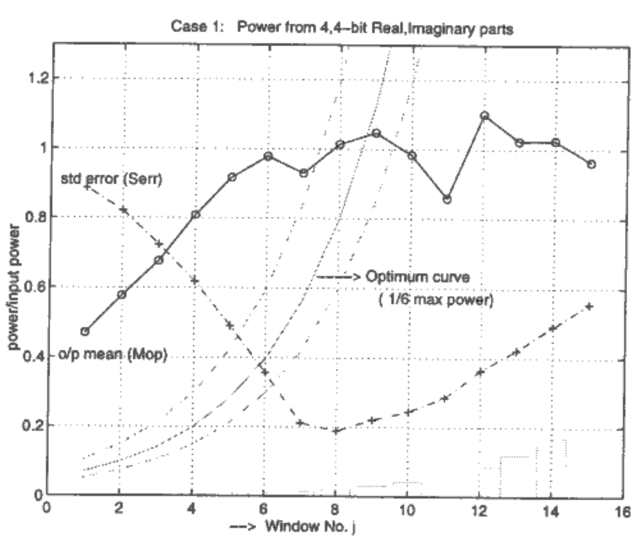

FIG. 5 - 9 Gain α -(1.5 j)dB *and* input range α (1.5 j)dB

The result obtained for cases-1, 2 , 3 (corresponding to the power obtained from the (4,4), (5,5), (6,6) bit representations respectively for the real, imaginary parts) are given here in figures 5-9, 5-10, 5-11 respectivlely. *The bar plots are shown here to indicate the step size of a given gain-window.*

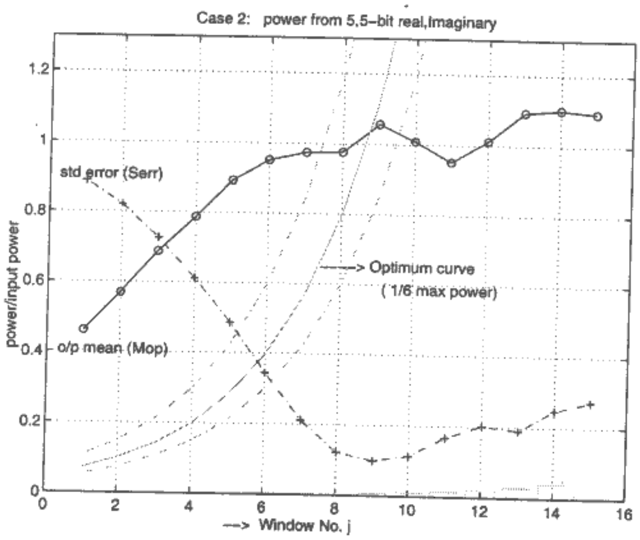

FIG. 5 -10 Gain ∝ -(1.5 j)dB *and* input range ∝ (1.5 j)dB

In these fingures the mean of the output power, and the standard deviation of the error in the estimation are plotted against the number of the gain-windows used. The successive gain-windows differ by -1.5 dB gain (input range increases by +1.5 dB) as one moves to higher window number. The y-axis are the output power, normalised to the input mean.

One of two prominent curves in these plots (fig 5-9, 5-10, 5-11) shows the output mean (Mop), the other one shows the standard deviation of the error (Serr) in the output. The output mean is the mean of the output power as measured by the different gain-windows. As it can be seen, the output mean measured by the gain-window 1 is less than the true mean. The input range is not sufficient and hence the signals are clipped due to saturation and this causes under estimation of the mean. The standard deviation of the error seen in the output is very large, and is comparable to the input mean.

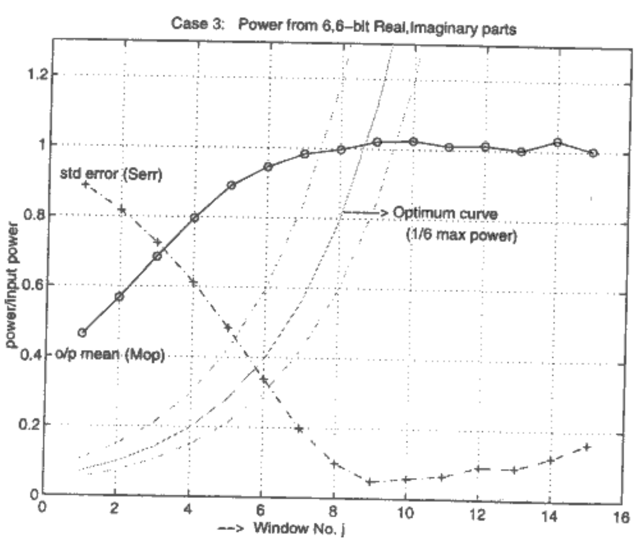

FIG. 5 - 11 Gain ∝ -(1.5 j)dB *and* input range ∝ (1.5 j)dB

As the input range is increased by moving to a higher gain-window number (lower gain), saturation and clipping effects are progressively reduced. Then the estimated mean slowly approaches the true mean. But until about gain window-3 the standard deviation of the error is larger than the estimated mean. The cross over takes place between the gain-windows 3 and 4. At this place, the estimated mean and the standard deviation of the error are about equal.

As the input range is further increased the estimated mean reaches the true input mean (Y=1) around X=9. At this time the standard deviation of the error also comes down to a minimum value.

Around this place and beyond, the features of the plots (fig 5-9, 5-10, 5-11) start to look significantly different. The mean value (Moi) curves start to fluctuate differently, and the standard deviation of the errors (Serr) are significantly different. This differences can be seen readily from fig.5-12, where the error curves from all the three cases (fig 5-9, 5-10 and 5-11) are plotted together.

The error committed in the estimation of the input power varies as a function of the gain-window used and as a function of the number of bits used in the output representation.

The following summarises the information obtained from these plots so far,

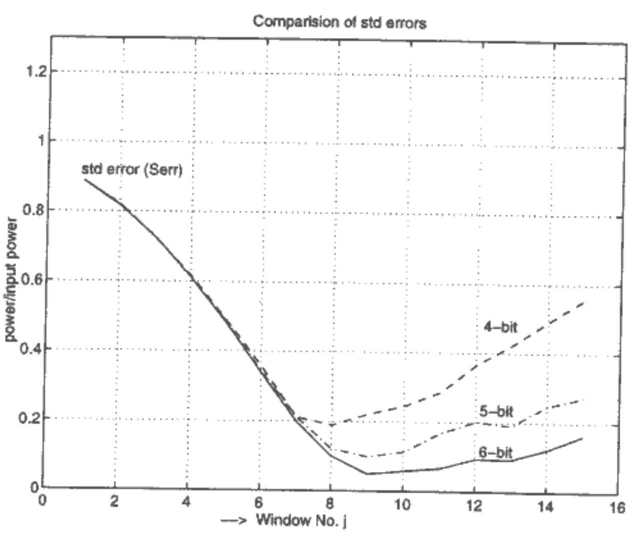

FIG. 5 - 12 Gain $\propto$ -(1.5 j)dB *and* input range $\propto$ (1.5 j)dB

- In all the three cases, the error shows a well defined minimum at an optimum gain-window.
- The optimum window number shifts towards the left for the 4-bit (smaller bit size) output (case 1), and error minimises at gain-window 8, where as for the 6-bit output it is at window 9. This is due to the bigger step sizes of the 4-bit output representation.
- At the optimum table the error introduced by the 6-bit representation is about 5%, 5-bit representation is about 9% ,and 4-bit representation is about 19%

The region of the gain-window corresponding to the minimal error is the *optimal operating region* for the assumed input power. At this region one will get the best reproduction of the signal from this hardware.

The optimal operating window is dictated by the distribution of the input signal. In this case the complex voltages have zero-mean and are gaussian distributed. From these results it can be observed that, the window that allows up to 6 times the average peak signal value gives the best reproduction and the signa-to-noise ratio. This is shown by the 'optimum curve' corresponding to 1/6th window maximum. In the voltage window (PA) this curve corresponds to it is 1/2.45 (about 0.4) of the maximum (unsaturated) voltage allowed in a given window. It can be seen that the 9th window is the optimum, where the error committed is the minimum. In the case of the 4-bit plots the minimum error window shifts to the left (towards the lower dynamic range window).

Hence for 'optimum' performance, given a mean input signal power, a suitable window that gives the minimum percentage error is to be chosen. As the mean input power is varied along the y-axis, different optimum gain-windows should be selected.

Near the optimal region the error minimises but the output mean starts fluctuating around the input mean (here y=1). This fluctuations are more seen in the case of the 4-bit output (case 1) system. It is less in the 5-bit system and it disappears in the case of the 6-bit system. This nature is related with the input distribution, quantisation sizes used in the measurement, and the round-off scheme used in deciding the output.

The software model simulates one channel (dish) operation. Hence the results shown here are for one dish input. The results can be appropriately scaled to see the effect on the multiple dish outputs, where only the ouput error will reduce by square-root of the number of dishes used, assuming operation at the optimum input range (Gain selection).

•

5. 3 Field-Test Results

The *Array Combiner* was taken to the observatory at the *Radio Astronomy Centre, Ooty, and GMRT, Poona*. There it was connected to the *Telescopes* and tested again. The *Pulsar Search Pre-processor* was connected to the *Combiner* hardware and the noise sources and CW signals were used as the test inputs. The linear operating regions of the combiner were verified. Pass-band filter shapes were recorded. Some of the results are presented here.

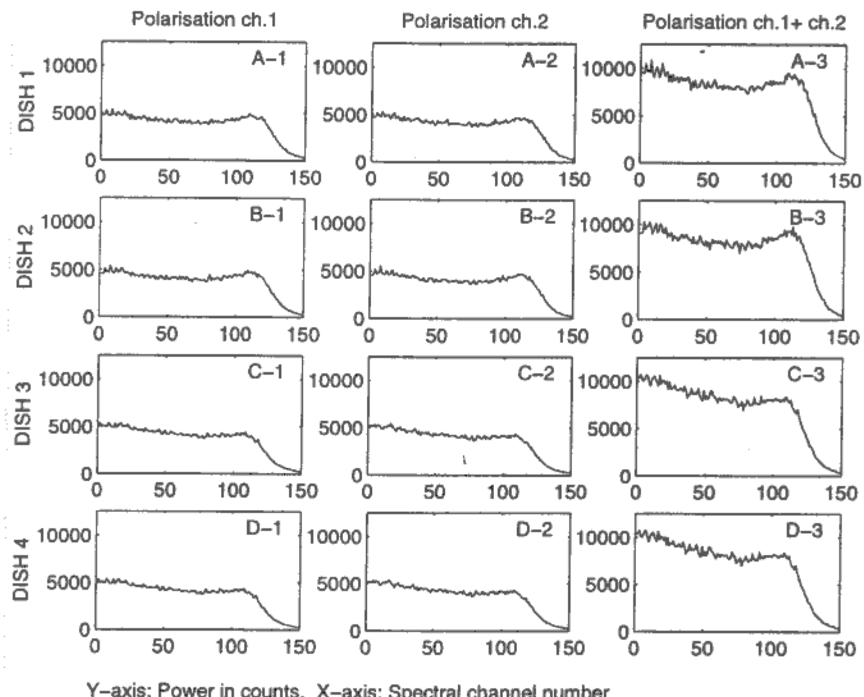

FIG. 5 - 13 *Noise Bandshapes for Dish 1 to 4 x 2 Pol. Channels*

The noise source bandshapes shown In fig. 5-13 are the test results obtained while checking the Array Combiner system. These tests were carried out at the *GMRT observatory*. The details about these plots are given here. Antenna noise were given as input to the FFT system. The FFT outputs were fed to each of the 16 channel inputs (two polarisations X eight dishes) of the Array Combiner. The outputs from the Array Combiner was verified on a back end system. The plots thus obtained verifies the proper functioning of the Array Combiner. Bandshapes obtained from 4 dishes and two polarisation channels are shown In this figure. Bandshape A-1 was obtained by processing signals from Dish 1, polarisation channel 1. Bandshape A-2 is from Dish 2, polarisation channel 2, and A-3 is the sum of the two polarisation channels A-1 and A-2. (as seen by the back-end instrument). Similarly for B-1..., C-1..., D-1... etc are for Dish 2, Dish 3 and Dish 4 channel bandshapes.

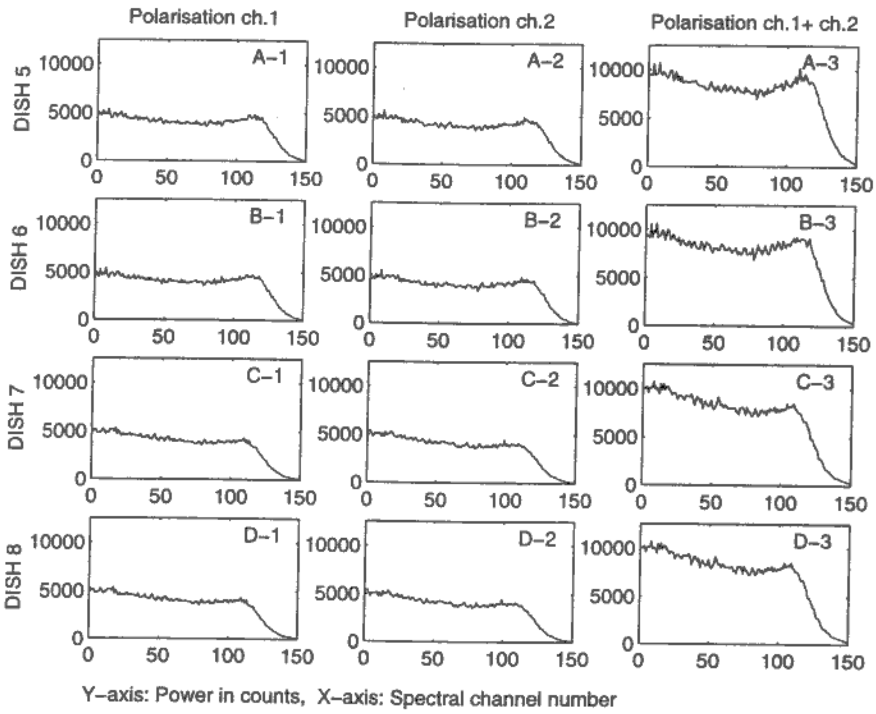

FIG. 5 - 14 *Noise Bandshapes for Dish 5 to 8 x 2 Pol. Channels*

The test results from the second set of four dishes (dish 5 to dish 8) are given in figure 5-14. Bandshape A-1 was obtained from Dish 5, polarisation channel 1. Bandshape A-2 is from Dish 6, polarisation channel 2, and A-3 is the sum of the two polarisation channels A-1 and A-2 (as seen by the back-end instrument). Similarly for B-1.., C--1.., D-1.. etc are for Dish 6, Dish 7 and Dish 8 channel bandshapes.

polarisation channel 2, and A-3 is the sum of the two polarisation channels A-1 and A-2. (as seen by the back-end instrument). Similarly for B-1..., C-1..., D-1... etc are for Dish 2, Dish 3 and Dish 4 channel bandshapes.

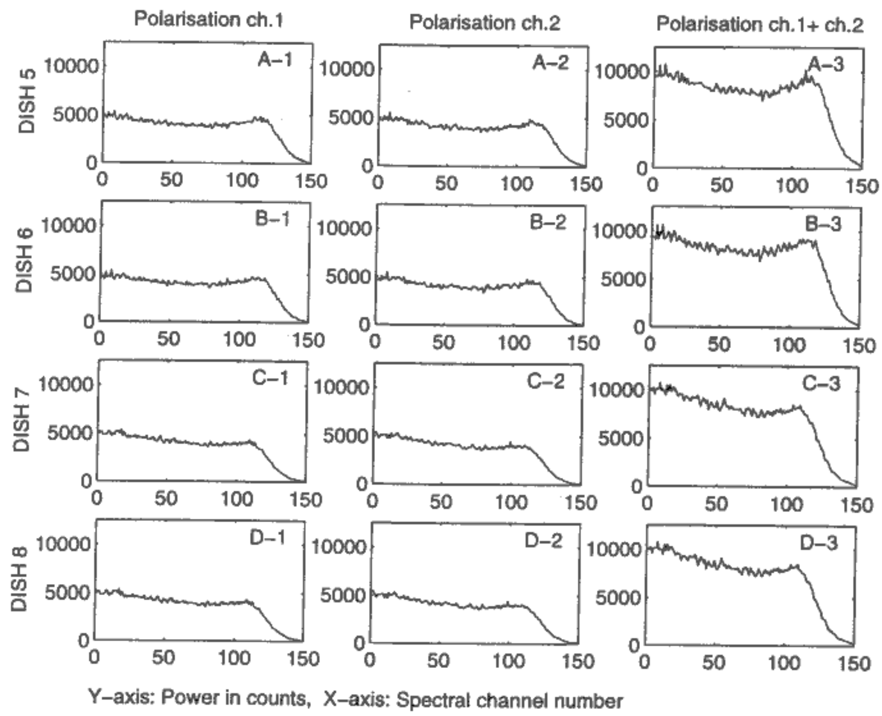

FIG. 5 - 14 *Noise Bandshapes for Dish 5 to 8 x 2 Pol. Channels*

The test results from the second set of four dishes (dish 5 to dish 8) are given in figure 5-14. Bandshape A-1 was obtained from Dish 5, polarisation channel 1. Bandshape A-2 is from Dish 6, polarisation channel 2, and A-3 is the sum of the two polarisation channels A-1 and A-2 (as seen by the back-end instrument). Similarly for B-1.., C--1.., D-1.. etc are for Dish 6, Dish 7 and Dish 8 channel bandshapes.

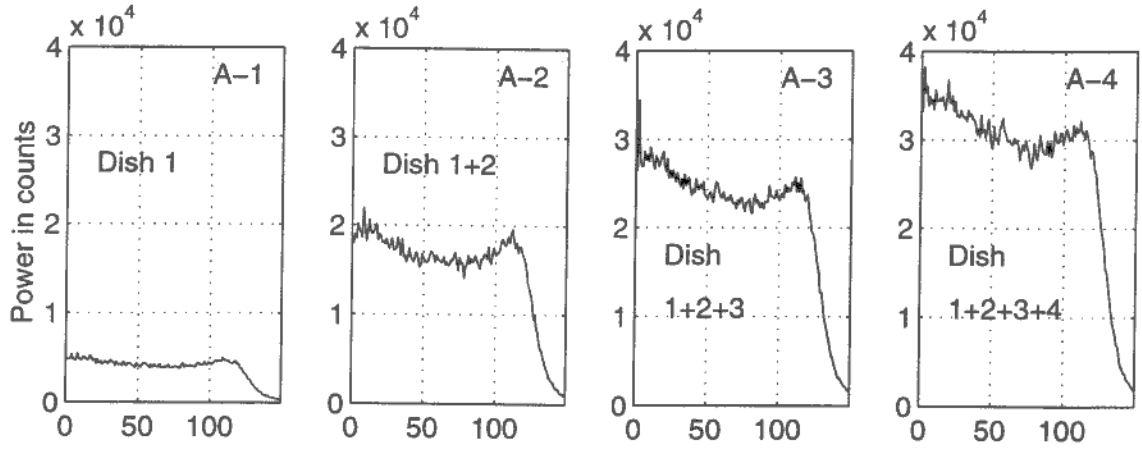

FIG. 5 - 15 *Adding signals from many inputs*

A sample of a typical result obtained while combining more than one dish input are presented here in figure 5-15

Noise spectrum outputs from the FFT system were fed to four dish inputs of the array combiner. The combined outputs from the array combiner were integrated and recorded using a back end instrument. In figure 5-15 the bandshapes A-1, 2, 3, 4 correspond to a single, two dish, three dish, and four dish inputs respectively. It can be observed that the combined output signal power increases as the number of dishes combined increases. These results verify the summing operation of the Array Combiner. Note that the input signal powers from different dishes were not same and that the gain windows used however were same.

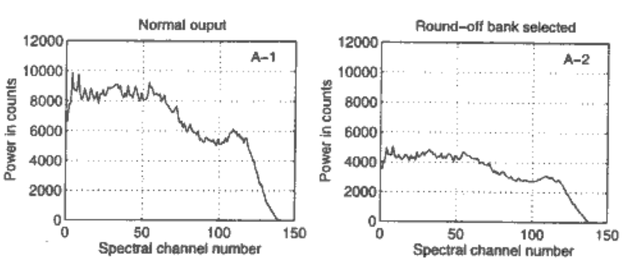

FIG. 5 - 16 *Output Format Control*

The last stage of the combiner has an output format control facility. The bandshapes shown in fig 5-16 verifies the operation of this stage. The input spectral voltages were fed to the Array combiner. Bandshape plot corresponding to the normal mode operation was recorded, which is shown in A-1. And one of the output format, the round-off mode was selected, and output bandshape A-2 was recorded. In the round-off mode the output will be produced after a divide by two operation. Hence the output bandshape (A-2) shows half the power of A-1 band.

FIG. 5 - 17 Band-shape plots for different Windows

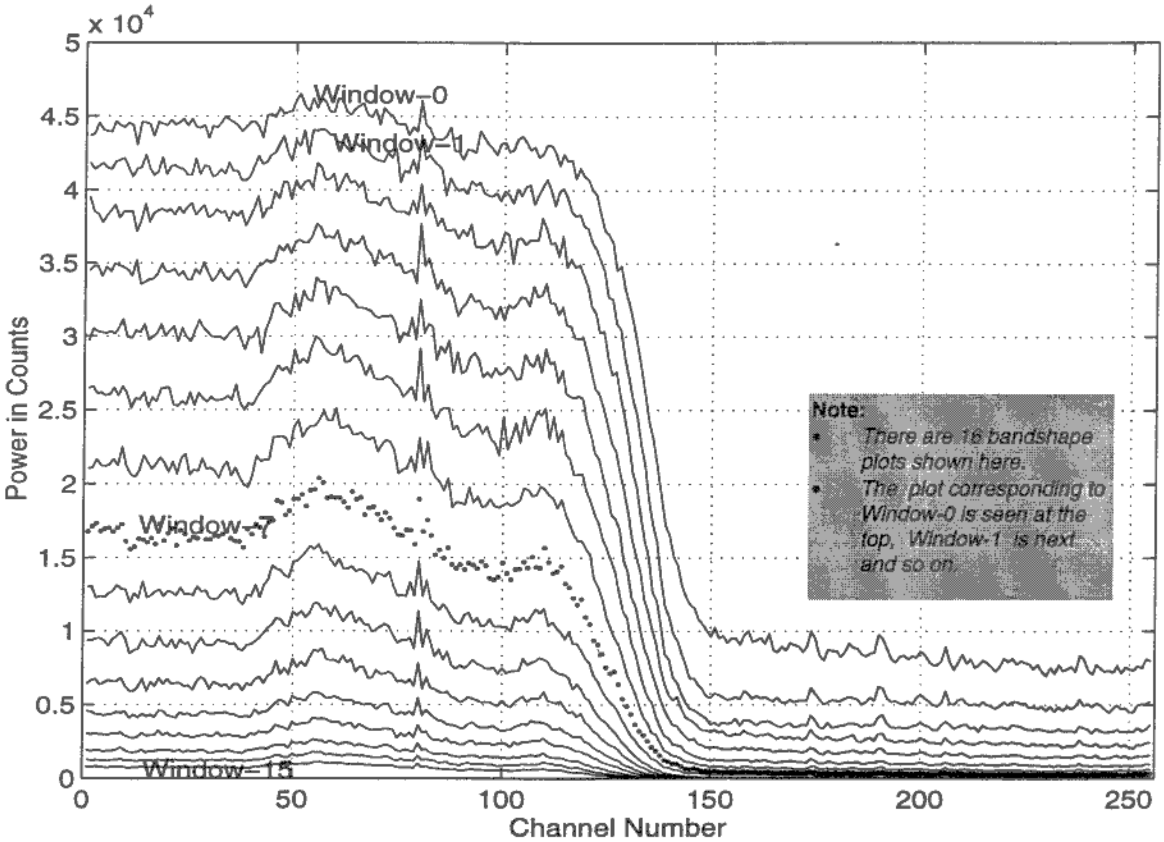

The Array Combiner has the programmable gain control facility. The operation of this stage was verified by observing the noise bandshape for various gain levels. The different band shapes thus obtained are given here in figure 5-17.

Noise spectrum was fed to the Array Combiner (only one dish input used). The output bandshapes were observed by changing the gain-windows. The gain-window was varied in steps of -1.5 dB. The 16 bandshape plots, thus obtained are overlaid and shown in fig. 5-17. The Lookup-0 plot corresponds to the highest gain window, and Lookup-15 plot corresponds to the lowest gain window. It should be noted that the gain-window corresponding to Lookup-15 accommodates, large input range variations in the signal but uses coarse steps, where as Lookup-0, gain-window accommodates smaller input range with fine steps. And in all these cases the total number of steps are the same. The results shown here are for the 6-bit resolution.

The linearity is assessed by the ratio of the outputs produced for two such channels that have significantly different input contribution. These ratios are derived from the bandshapes plot of fig. 5-17. One of the channel (ch 50) is taken from relatively a higher power section of the band, and the other one is (ch 125) chosen from the lower power (fall-off) section of the band. In fig. 5-18, the gain for the two channels as a function of the window number is shown. As can seen the gain variation is not identical for the two channels. The reason is that they have different input powers. This aspect can be more clearly seen from fig.5-19, where we plot the ratio of the powers from the same two channels as a function of window number. The common linear region is confined to a very small section between window 1 and 7. In otherwords, the gain-window which optimally matches for one section of the band need not be optimal for another section. Especially when the pass-band has significant gain variation across frequency, this aspect will cause signal to noise degradation across band. This problem is completely solved by the *Channel-wise gain correction* feature incorporated in the *Array Combiner* design.

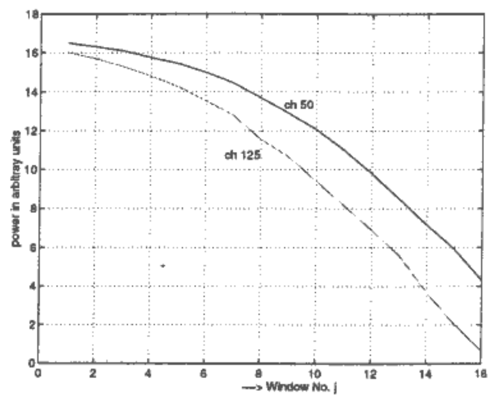

FIG. 5 - 18 *Lieanity Plot - 1*

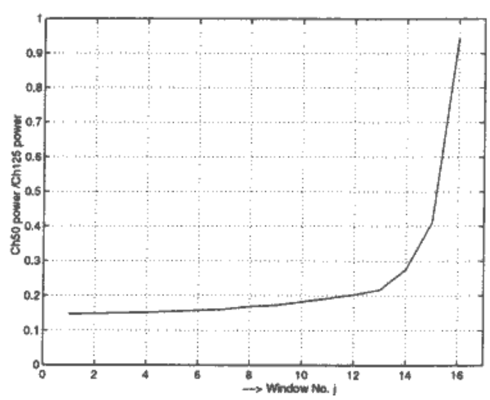

FIG. 5 - 19 *Linearity Plot - 2*

5. 4 Astronomical Observational Results

The proto-type *Array Combiner* has beeen used in many astronomical observations. One of the most useful participation of the *Array Combiner* is in the survey, study, and general observations of the radio *Pulsars*[1], which give periodic pulses of radio emission.

The Antenna was pointed to a pulsar direction in the sky. The baseband outputs were digitised and fed to a *Fast Fourier Transform (FFT)* hardware. The output from the *FFT* was fed to the *Array Combiner*. The *Array Combiner* outputs were connected to a *Pulsar Search Preprocessor.* The *Pulsar Search Preprocessor* acquired the data from the *Array Combiner*. Integrated power spectra were output at intervals 0.5 msec. and were recorded for off-line processing. The recorded data was further processed[2] by software programs to detect the presence of pulse signal. The obtained pulse profiles are shown here.

The following figures shows some of the observations made on pulsar signals at 327 MHz using the *Ooty Radio Telescope*.

[1] *Pulsars: Nuclear fuel is the lifeblood of a star. Stars with larger masses than 1.4 Suns, after using up all the fuels die a more violent death by explosion. A part of the star collapses, to become a heavy material at its core. It forms a tiny star of about 20 Kms in radius with an incredibly high density of about 100,000,000 tonnes per cubic centimetre. At this pressure the electrons are forced into the nuclei with the protons, forming a neutron star. Some of these are rotating at a very high rates of up to several turns per second, and send out beams of radiation which we detect each time a beam passes us. Since we receive the energy in pulses, we call these stars Pulsars.*

[2] *Different spectral channel data was suitably delayed to acount for dispersion delays introduced in the intervening medium and then combined. The dedispersed time sequence was folded at the intervals of the Pulsar period to obtain an average estimate of the emission profile over one period.*

FIG. 5 - 20 **Pulsar Profile -1** *(PSR 0834+06)*

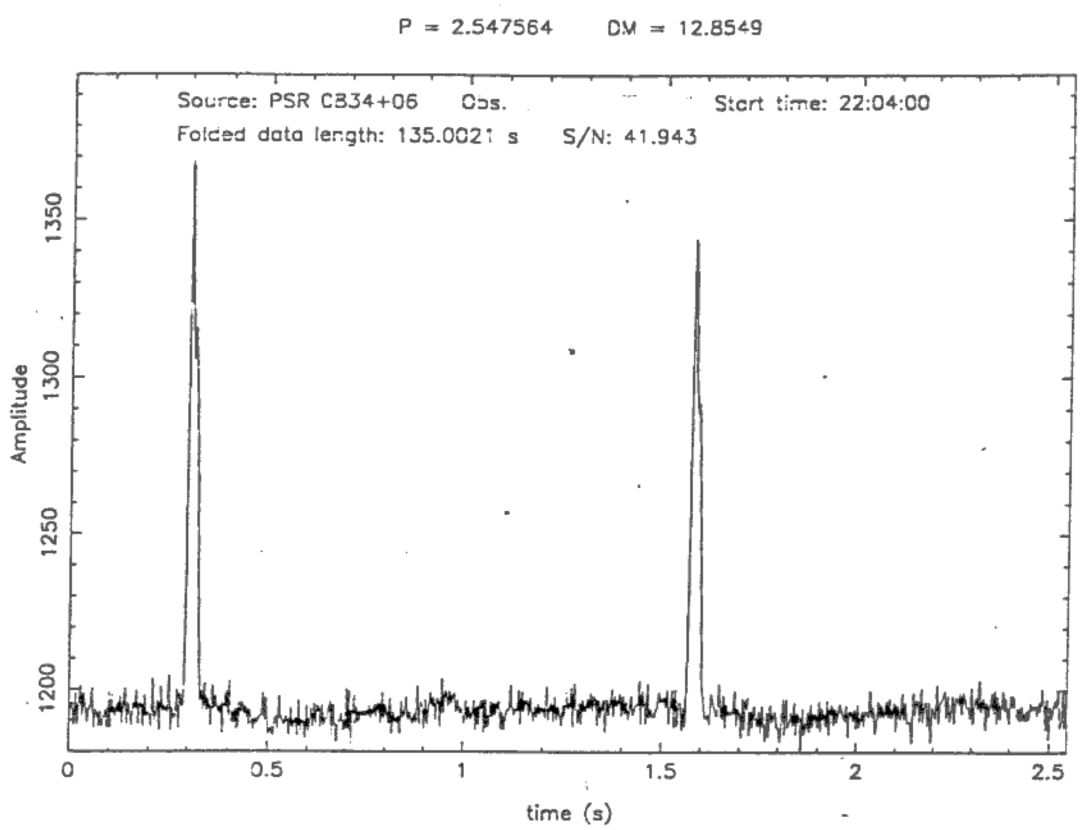

Figure 5-20 , is pulse profile obtained by observing a pulsar PSR 0834+06 (*the numbers indicate their location in the sky*). This particular pulsar rotates at rate of about one revolution every 2.547564 seconds. In this figure two pulse periods are shown. In most cases, the data acquired from the sky does not have any significant indication about the presence or absence of the pulse. A priori knowledge about the expected nature of the pulsar radiations, good estimates about the characteristics of the media through which pulse radiation has travelled, and the signal processing techniques adopted makes the detection of the Pulsar radiation possible on Earth. The signals that are buried deep in the sky and receiver noise can thus be detected with a remarkably high signal to noise ratios (SNR). Here, the SNR achieved is about 42 from a data collected for about 135 seconds. To make such detections feasible the instruments used have to work with sufficient accuracy and precision to cater for the weak nature of the signals received in the telescopes.

FIG. 5 - 21 ***Pulsar Profile-2 (PSR 1237-41)***

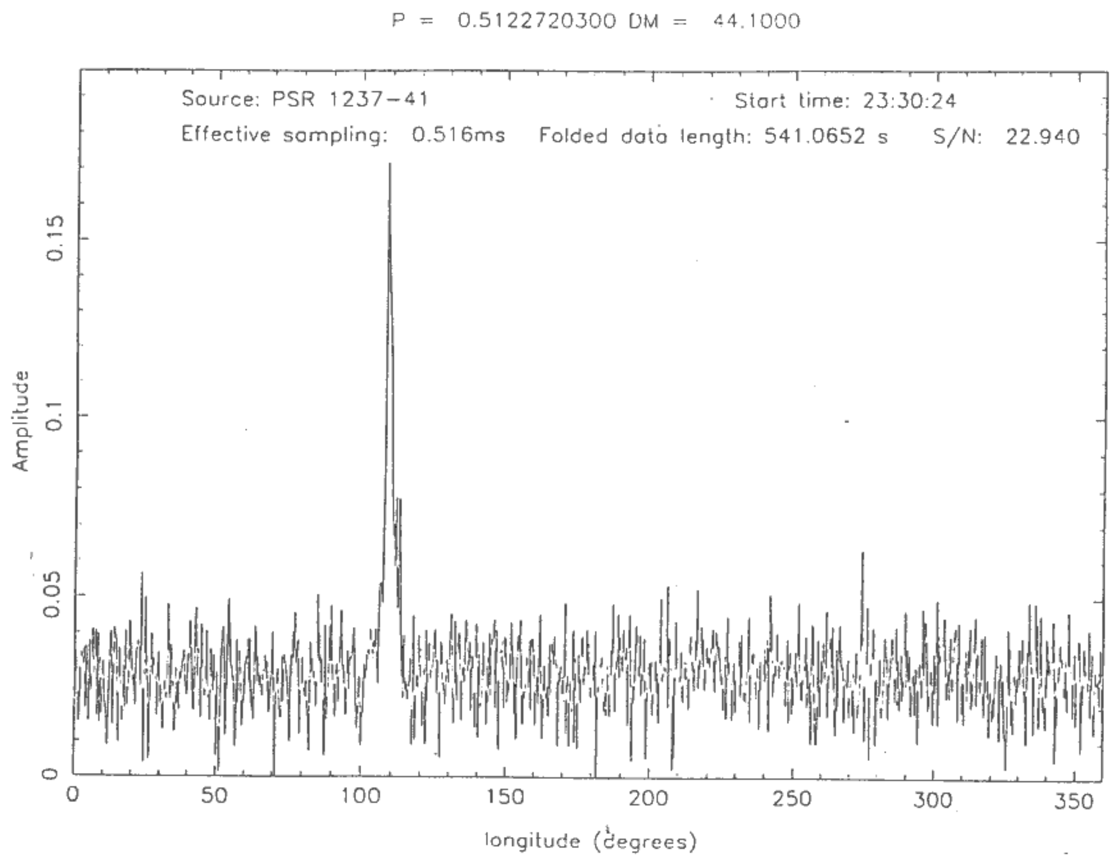

Figure 5-21 is a pulse profile obtained by observing a pulsar PSR 1237-41. This pulsar rotates once every 0.5122720300 sec. (incidentally the rotation periods are known to better than such accuracy!). This folded pulse profile has a SNR of about 23 from a data collected for about 541 seconds.

FIG. 5 - 22 **Pulsar Profile-3** *(PSR 0740-28)*

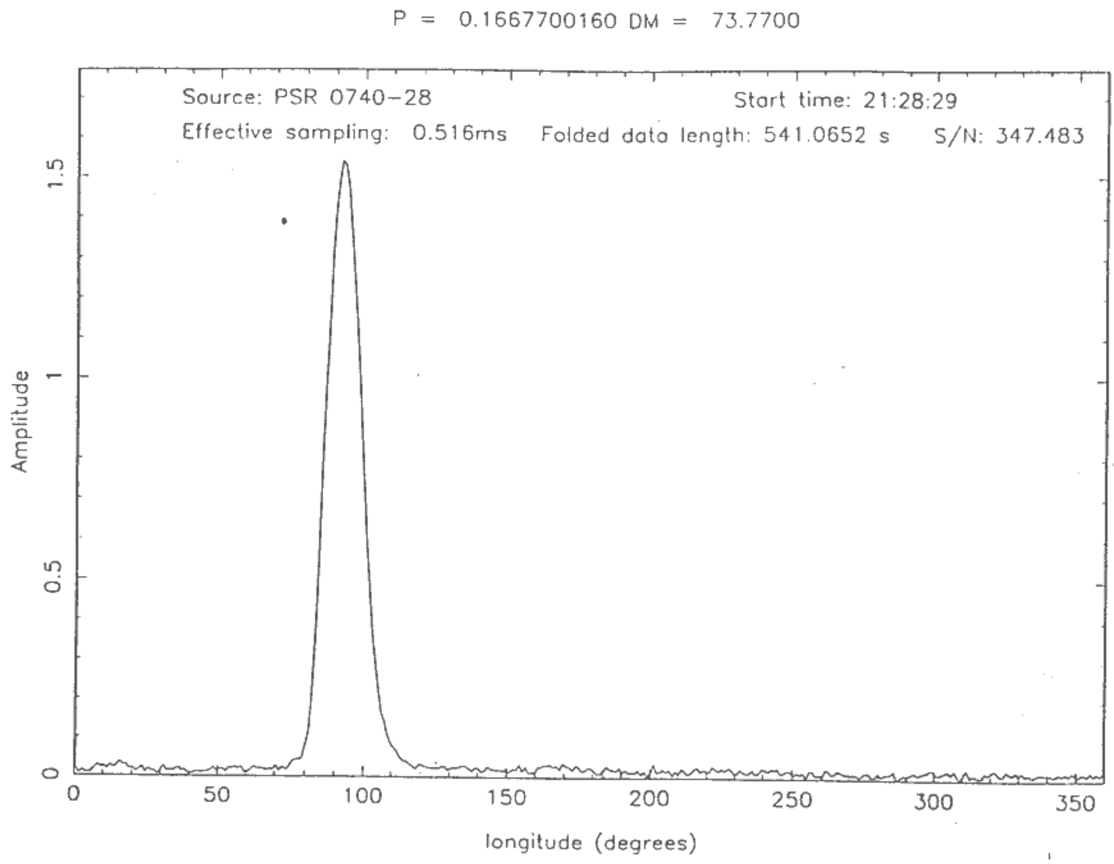

Figure 5-22 is another fast pulsar PSR 0740-28, with a rotational period of 0.1667700160 seconds. This profile was raised above the noise with a SNR of about 347 from a data collected for about 540 seconds.

In these cases the proto-type Array Combiner was used. The instrument is still in use for many other major observations like search, timing study, flux calibration of pulsar signals, etc..

5. 5 Conclusion

The error analysis performed has yielded a very useful information about the characteristics of the instrument. The optimum curves identified will help to use the instrument at its best performing region. To summarise the cumulative results from the IA and PA error curves are presented here again.

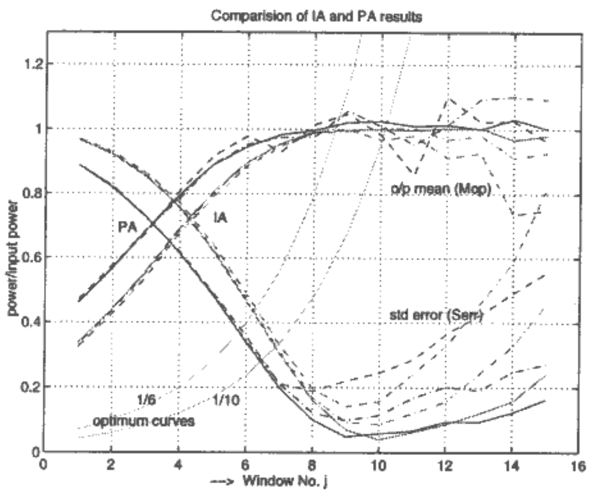

FIG. 5-23 Gain α -(1.5 j)dB *and* input range α (1.5 j)dB

The plots can also be interpreted as though the windows are not changed but the signal power is varied from left to right in steps of -1.5dB.

The error committed in the estimation of input mean varies as a function of the gain-window used and as a function of the quantisation step sizes used. The error minimises at an optimum gain-window in a particular fashion. It should be noted, however, that the error values and the optimum value vary for the IA and the PA stages.

The performance of the machine in practice depends on how carefully one selects the gain-windows. For this purpose an automatic calibration procedure has been developed to aid the user. It is also possible to selectively attenuate any given frequency channels, especially when there are interferences. All these features, improve the performance of this instrument.

For observations like *pulsar*, where there is an expected positive growth in the signal power it is best to operate at the one extreme (towards the higher window side) of the linear region of the *Array Combiner*. The error values seen in this plot are for one dish input. These values will go down to an appreciably very small value when more dish inputs are combined.

Chapter 6 ***Conclusions***

Chapter 6

Conclusions

6. 1 Summary of the work

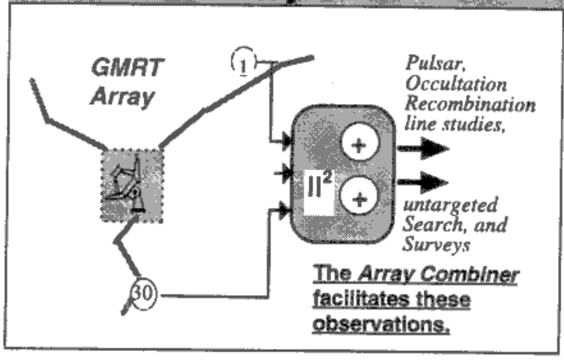

The ***Array Combiner*** presented in this *thesis* is designed and developed to provide the two possible simultaneous single-beam modes for the GMRT Array. One of the single beam mode is the Incoherent Array (IA) mode and the other one is the Phased Array (PA) mode. The outputs in these modes are produced by suitably combining the different dish outputs. Such single beam mode helps in terms of reduced hardware complexities and data rates, etc., in observations requiring high time/spectral resolution.

The IA *output* is formed by combining the detected power outputs from the array elements, while the PA output is formed by coherently combining the voltage signals from the array elements. The IA mode yields a broader sky coverage at the expense of reduced sensitivity, and is best suited for survey kind of observations. The PA mode is useful for observations of small sky area that require a very high sensitivity.

A detailed quantitative analysis of the performance evaluation is carried-out using computer simulations. These simulation studies yielded useful information about the choice of parameter to optimise the performance of the *Array Combiner.*

The design was carefully analysed and the two main sections were identified, viz., 1) the Input Conversion stage, 2) the Summing stage. Suitable techniques were found out to simplify the design complexities in these stages. To validate the design, a reduced version of the instrument working at 16 MHz was built and tested at the telescope site with astronomical signals. The test results showed that the basic design works satisfactorily. Currently, this version is being used for the astronomical observations. In this design, the major computations were simplified using the look-up tables, and erasable programmable logic devices were used for performing the addition. In the final design, the hardware complexities were further reduced by running the system at twice the speed. The final system also incorporates a facility to optimise the quantisation levels (in the look-up tables) in accordance with each spectral channel input independently. It has been designed with a scalable architecture.

It is important to note that the speed of operation of the final system is about 32 MHz. Running the system at the higher speed introduced new constraints. The hardware technology required was completely different from what was used in the proto-type design. The realisation of the final system hinged on the availability of faster components in the market and the knowledge from literature for building such high speed systems. For this purpose, the high speed circuit design aspects were carefully studied. The techniques for performing processing of signals at the required speed were identified and circuit layouts were carefully made to suit for the high speed design. The full system design was completed. The design taking into account all the additional factors is implemented in the final version of the hardware.

The PCBs required for a main section of the instrument, supporting an eight dish system (two polarisation) were made, assembled and tested. This new version is presently installed at the GMRT telescope site. The test results show that the design goals are adequately met in the final system.

6. 2 Special Features & Scopes for Future Work

1. In this design many Engineering design challenges have been met by suitable design ideas and techniques. Especially to handle large number of inputs at the high speed, many new design ideas were considered. The techniques developed and identified for making the high speed boards should find use in many other new applications.

2. One of the important features of this instrument is its complete programmability. By suitably arranging the hardware and the memory chips, the instrument can be made to handle a variety of different tasks at high speeds, apart from being an *Array Combiner.*

3. The main circuit cards are made using 4-layer PCBs. In all these cards the inner layers are the power planes and the signal tracks are laid only in the outer layers. Such layouts, enable quick and easy testing of the circuits during the development stages.

4. The Computer Interface provided at present satisfies all the present requirements. However it has a lot of scope for further improvements. A dedicated controller can be incorporated with a standard interface (like RS 232) to the Control Computer. The user interface program can be further improved. The *remote* user interface can be provided by adding additional features through the *ethernet* connectivity

5. The FCT series ICs and the CMOS PROMS used in the system reduced the total power consumption to a good extend. The ECL differential driver and receiver ICs used in the system consume a lot of power and dissipate heat. With the present state of the technology, it would be possible to consider an alternative scheme for such purposes.

6. A facility to introduce a special-purpose Marker channel during the dead time of the FFT cycles for use by the back-end systems for any hardware synchronisation purposes is provided. This is achieved by suitably loading the Gain RAMs.

7. At present, the system *calibration* depends on the Pulsar Search Pre-processor as a back-end to collect and integrate the data coming from the *Array Combiner.* If an *Integrator* can be incorporated along with the *Array Combiner* itself, it will reduce the dependence on a back-end system and make the *Array Combiner* as a self-contained system.

8. The final system, capable of handling all the GMRT dishes (30 dishes X 2 Polarisation channels X 2 sidebands) consists of 22 main cards of about 11" x 9" size (with totally about 1500 ICs). The further size reduction of the system may be possible, if, fast PROMs with much higher density or high speed EPLD range devices are available.

9. It is possible to operate the Array Combiner for up to 512 channels per polarisation per FFT frame in case the FFT system gets upgraded to 512 channels in future. For this purpose, the *Gain RAMs* will have to be loaded and the Clock sequencer reset (sync) will have to be generated appropriately.

10. There are general purpose signal lines provided in circuit cards, from the EURO connectors to the EPLDs and between the EPLDs. These lines can be used to accommodate future requirements, if any. For example, the *Gain RAM* channel counters can *start*, *stop*, or the count order can be reversed etc., by sending a specific input signal through these general purpose lines.

11. The Array Combiner has 32 input channels. One of the two spare inputs can be fed with test patterns to enable easy diagnostics of the system.

12. It is possible to use the Array Combiner to form a *Broader Beam*. For this purpose, the individual antennas being combined can be made to point to a non overlapped grid positions in the sky, and when 'n' such antenna signals are combined, it will produce a beam that will cover areas in the sky 'n' times that of a single dish. Although the sensitivity will be poor, such a beam may be useful to detect and follow strong and fast moving phenomena in the sky.

13. The Array Combiner, with minor changes in the configuration (PROMs), can be used to correlate signals between two antennas or two groups.

14. The final stage of the Array Combiner demultiplexes the two polarisation channels. In any specific application, if the multiplexed outputs are desirable, the

hardware can provide these outputs with only a minor modification on the clock lines. This is possible by feeding the 32 MHz clocks, in the place of two (two phased) 16 MHz clocks, that are going to the Demultiplexer section. This 32 MHz clocks can be fed at the back-plane connector pins or inside the *Clock Control* card. When the demultiplexing is disabled this way, the same output will appear on the Pol-1 and Pol-2 connectors at the 32 MHz rate. But the data from the Pol-2 connector will appear one clock earlier to the data from the Pol-1 connector.

15. The simulation study results can easily be verified for the various windows by using test *noise* or suitable astronomical *calibration sources*, and by comparing the corresponding results. The calibrated system performance can be evaluated using the astronomical observations of well known sources.

The astronomical observations that will use the Array Combiner's single beam modes (IA and PA) are:

- *Pulsar Search Observations,*
- *Pulsar Polarisation Study,*
- *Pulsar microstructure studies*
- *Recombination line observations,*
- *Occultation studies,*
- *VLBI Observations, etc.,*

To summarise, the test results show that the design goals are adequately met in the final system and hence the *Array Combiner* with all its programmable features will surely add significantly to the GMRT capabilities and contribute in all these scientific studies planned with the *Giant Metrewave Radio Telescope.*